Geology, Mining History, Mineralogy, and Paragenesis of the McDermitt Caldera Complex, Opalite Mining District, Humboldt County, Nevada, and Malheur County, Oregon

Gail E. DUNNING[1]

773 Durshire Way, Sunnyvale, California 94087

Michael F. COX

P.O. Box 786, Soquel, California 95073

Andrew G. CHRISTY

School of Earth and Environmental Sciences, University of Queensland, St Lucia, Queensland 4072, and Geosciences, The Queensland Museum, 122 Gerler Road, Hendra, Queensland 4011, Australia

Ted A. HADLEY

907 Anaconda Way, Sunnyvale, California 94087

Joe MARTY

5199 Silver Creek Road, Salt Lake City, Utah 84108

[1] Corresponding author; email: gedunning1937@gmail.com

A Bay Area Mineralogists Report

Table of Contents

ABSTRACT

From the first discovery in 1917 until the present, the abandoned mercury and uranium mines within the boundaries of the McDermitt Caldera, Opalite mining district, Humboldt County, Nevada and Malheur County, Oregon, have yielded an important suite of epithermal mercury and uranium-bearing minerals related to Yellowstone-type volcanogenic and hydrothermal processes and activity lasting over a short span of about 16.6 to 15.7 Ma. Mercury ore formation appears to be a combination of structural control along caldera-collapse fractures, as well as the mixing of paleo ground and surface waters with epithermal fluids originating from undefined deeper hydrothermal sources. Mercury-bearing minerals identified within volcanic rocks and overlying tuffaceous lake sediments include calomel, cinnabar, corderoite, eglestonite, kenhsuite, kleinite, mercury, montroydite, mosesite, radtkeite, schuetteite, shakhovite, terlinguacreekite, terlinguaite, and thirteen new and rare mercury phases currently under study, one being the unnamed cubic β-$Hg_3S_2Cl_2$ phase and another the first natural mercury carbide oxy-chloride derivative of Hofmann's base. Several of these new phases constitute a substitution family of mercury compounds not recognized before. Uranium-bearing minerals within the western and northern areas of rhyolitic rocks and tuffaceous lake deposits include autunite, coffinite, "gummite", meta-autunite, metazeunerite, torbernite, and uraninite. Accessory minerals of interest include chapmanite, conichalcite, cryptomelane, kermesite, lithiophorite, quintinite-2H, senarmontite, stibnite, tripuhyite, and valentinite. Important concentrations of gold, silver and gallium have been recorded from recent exploratory core drilling in the area east of the old Cordero mine. Lithium-rich clay deposits are currently being explored in the area.

INTRODUCTION

The McDermitt Caldera is a Miocene-age volcanic structure straddling the Nevada-Oregon border, approximately 200 miles (322 km) northeast of Reno, Nevada. Most of the caldera structure is in the state of Nevada. It is oval shaped based on recent mapping, and the structure is about 27 miles (43 km) in a northerly direction and 21 miles (34 km) in an easterly direction. The caldera has been interpreted as a superposition of several collapse-type calderas located in a region of Basin-and-Range normal faulting (Rytuba 1976; Rytuba and Glanzman 1978; Rytuba and McKee 1984), but most recently is argued to be a single collapse structure within a larger area of Miocene collapse structures called the McDermitt Volcanic Field (MVF) (Benson, 2017; Henry 2017).

Locally, the volcanic complex hosting the mining area is reached via a paved road about 11 miles (18 km) south from the small unincorporated community of McDermitt, originally called Dugout, which straddles the Nevada-Oregon border. The area is in the Oregon High Desert, with a semi-arid climate and an average rainfall of 9.2 inches (234 mm) annually, with hot dry summers and cold winters.

Figure 1. *View of McDermitt, Nevada looking north to Oregon along Highway 95 (after Commons, Wikimedia, 2010).*

Situated near the northeastern and eastern periphery of the caldera complex are eight mining claims which contained significant quantities of mercury mineralization. The McDermitt mine is the largest and was the largest mercury producer in the western hemisphere in the late 1980s (Noble et al. 1988), as well as the last in production. The McDermitt deposit possesses a tabular, gently dipping configuration within 150 feet (46 m) of the surface over an area of 2200 × 2500 feet (670 × 760 m) (Roper 1976) and was mined as an open pit. The mercury ore consists of cinnabar and corderoite deposited parallel to bedding in argillized Miocene-age tuffaceous lacustrine sediments above a paleolake-bed of silicified "opalite" volcaniclastic breccia.

The uranium mineralization is confined to the northwestern and southwestern regions of the caldera complex periphery, within rhyolite domes whose emplacement is controlled by fault zones. Minerals include uraninite and coffinite with minor secondary uranium phosphates and arsenates.

GEOLOGICAL SETTING

Geological and mineralogical reports for the region span eighty years of significant scientific progress. Reports fall into three groups: 1) areal geologic characterization; 2) geology of the caldera; and, 3) individual features such as mines and mineral deposits. Studies involving the geology and geological evolution of the northwestern United States are beyond the scope of this compilation. The geology of the MVF has been intensely studied because of its prominent features and ore deposits. These features include radiating dikes of basalt and rhyolite filling Miocene fracture zones, flood basalts, silicic eruptive centers and associated ignimbrites and flows, proximity to the Miocene edge of the North American craton, relationship to the northeast-trending volcanic track of the Yellowstone hot spot YHS), location just west of the northern terminus of the south-southeast trending Nevada Rift Zone, and an abundance of interesting and significant mineral deposits. With respect to the caldera, essential professional studies that clarify the geological setting and origin include Wilden 1964; Greene 1972, 1976; McKee et al. 1975; McKee 1976; Rytuba 1976; Rytuba et al. 1979, 1984; Noble et al. 1988; Pierce and Morgan 1992; Camp et al. 2003; Coble and Mahood 2008, 2012, 2016; Christiansen et al. 2012; Henry et al. 2012, 2013, 2016, 2017; Benson et al. 2013, 2014, 2015, 2016, 2017; Camp and Ross 2014; Starkel 2014; and, Benson 2017. Recent investigations of the McDermitt caldera and its geologic setting are provided by Starkel 2014; Henry et al. 2016, 2017; Benson 2017; and, Benson and Mahood 2017.

In general, the caldera is related to Miocene volcanic activity that is postulated to have accompanied subducted slab thinning or breakoff beneath the western edge of the North American craton, as well as impingement of a hot spot on the same edge. Pierce and Morgan (1992) provide a comprehensive discussion of the YHS track and the possibility that the YHS first migrated beneath the stable craton margin in the vicinity of the McDermitt caldera. Researchers currently propose that the MVF is part of a complex formed by dikes propagating southward from an eruptive focus at the Steens Mountain. The propagation of the dikes caused mid-level crustal melting and magmatic assimilation, fractionization, crystallization, and caldera-forming eruptions.

MVF eruptive centers formed during a relatively short interval of time (~16.8 – 14.6 Ma) (Noble et al. 1988; Wallace 2003; Henry et al. 2017; Benson 2017) and are associated with basalt and rhyolite volcanic suites like those at McDermitt (Rytuba and McKee 1984). The basalts are mantle-derived, and the rhyolites are produced by partial melting of the lower crust (Wallace 2003 and references therein). Figure 2 illustrates some of the regional geologic features. Figure 3 illustrates a possible mechanism for the formation of the MVF.

Although the MVF is frequently cited as the location of the initial impingement of the Yellowstone hot spot, recent studies find that the area affected by Miocene volcanism is larger than the MVF and extends further to the southwest. None the less, modern studies support the theory that the McDermitt caldera is associated with Miocene YHS volcanism at the then margin of the North American craton. Using precision $^{40}Ar/^{39}Ar$ dating of 47 new samples, Benson (2017) provides an age of 16.328 ±± 0.013 for the main caldera-forming ignimbrite, the Tuff of Long Ridge. Henry et al. (2017) provide a precision $^{40}Ar/^{39}Ar$ age of 16.39 ± 0.02 (n = 3) for the same unit, which they call McDermitt Tuff, and they estimate the primary hydrothermal mineral deposits formed during the collapse or shortly thereafter, probably over an interval of not more than 600,000 years.

Mafic basalts and silicic rhyolites are the primary volcanic rock types and the McDermitt caldera is the largest of the Miocene collapse structures in the MVF. The volcanics, of unknown thickness, overly pre-Tertiary rocks that rest on Precambrian basement. The nature of the deeper rocks is not known exactly, but deformed Paleozoic and Mesozoic sediments occur throughout Humboldt County (Wilden, 1964). Triassic-Jurassic slates and phyllites, intruded by Cretaceous granitic rocks, are exposed at the Sleeper Au-Ag deposit, only about 15 miles (24 km) south of the MVF (Conrad et al., 1993). Benson et al. (2017) state: "The Paleozoic to Jurassic Black Rock terrane

basement that underlies the McDermitt volcanic field is composed of Paleozoic sedimentary rocks, early Mesozoic arc-related mafic volcanic rocks, and Late Triassic to Early Jurassic deep-marine back-arc basin sediments (Wyld and Wright 2001, and references therein). These rocks are intruded by middle Cretaceous granitic rocks (N. van Buer, 2012, personal communication), upon which most of the Miocene volcanic strata were deposited."

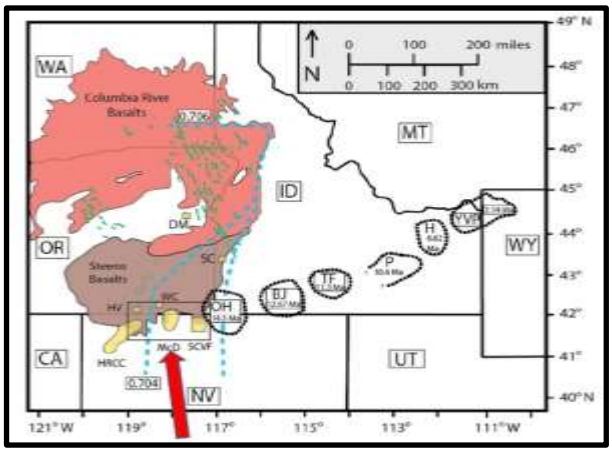

Figure 2. *McDermitt caldera location relative to regional volcanic features, modified from Starkel (2014, fig. 1). Stippled black circles are "hot-spot" eruptive centers progressively younger toward the east. Dikes of intrusive igneous rock related to the outpouring of basalts from 17.5 Ma to 16 Ma are colored green. In yellow are silicic eruptive centers coeval with the main basalt outpourings. The blue dashed lines are strontium 87 to 86 isotope ratios. A ratio less than 0.704 is interpreted as accreted oceanic crust and greater than 0.706 is interpreted to be craton rocks. Abbreviations: BJ, Bruneau – Jarbidge; DM, Dooley Mountain; H, Heise; HRCC, High Rock Caldera Complex; HV, Hawkes Valley; McD, McDermitt; OH, Owyhee – Humboldt; P, Picabo; SCVF, Santa Rosa-Calico Volcanic Field; TF, Twin Falls; WC, Whitehorse; and, YVP, Yellowstone Volcanic Plateau.*

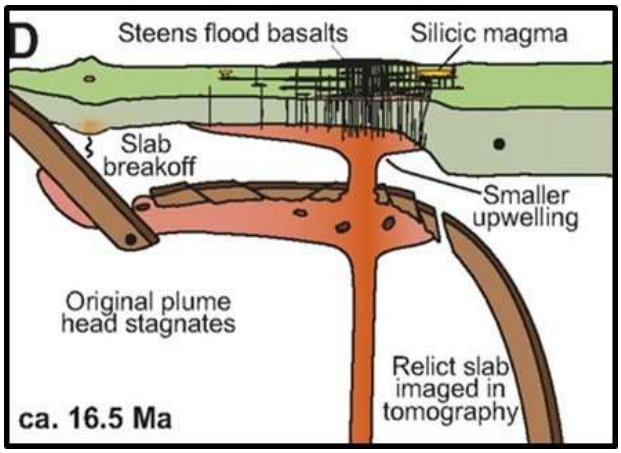

Figure 3. *From Coble and Mahood (2012, fig. 3D), illustrating a possible mechanism for the formation of the basalt flows and silicic magmatic eruptions of the region. About 25 Ma, the Juan de Fuca slab subduction stalled. The slab was uplifted by rising magma from a mantle hotspot. This caused slab thinning and melting. Breakthrough formed a second zone of magma at the base of the lithospheric crust, which was also thinning. This magma fed hundreds of basalt dikes and caused flood basalt outpourings at the surface. To the southeast, where the dikes were less numerous, a zone of mid-level crustal melting formed. The mid-level melting caused a rapid transition, in both space and time, from eruptions of voluminous basalt to eruptions of rhyolite. The slab momentum caused eastward volcanic migration over time.*

CALDERA & MINERAL DEPOSIT GEOLOGY and TIMING

Recent academic geologic theses and the work of Henry et al. (2016, 2017) provide a comprehensive review and characterization of the McDermitt caldera geology. Figure 4 is a comprehensive geologic map of the caldera from Henry et al. (2016). There is no single modern and comprehensive examination of the known mineral deposits and mining activity in the entire caldera, but Henry et al. (2016) tabulated significant known deposits (Table 1 herein). Vickre et al. (2016) provide a synthesis of published geologic and mineral resource data for a very large area of Bureau of Land Management resources, including the McDermitt caldera. Principle academic theses on the geology and ore deposits associated with the McDermitt caldera include Curry 1960; Speer 1977; Hetherington 1983; Giraud 1986; McCormack 1986, 1997; Minor 1986; Starkel 2014; and, Benson 2017. The doctorial theses of Starkel (2014) and Benson (2017) are significant contributions with respect to advancing the geologic characterization and timing of the McDermitt caldera rocks. Geologic mapping and analytical studies by geologists from government agencies, universities, and private industry illuminate the characteristics, dimensions, timing, and mineralization of the McDermitt caldera.

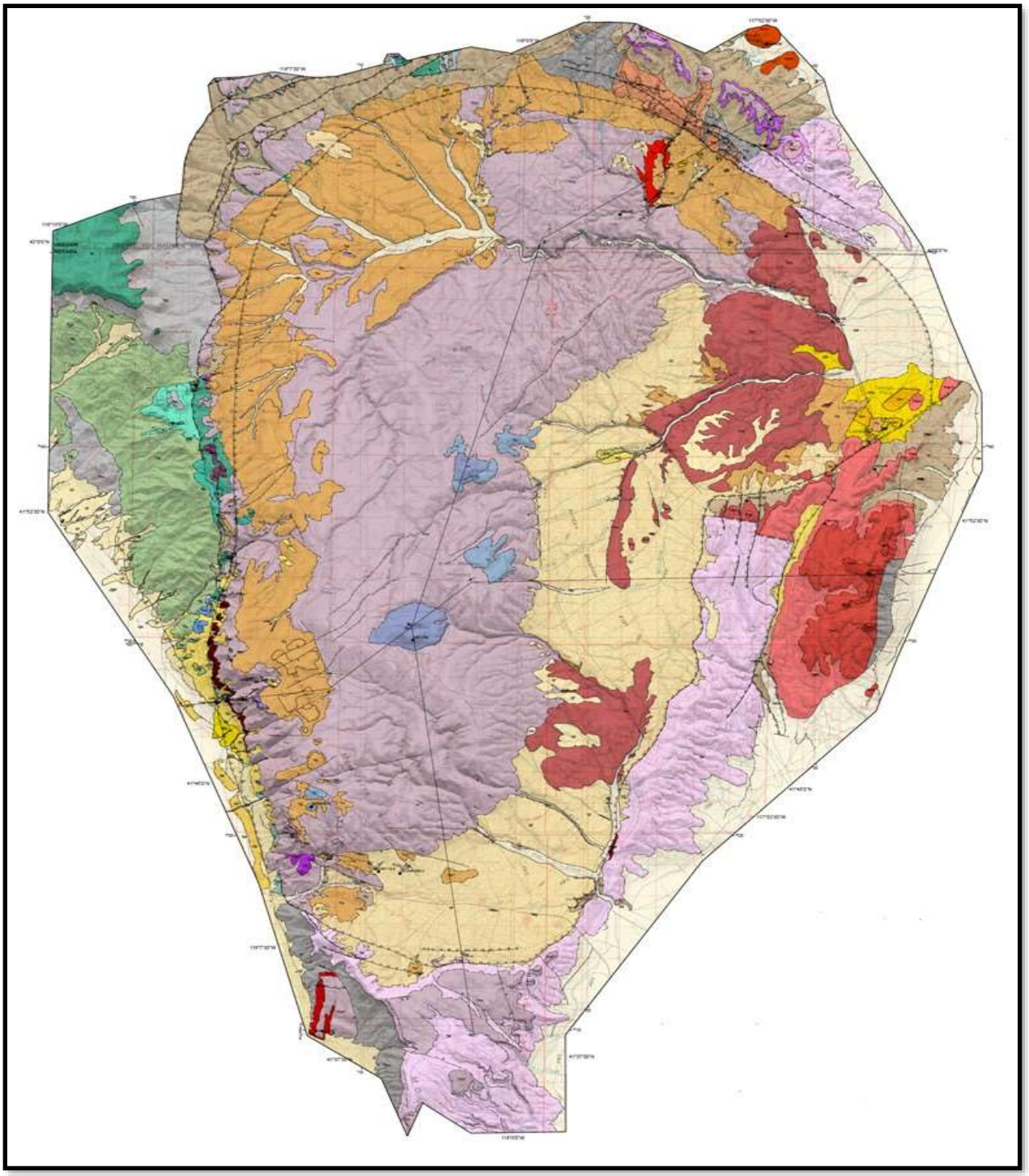

Figure 4. *Preliminary Geologic Map of the McDermitt Caldera, Humboldt County, Nevada and Harney and Malheur Counties, Oregon, by Christopher D. Henry et al. (2016) Nevada Bureau of Mines and Geology Open File Report 16-1, available from the Nevada Bureau of Mines and Geology Open File Report 16-1, available from the Nevada Bureau of Mines and Geology and website. Readers should also obtain the accompanying report, which includes a map key and geologic descriptions. Portions of the ring fractures and sediments (orange color) shown above can be discerned in aerial photographs, such as Figure 5 herein. Arcuate sedimentary deposits in the east and southeast portion of the caldera have been eroded, and alluvium (light tan to yellow colors) covers much of the eroded geology. The rocks exposed in the west half of the caldera, in addition to the arcuate sediments, is mostly McDermitt Tuff, called Tuff of Long Ridge by Benson (2017). The inverted pear or tear-drop shaped caldera measures about 25 miles (40 km) north-south by 19 miles (30 km) east-west at its widest point. The maximum vertical extent of the collapse is not known precisely but based on available reports is estimated to be not more than 0.6 miles (1 km).*

Table 1. *Mineral deposits and prospects associated with the McDermitt Caldera (After Henry et al., 2017, Table 5).*

Major component	Mine or prospect	Associated elements		Estimated *T** (°C)	Host rock§	Age and relative age	Age source	Notes	References†
		Major	Minor						
Uranium									
	Moonlight	Zr, As, Sb, F, Cu, Mo, Ag, Te, Tl	Bi, Hg, Au	330?, 340 ± 7	Tbr, Kg	16.32 ± 0.10 Ma	Adularia	Much U in hydrothermal	1, 2, 3, 4, 5
	Horse Creek	Zr, As, Sb, F, Ag, Au, Bi, Mo, Tl	Cu, Hg, Te, REE		Tb, Tpi, Tpr, Tmt	Same as Moonlight?	Host rock	U-rich zircon	1, 2, 3, 4, 5
	Big Bend Spring	Zr, As, Sb, Hg	Mo		Tmt	≤Tmt	Host rock	U-rich zircon present	1, 2, 3
	Old Man Spring	Th, Sb, As, Mo, Hg, Y	Zr, F		Tmt, basal Tis?	≤Basal Tis	Host rock	U-rich zircon present	1, 2, 3
	Aurora	As, Tl, Sb, Mo, F, Hg, Li			Tia, Tis, Tmt	~Tis	Host rock		2, 3, 4, 5, 6, 7, 8
Mercury, uranium									
	Bretz	As, Sb, Mo, F	Zr, Au, Ag	205 ± 5	Tis	<16.4 Ma, ~Tis	Host rock		1, 3, 5, 6, 7, 9
	Opalite	Sb	Zr, As, Mo	195 ± 5	Tis	~Tis	Host rock		1, 3, 5, 6, 7, 9
Mercury									
	Cordero	Au, Ag, Ga	Cu, Mo, Zn, Pb		Trau?, Tar?	≤16.4 Ma	Host rock	Ag, Au possibly deeper part of Hg system	10, 11, 12
	McDermitt	As, Sb, Se, Cu, Mo, Tl, F, Te		200 ± 5	Tis	16.67 ± 0.14; 15.7 ± 0.4 Ma	Adularia and K-Ar		4, 10, 11, 14, 15, 16
						12.6 ± 0.7 Ma	Alunite K-Ar, supergene?		13
Lithium									
	Kings Valley I	F, Rb	Mo	low	Tis	14.87 ± 0.05 Ma	On spatially associated K-feldspar	Mineral assemblage is typical of closed hydrologic system diagenesis	4, 5, 9, 17, 18
Hectorite									
	Thacker Pass				Tis	≤Tis	Host rock	In upper part of lithium deposit	19
	Bull Basin				Tis	≤Tis	Host rock		
Gallium									
	McDermitt	As, Sb, Zn			Tis	~Tis	Host rock		20
Gold				low					
	Albisu	Ag, As, Hg	Mo, Sb, Co		Tmt, Tpi	≤Tmt	Host rock		21, 22

*T—temperature estimates from Rytuba (1976) and Rytuba and Glanzman (1979) except for hectorite and lithium, which is based on young age and association with diagenetic minerals. ? indicates uncertainty (see text for details).
†References: 1—Castor et al. (1982), 2—Dayvault et al. (1985), 3—Castor and Henry (2000), 4—Rytuba (1976), 5—Rytuba and Glanzman (1979), 6—Wallace and Roper (1981), 7—Roper and Wallace (1981), 8—Myers (2005), 9—Glanzman et al. (1978), 10—Yates (192), 11—Fisk (1968), 12—Childs (2007), 13—Rytuba and McKee (1984), 14—Hetherington and Cheney (1985), 15—McCormack (1986), 16—Noble et al. (1988), 17—Western Lithium Corporation (2014), 18—Stillings and Morissette (2012), 19—Odom (1992), 20—Rytuba et al. (2003), 21—Minor et al. (1988), 22—Western Lithium Corporation, D.P. Bryan (2015, written commun.).
§For host rock symbols, see text Figures 6 and 7.

The reconnaissance geologic map of the Adel, Oregon quadrangle (Walker and Repenning 1965) suggested the existence of a caldera in the McDermitt area. Albers and Kleinhampl (1970) reported that workers in the area for several years prior to 1970 had recognized the surface geology to be underlain by a caldera-like structure. The first geologic mapping that helped to delineate a possible caldera collapse structure was provided by Greene (1972) during preliminary geologic mapping of the Jordan Meadows quadrangle for the U.S. Geological Survey. Greene subsequently teamed up with McKee and Foord (1975) to examine the evolution of the caldera and its mineral deposits. Rytuba of the U.S.G.S. became interested in the caldera and was involved in explorations for uranium soon after Greene's preliminary work.

In 1976 Rytuba published an open file report regarding the known caldera geology and ore deposits. Rytuba's on-going interest in the caldera resulted in many publications (Rytuba et al. 1978, 1979a, 1979b, 1983, 1984, 1992, 2003 and Glanzman et al. 1978, 1979). Research since 1984 has significantly refined the MVF geology, mineralogy, and stratigraphy. Rytuba has also worked behind the scenes to aid the investigations of others, particularly the work of graduate students, including Benson (2017).

Rytuba and McKee (1984) describe the McDermitt caldera as a complex of seven nested caldera structures, each producing a distinct peralkaline rhyolitic ignimbrite unit. They and others gave separate names to the collapse structures. Already mentioned above, recently both Henry et al. (2016, 2017) and Benson (2017) determine that the caldera is a single collapse structure formed from the eruption of a single unit of related ignimbrites. Henry et al. (2017) call the main collapse-related ignimbrite unit the McDermitt Tuff, a name proposed by Starkel (2014). Benson recommends changing the name to the Tuff of Long Ridge, and that is the name used here.

Starkel's work, focused on the magmatic petrogenesis of the volcanic rocks, was integrated into the comprehensive geologic work of Henry et al. (2016). Benson worked closely with Mahood and Coble, and his work contributed to several published studies and his PhD thesis (Luckett et al. 2013; Benson et al. 2013, 2014, 2015a, 2015b, 2016a, 2016b, 2017a, and 2017b; Mahood and Benson 2016, 2017; Benson 2017). The recent studies include geologic mapping, geomagnetic evaluation, geochemistry, petrology, volcanology, age dating, and stratigraphy.

Starkel (2014) and Henry et al. (2016, 2017) closely examine questions of magma formation and composition in the evolution and petrogenesis of the center. They use precision age dating and geochemistry to further define and organize the various geologic units, as do the other significant studies of the current decade. The latter group of researchers also examine broader questions of the MVF evolution and its relation to the Mid-Miocene Columbia River flood basalts, as well as specific mechanisms for the enrichment of critical elements, such as rare earths, gallium, lithium, and uranium. Henry et al. (2016, 2017) provided a summary of the major geological events for the Cenozoic volcanism of the MVF, abbreviated in Table 2 herein. Work by Benson (2017) and Coble and Mahood (2008) generally agrees with the ages and interpretations of Henry et al. (2016). Benson notes that starting about 12 Ma, high-angle normal faulting dissected the MVF with up to 1 km escarpments. Again, the recent age-dating work lead by Benson (2017) has centered on 16.328 ±± 0.013 for the age of the Tuff of Long Ridge, whereas Henry et al. provide a best estimate of the average eruption age of 16.388 ± 0.015 Ma for the intracaldera tuff.

Table 2. *Cenozoic volcanism and development of the McDermitt Caldera (after Henry et al. 2016, 2017).*

TIMELINE	MAJOR EVENTS
46.7 and 39.2 Ma	Two pulses of dacite to andesite lavas were deposited along western margin of the caldera.
≥16.69 ± 0.02 Ma	Steens Basalt lavas began to erupt from unknown sources and flowed into the northwestern area of the caldera. Eruptions were nearly continuous until the caldera formation.
16.69 ± 0.02 to 16.35 ± 0.04 Ma	Silicic magmatism began based on the range of ages on sparsely anorthoclase-phyric rhyolite lavas from the lowest exposed unit underlying icelandites north of the caldera. At 16.65 ± 0.01 Ma, an anorthoclase-phyric ash-flow tuff was emplaced along the western caldera wall.
16.62 ± 0.02 Ma	First of three pulses of biotite-quartz-sanidine-plagioclase metaluminous rhyolite emplaced as lavas and domes of the Moonlight mine western margin of the caldera.
16.56 ± 0.02 and 16.49 ± 0.03 Ma	Tuffs of Oregon Canyon and Trout Creek Mountains and widespread peralkaline ash-flow tuffs, flowed into the area from the northwest or west.
16.40 ± 0.02 Ma	Deposition of one or more sanidine-quartz ± sodic amphibole-phyric peralkaline rhyolite lavas emplaced around the western, southwestern, and southeastern margins of the caldera.

TIMELINE	MAJOR EVENTS
~16.60-16.40 Ma	Numerous aphyric rhyolites were emplaced around most of the caldera except in the western and northwestern margins.
16.38 ± 0.07 to 16.36 ± 0.02 Ma	Eruption of at least three biotite-sanidine-quartz-plagioclase rhyolite flows of Hoppin Peaks outside the eastern margin of the caldera.
16.35 ± 0.03 Ma	Eruption of the McDermitt Tuff (Tuff of Long Ridge) and formation of the McDermitt caldera. The tuff is strongly zoned from peralkaline, aphyric high-Si rhyolite to anorthoclase-rich, Fe-rich dacite and icelandite. Intense rheomorphic flow intimately intermixed these rock types in the caldera. Most of the McDermitt Tuff ponded in the caldera. Thin outflow (mostly ≤160 feet (50 m) thick) was deposited north, west, and south of the caldera.
16.34 ± 0.06 Ma	Hydrothermal activity began that generated the Moonlight U deposit and along the western margin of the caldera, and possibly other areas of widespread U mineralization.
16.4-16.1 Ma	Large area of post-collapse resurgent uplift formed in the caldera. Intra-caldera volcanism consisting of lavas with lesser dacitic to rhyolitic lavas were extruded widely in the caldera. As much as 200 m of tuffaceous lacustrine sedimentary deposits (Tis) accumulated in the caldera.
15.67 ± 0.05 Ma	Eruption of the tuff of Whitehorse Creek and formation of the Whitehorse Creek caldera (Rytuba and McKee, 1984) 13.7 miles (22 km) northwest of the McDermitt caldera.
14.90 ± 0.74 Ma	Emplacement of late basaltic lavas in the southeastern part of the caldera.
14.87 ± 0.05 Ma	Formation of K feldspar spatially and probably temporally related to Li mineralization in tuffaceous sedimentary deposits.

The caldera collapse involved the accumulation of volcanics at the surface and resurgent rhyolite magma under the collapse structure. Layered ignimbrites built up during the eruption and collapse, as well as fluvial and lacustrine sedimentary deposits, especially in shallow bogs and lakes at the base of the escarpments formed by the caldera ring fractures. Henry et al. (2016, 2017) estimate the total erupted volume of the McDermitt tuff (Tuff of Long Ridge) to be ~144 mi^3 (600 km^3) to as much as 240 mi^3 (1000 km^3), of which as least 50% and possibly as much as 85% ponded in the caldera. Benson (2017) estimates the volume as 1080 km^3.

Tuff that flowed out of the caldera reportedly crops out up to 7.5 miles (12 km) south of the southern caldera margin and up to 12.4 miles (20 km) north of the northern margin but outflow probably was never much more extensive. Excepting accumulation in local topographic lows, the outflow is reportedly no more than ~50 m thick, and outflow volume was likely <64.8 mi^3 (270 km^3) Subsequent basin and range faulting and erosion have respectively complicated and removed or covered over some parts of the caldera, but in general the feature is well preserved despite its shallow nature.

During and subsequent to the caldera collapse, it is likely hydrothermal waters circulated through the caldera fill, possibly aided by resurgent magma after the collapse and periodic episodes of waning volcanism with hydrothermal activity. It is not unreasonable to assume that later basin-and-range faulting may have caused some additional local hydrothermal alteration and/or invasion of meteoric waters and oxidation. Hydrothermal activity related to the caldera collapse likely generated the bulk of the known and probable mineral deposits in and around the caldera, especially of the strategically important minerals containing U, Ga and Hg. The work of Benson (2017) states that the lithium deposits are also related to hydrothermal activity, but to a later episode of renewed volcanism at about 14.9 Ma. The MVF is one of many volcanic centers in the northern Great Basin that host hydrothermal Au-Ag-Hg mineralization.

In the McDermitt caldera, hydrothermal fluids migrated along caldera ring fractures. These fluids initially deposited stibnite, pyrite, quartz, cinnabar, alunite and other minerals in pre-existing rocks. Secondary oxidation products formed during the later stages of the main activity. Mining has been limited to shallow rocks, mainly rhyolite ignimbrite and fluvially reworked ignimbrite, as well as tuffaceous lake-bed sediments and clays formed from diagenesis of the tuffaceous rocks. The ore-forming solutions may have included one or several of a residuum from the silicic magma, connate water, and ground water heated by magma in the resurgent central domes of the calderas (McKee 1976). The figures below provide the locations of significant mineral deposits within the caldera.

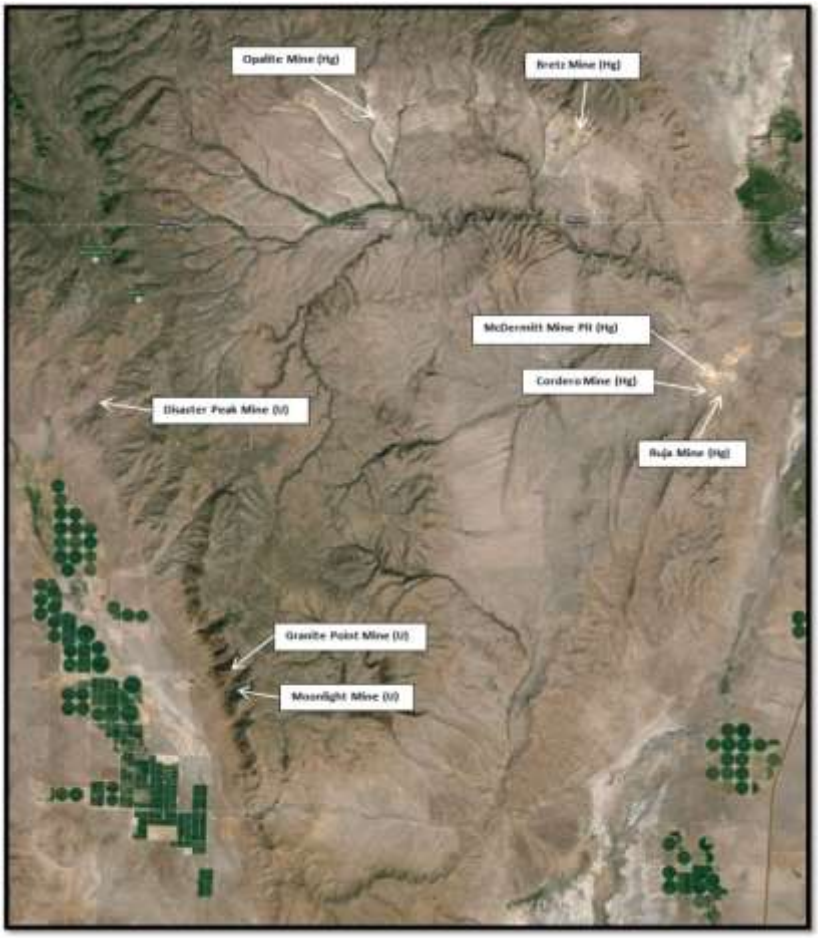

Figure 5. *GoogleEarth™ satellite view of the McDermitt Caldera Complex area showing the location of the mercury and uranium mines. The green geometric zones represent areas of reclaimed desert where alfalfa is grown.*

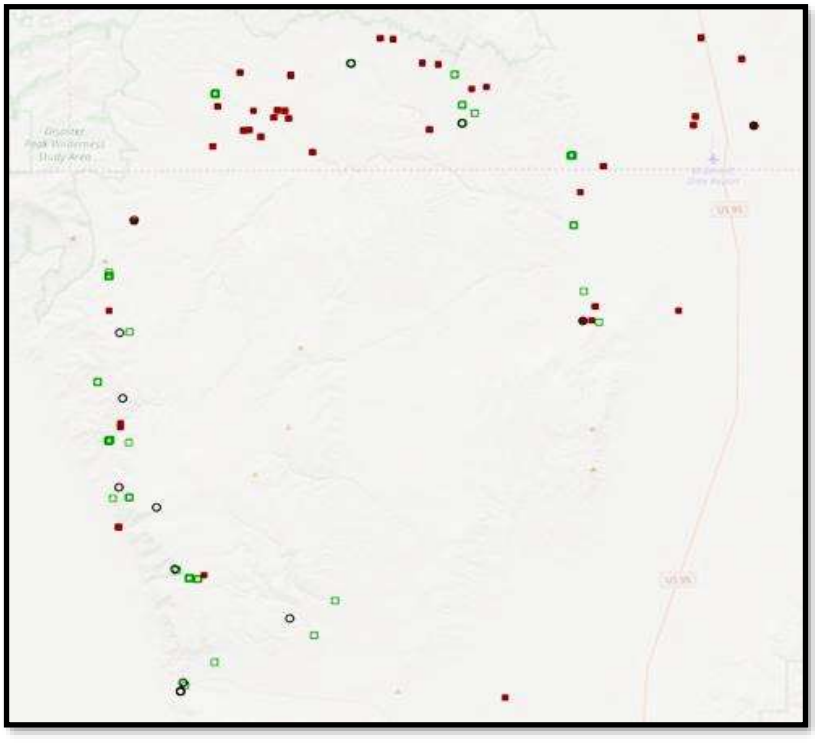

Figure 6. *Vicinity of the McDermitt caldera showing principle mineral occurrences and mines from the U.S. Geological Survey Mineral Resource DatSystem (MRDS) web-based viewer. There is no scale provided. The solid red squares are a mine or location with some past production. The open green squares are prospects or occurrences with no recorded production.*

The primary commodities for the caldera are mercury to the north and east, and hectorite clay to the west and southwest. Lapidary material is found principally to the north, primarily petrified wood in ancient lake deposits, jasper comprised of thoroughly silicified volcaniclastic sediments, and less common agate and lithophysae (thundereggs) in rhyolite tuff and lava.

Gold is a minor commodity, with just a few prospects to the west. Trace elements of interest, but unmined, and primarily near or associated with the mercury deposits along caldera ring fractures, are gallium, silver, and uranium.

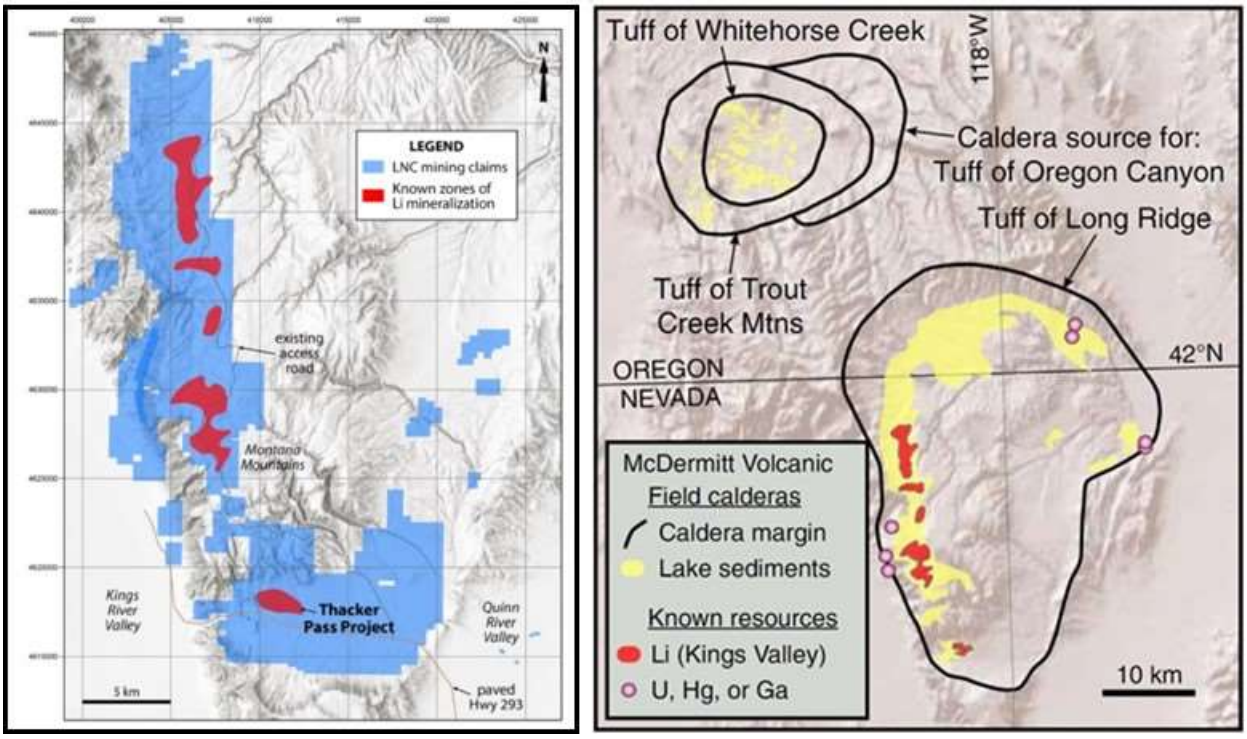

Figure 7 a & b. *Left: location Map of the McDermitt Caldera, Thacker Pass Project, and Other Known Lithium Mineralized Zones, Figure 4-1, Fourie and Peldiak (2018). This figure is from feasibility studies for the southernmost Li project, called Thacker Pass. The lithium deposits are associated with clays formed from the diagenesis of volcaniclastic lake sediments. Right: location of the Kings Valley lithium deposits, said to be the largest reserve of lithium in the continental United States. Also shown are the location of the volcaniclastic caldera fill sediments and mercury, gallium, and uranium resources (Benson et al. 2017, Figure 2b).*

Economic to sub-economic trace elements of interest in and around the McDermitt caldera include Ag, Au, Ga, Hg, Li, Zr-rich U, and Sb. Many other elements occur in somewhat elevated concentrations compared to background. Only mercury has been mined to a significant degree. Interest in the other elements remains largely speculative, but, as mentioned above, plans are in progress to develop lithium mines along the southwest caldera margin. Trace elements are concentrated along ring fractures and in volcaniclastic sedimentary rocks around the margins of the caldera, and, at least in the case of the McDermitt mercury mine, possibly in zones where hydrothermal fluids encountered meteoric water mixing or buffering (McCormack, 1986).

For the contemporaneous Mule Canyon epithermal Au-Ag deposit, about 110 miles (170 km) southeast of McDermitt, John et al. (2003b) deduced from isotopic data that the water was predominantly meteoric, but with precious metals leached from underlying Paleozoic sediments and sulfur derived from both those sediments and degassing Miocene basalts and andesites. The mineralization is broadly typical of a classical hot spring deposit, however, at McDermitt, Hetherington and Cheney (1985) argue that the hydrothermal alteration minerals correspond to depths below the original water table rather than to the paleosurface.

Mercury is unusually abundant in the host rocks of the caldera complex. From published reports, the Hg content is about 0.25-0.65 ppm in the ash-flow tuffs, 1 ppm in the rhyolites, and 0.5 ppm in volcaniclastic sediments (tuffaceous sandstone). These concentrations are one to two orders of magnitude greater than typical for rhyolite and might be very efficiently leached by hydrothermal fluids at 200°C (Rytuba and Glanzman 1979).

The radioactive prospects and deposits are enriched in a suite of elements typical of epithermal deposits, including As, Bi, Mo, Te, Tl and Hg. Significant anomalies are also found for Li, Th and Zr-rich U, from the highly differentiated rhyolitic magmas. Uraninite, coffinite, botryoidal pyrite, marcasite, arsenopyrite, cinnabar, and fluorite were the primary minerals deposited (Castor and Henry, 2000). Uranium at the Aurora prospect is hosted at depth in the iron-rich andesites of the "Aurora series" (Roper and Wallace 1981; Wallace and Roper 1981). This volcanic unit has been dated at 15.3 ± 0.4 Ma (Noble et al. 1988).

Lithium also reaches economic concentrations in the moat-filling lacustrine sediments of the caldera complex. Rytuba and Glanzman (1979) note Li concentrations up to 0.68%, occurring as hectorite and possibly other,

unidentified Li-bearing minerals. The extensive areas of high Li concentration in the western parts of the Long Ridge, Jordan Meadow and Calavera calderas represent a major economic reserve (Rytuba and Glanzman 1979). Figure 8 (Benson 2017) is schematic model for the formation of the caldera Li deposits, but is broadly applicable to the other economic mineral deposits as well.

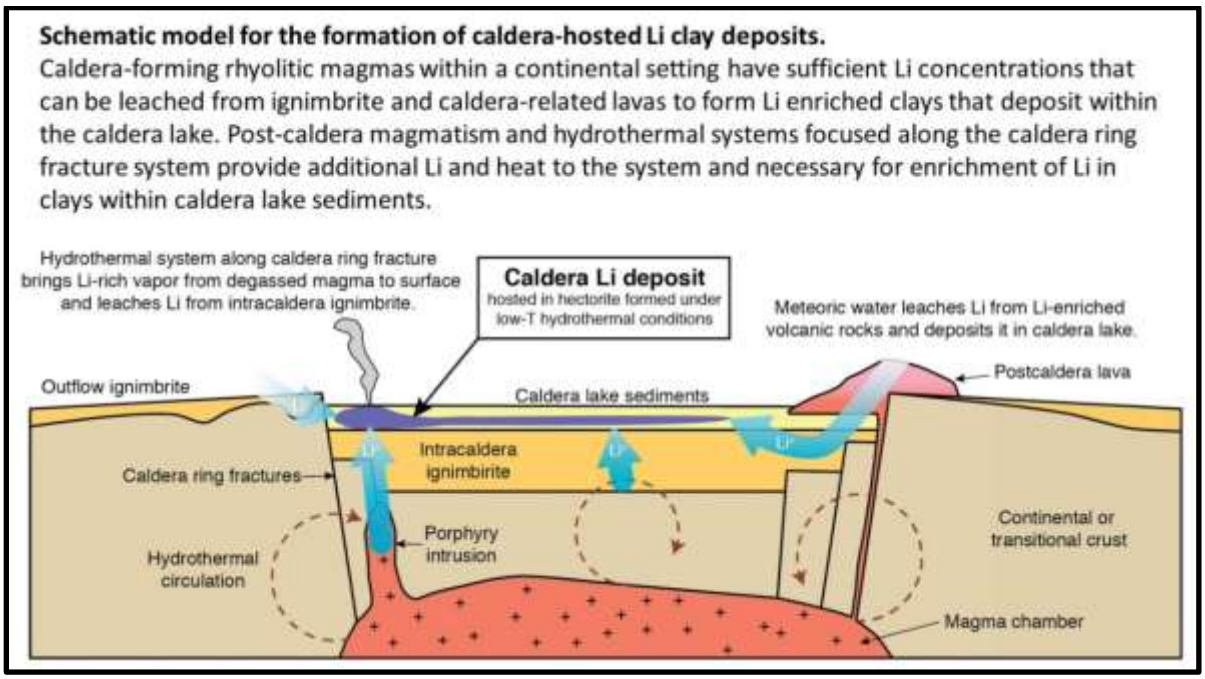

Figure 8. *This model, Figure 3.5 from Benson (2017), can be used to explain the uranium, mercury, and gallium deposits inside the caldera. It is important to note that the east side of the caldera (right side of the figure) has been eroded down, exposing rocks with hydrothermal alteration that formed perhaps ≥650 feet (200 meters) or so below the surface. The McDermitt open pit mercury mine is in tuffaceous sediments and interlayered tuff that were invaded by fluids that probably migrated up a ring fracture and into the tuffaceous sediments of the upper caldera fill. The Cordero mine orebody corresponds to hydrothermal alteration associated with resurgent volcanism adjacent to a ring fracture, such as on the left side of the figure, with most of the orebody hosted in a nearly vertical rhyolite breccia "pipe" and some of the shallow ore body hosted in tuff and tuffaceous sediment.*

In summary, with respect to the formation of the volcanic deposits and the caldera, Starkel (2014) states that the "onset of silicic volcanism at McDermitt began at 16.69 ± 0.03 Ma with effusive eruptions that were prevalent through the duration of activity at McDermitt; silicic magmatism climaxed with the caldera-forming eruption of the McDermitt Tuff (MDT) at 16.35 ± 0.03 Ma. The geochemistry of the McDermitt rhyolites is quite variable, a direct result of the myriad magma evolutionary mechanisms invoked in our petrogenetic models. The primary evolutionary track, comprised of most of the McDermitt Tuff samples and the Calavera Canyon (CC) rhyolites, is best modeled by evolution of McDermitt intermediate magmas by AFC (assimilation–fractional crystallization) processes with crystal fractionation being the most dominant mechanism. The compositional variation of the MDT/CC samples is the result interactions recharge magmas and remobilized cumulates at the base of the MDT/CC magma chamber."

Benson (2017) summarizes that "new mapping and geochronology at the McDermitt Volcanic Field delineates three regionally extensive peralkaline ignimbrites and one smaller metaluminous ignimbrite associated with flood basalt volcanism. Peralkaline volcanism continued in the southeast part of the field on eruption of the 16.328 ± 0.013 Ma Tuff of Long Ridge (~1000 km^3), resulting in the collapse of the McDermitt Caldera. After a ~770 ky hiatus, silicic volcanism renewed on eruption of the ~110 km^3 metaluminous Tuff of Whitehorse Creek and collapse of the ~13 x 12 km Whitehorse Caldera nested within the Pole Canyon Caldera. Volcanic activity in McDermitt Volcanic Field ended at 15.37 Ma on eruption of hornblende- and zircon-bearing rhyolite lavas along the western ring fracture of the Whitehorse Caldera."

Benson (2017) also states that "ignimbrites within this trend of volcanism young southeastward between 16.5 and 15.7 Ma, reflecting a basaltic dike swarm emanating from Steens Mountain and propagating at a rate of ~12

cm/a. Contemporaneously, 16.5 to 15.7 Ma caldera volcanism fueled by flood basalt in the High Rock Caldera Complex and Hawks Valley – Lone Mountain center propagated southwest from Steens Mountain at a similar rate of ~14 cm/a. Collectively, these two synchronous swarms and the north- to northwest-propagating Chief Joseph and Monument dike swarms make clear that Columbia River flood basalts and related volcanism form a giant radiating dike swarm centered in the vicinity of Steens Mountain. This pattern of volcanism is consistent with a model in which a Yellowstone plume head impinged on lithosphere, generating radiating dike swarms that rapidly spread laterally, leading to voluminous effusions of flood basalt, or, where the crust was more felsic, fueling the formation of subordinate volumes of rhyolitic magmas."

Henry et al. (2017), provide the following summary. "The McDermitt caldera formed ca. 16.39 Ma in an area that had undergone abundant prior igneous activity, the most important being major middle Miocene volcanism that led continuously to caldera formation, as well as two preceding episodes of Eocene intermediate volcanism at 47 and 39 Ma." Additionally, "although not the oldest caldera of the Yellowstone hotspot, the McDermitt area has the oldest documented rhyolitic activity. The resultant caldera is ~40 × 30–22 km in area, and total collapse was no more than ~1 km. Total erupted volume was ~1000 km^3, 50%–85% of which accumulated within the caldera. Continuity of intracaldera tuff, the caldera ring-fracture system, and intracaldera sedimentary deposits demonstrate a single caldera. . . .

The caldera underwent post-collapse resurgence and several episodes of dominantly icelanditic magmatism until ca. 16.1 Ma, when almost all magmatism ceased. Late high-alumina olivine tholeiite lavas erupted ca. 14.9 Ma but are probably unrelated to the caldera system. Understanding the petrogenesis of the caldera magmatic system as well as the diverse pre-caldera and post-caldera rocks will require extensive geochemistry, mineralogic characterization, and isotopic analyses."

Henry et al. (2017) also states that "the McDermitt caldera and other ca. 16 Ma and older rhyolite centers extend over a large area in northern Nevada and southeastern Oregon. Their wide distribution is consistent with initiation of the Yellowstone hotspot over an equally wide area. Curiously, however, these rhyolite-dominated centers only partly overlap with, and partly are south of, the immediately preceding to contemporaneous Steens Basalt lavas. Full delineation of the Steens Basalt in the subsurface in northern Nevada and of ca. 16 Ma and older rhyolite centers is needed. . . .

Hydrothermal waters circulating along collapse fractures and possibly some pre-existing faults resulted in local enrichment of a variety of trace elements, but only mercury has been exploited to any significant degree, although it appears that lithium is likely to be mined in the near future. Uranium and gallium resources have also been delineated and appear promising. . . .The McDermitt caldera is highly mineralized, with significant deposits of Hg, U, Zr, and Li as well as lesser accumulations of Au, Ga, and Mo. Most, possibly all, mineralization is related to the caldera magmatic and structural system, although considerably more work is needed to fully understand how the deposits relate to that system."

TRACE ELEMENT, GEOCHEMISTRY AND AGES

Again, economic trace elements of interest in and around the McDermitt caldera include Ag, Au, Ga, Hg, Li, Mo, U, Sb, and Zr. Only Hg has been mined to a significant degree. Interest in the other elements remains largely speculative. Elevated trace elements are likely related to caldera formation and development. Trace elements concentrated along ring fractures and in volcaniclastic sedimentary rocks around the margins of the caldera, and, at least in the case of the McDermitt mercury mine, possibly in zones of meteoric water mixing or buffering (McCormack 1986).

The duration of hydrothermal activity and mineralization before and after the caldera collapse is not known precisely, but age dating of minerals suggests activity both during and within a few million years of the collapse. One reason for the uncertainty is the overlapping activity before, during, and after the main intervals of volcanism, as well as activity possibly related to basin and range crustal extension. According to Henry et al., (2017), adularia in U-Zr±Mo±Au±Ag deposits in the western part of the caldera, dated at 16.34 ± 0.06 Ma, are indistinguishable from the age of the Tuff of Long Ridge (McDermitt Tuff), but younger based on field relations. Henry et al. (2017) believe that geochemically different uranium enrichment in the north part of the caldera may have taken place at about the same time, and the lithium deposits in the tuffaceous intracaldera sediments probably formed at 14.87 ± 0.05 Ma based on the age of spatially related K-feldspar.

With respect to the mercury deposits in the north and northeast part of the caldera, mined for many years, Henry et al. (2017) believe they were deposited at 15.7 ± 0.4 Ma based on K-Ar age dating of adularia associated

with cinnabar from the McDermitt mine (Noble et al. 1988). Noble et al. (2018) also obtained an age of 12.4 ± 0.7 Ma on vein alunite from the Cordero mine. They suggest, as does Rytuba and Conrad (1981), that hydrothermal activity may have resumed or even continued along the southeastern margin of the caldera for several million years after collapse.

For the contemporaneous Mule Canyon epithermal Au-Ag deposit, about 110 miles (170 km) southeast of McDermitt, John et al. (2003b) deduced from isotopic data that the water was predominantly meteoric, but with precious metals leached from underlying Paleozoic sediments and sulfur derived from both those sediments and degassing Miocene basalts and andesites. The mineralization is broadly typical of a classical hot spring deposit, however, at McDermitt the hydrothermal alteration minerals correspond to depths below the original water table rather than to the paleosurface (Hetherington and Cheney 1985).

Mercury is unusually abundant in the host rocks of the caldera complex. The Hg content is 0.25-0.65 ppm in the ash-flow tuffs, 1 ppm in the rhyolites, and 0.5 ppm in volcaniclastic sediments (tuffaceous sandstone). These concentrations are one to two orders of magnitude greater than typical for rhyolite, and very efficiently leached by hydrothermal fluids at 200°C (Rytuba and Glanzman 1979).

The radioactive prospects and deposits are enriched in a suite of elements typical of epithermal deposits, including As, Bi, Mo, Te, Tl and Hg. Significant anomalies are also found for Li, Th and U, from the highly differentiated rhyolitic magmas. Uraninite, coffinite, botryoidal pyrite, marcasite, arsenopyrite, cinnabar, and fluorite were the primary minerals deposited (Castor and Henry 2000). Uranium at the Aurora prospect is hosted at depth in the iron-rich andesites of the "Aurora series" (Roper and Wallace 1981; Wallace and Roper 1981). This volcanic unit has been dated at 15.3 ± 0.4 Ma (Noble et al. 1988).

Lithium also reaches economic concentrations in the moat-filling lacustrine sediments of the caldera complex. Rytuba and Glanzman (1979) note Li concentrations up to 0.68%, occurring as hectorite and possibly other, unidentified Li-bearing minerals. The extensive areas of high Li concentration in the western parts of the Long Ridge, Jordan Meadow and Calavera calderas represent a major economic reserve (Rytuba and Glanzman 1979).

MINING HISTORY

AREA MINES

Area mines are predominantly along the margin of the caldera, located in zones of mineralization which contain significant quantities of either mercury or uranium. To the north, across the Oregon border in Malheur County, lie the Bretz and Opalite mines. These mines gave rise to the Opalite mining district name. Both are mercury-rich deposits situated in low rolling hills underlain by opalite and extrusive tuffaceous rhyolite and related rocks. The Aurora prospect, also in this area, contains significant amounts of uranium and gold. To the southwest of these mines, in Humboldt County, Nevada, are several uranium mines localized in rhyolite domes, including the Disaster Peak, Moonlight and Granite Point. Broadly, these mines exploit rocks that host small amounts of cinnabar, uraninite, coffinite and secondary uranium minerals. To the east are the majority of mines hosting rich deposits of mercury, including the Cordero, McDermitt, Crofoot, Lenway, and Ruja. The older Cordero mine explored mercury mineralization underground, with a series of shafts and adits in the rhyolite and lake sediments. In addition, there are a series of shafts in the same general area that are both named and unnamed. These include the Lenway shaft (mine), Blackey's shaft, Corderito shaft, Bradley shaft, Brown shaft, and the 614 shaft.

The first mineral exploitation in the caldera, at the beginning of the 20th Century, was for mercury. Schuette (1938) examined and reported on mercury mines in the Oregon portion of the Opalite mining district. Yates (1941) examined and reported on the district mercury mines in both Oregon and Nevada. According to Yates (1942), mercury was first discovered in the region by William Bretz in 1917, in the vicinity of the Bretz mercury mine. Bretz reportedly also found the nearby Opalite deposit in 1924, the same year that Tomas Alcorta discovered the Cordero deposit to the south. By the end of 1926, a furnace plant had been installed at the Opalite mine and was processing ore from the district mines. The operations were consolidated under the Bradley Mining Company, which operated intermittently. Yates (1942) states that the Bretz and Opalite mine ores appeared to be exhausted by April 1941.

Bailey and Phoenix (1944) reported on the Nevada portion of the Opalite district, providing new details for the Cordero mine. Unlike the shallow Bretz and Opalite mines, the Cordero proved to have an extensive fault-controlled vertical orebody and was able to sustain significant production. Largely on account of the success of the Cordero mine, several renewed but short-lived mining efforts were attempted at the Bretz and Opalite mines, but

none were significant and most resulted in no additional production. By 1949, the district mines were inactive, as reported in the "Reno Gazette Journal," "Nevada State Journal," newsletter of the Western Mining Association, and the "Ore Bin," published by the state of Oregon, Department of Geology and Mineral Industries.

Brooks (1957, 1959, 1963), Wilden (1964), and Holmes (1965) report depressed market conditions from 1945 until 1950, when prices began to gradually recover and encouraged several mines to reopen. In the 1960s, mercury demand and its price were rising significantly, primarily for chlor-alkali production. The late-1950s through the 1960s saw significant activity in the district, and the Cordero mine reached its peak development during this period,

In the 1960s, interest was growing in mercury as an indicator for shallow hydrothermal precious metal ore deposits, especially gold, and the operators of the Cordero mine carried out extensive shallow exploratory drilling in the vicinity of the district mercury deposits. It was this step-out exploration that eventually lead to the discovery of the McDermitt mine orebody in the late-1960s. Based on press articles in the "Ore Bin" and various lapidary and rock hounding journals and newsletters, the caldera was also a popular rock hounding location, due to discoveries of agatized (silicified) tuffaceous rocks and deposits of petrified wood. During this decade, Curry (1960) wrote the first MSc thesis for the area, focusing on the Cordero mine area, and Fisk (1961, 1968) provided exacting details concerning the Cordero mine and its operations.

Brooks (1959, 1963, 1971) updated Schutette's 1938 Oregon work, and produced a comprehensive map showing the location of quicksilver deposits in the state. Wilden (1964) examined mineral deposits in Humboldt County, Nevada. Although the Bretz and Opalite mines once again proved only capable of supporting intermittent production, the Cordero deposit generally sustained production until a rapid decline in the market price for mercury brought about the closure of the mine in 1970. By then, step-out exploration had discovered the adjacent McDermitt mercury mine and the mine was quickly developed and commenced production in 1974. Sisselman (1975) provides a summary of the mine discovery and development, as well as technical details concerning it early operation.

The McDermitt deposit increased interest in the unusual mercury minerals found in the Opalite district mercury deposits, thought to be mercury oxy-chlorides. Geologic mapping and mining-related exploration also increased and converged on the realization that the area deposits were related to a Miocene volcanic caldera and its extensive collapse-fracture system. The mapping and exploration work delineated unmined reserves of gallium, gold, lithium, silver, and uranium. Because of the McDermitt mine, the 1970s and 1980s were halcyon years for the Opalite mining district and mineral exploration in the caldera. During the boom years, numerous scientific papers and theses were published, as well as significant private studies and reports. 1990 ushered in the inevitable closure of the McDermitt mine, although stockpiled mercury was sold in 1991 and 1992. Work on the volcanic origins of the caldera continued, as did work on the unusual mercury oxychloride minerals. The mineral characterization culminated in McCormack's PhD thesis (1997), in which it was demonstrated the unusual mercury oxy-chlorides are sulf-halide minerals. In this paper, later, it will be shown that the best classification is as mercury nitrides.

The global consumer electronics explosion in the 1990s lead to additional interest in the caldera lithium, gallium, gold, and silver resources. Exploration for these has occurred intermittently. Today, the lithium-bearing clay deposits along the western side of the caldera are undergoing mining feasibility studies. Refer to the references herein for reports and information available to the general public. The archives of the University of Nevada, Reno, are also a significant source for historical information, and the files of the Security and Exchange Commission provide details for exploration and mining carried out by companies soliciting public investment. The MinDat (www.mindat.org) web pages for the Cordero mine complex and opalite district are useful resources for mineralogy, geology, location, and some history. The historical information for the individual mercury mines below is taken from the published reports of Schuette 1938; Yates 1941; Bailey and Phoenix 1944; Fisk 1961, 1968; Wilden 1964; Storey 1985; Placer Amex circa-1980.

Mentioned earlier, Vikre et al. (2016) published a comprehensive review of mineral resources for the area based on available reports. The production history provided is not complete with respect to many of the mines because of gaps in the published records. The inventory of resources is very thorough, because it includes records held by the Bureau of Land Management in connection with mining claims and mining exploration and extraction authorizations. The authors confirm that five mines in the district (Cordero, McDermitt, Bretz, Opalite, and Ruja) produced about 408,000 76-lb (34.5 kg) flasks of mercury (Yates, 1942; Bailey and Phoenix, 1944; Rytuba, 1976), and one uranium deposit was mined with recorded production of about 1,320 lbs. (600 kg) of uranium ore (Castor and Henry 2000; table 14; fig. 22).

Vikre et al. (2016) state: “At the Cordero (McDermitt) Mine a mercury resource (1,070,000 short tons at 7.25 pounds [lbs] of mercury per ton) overlies a drill-identified gallium resource (21,562,700 million metric tons at 46.5 ppm [parts per million] gallium). . . .Three uranium resources have been defined by drilling. The Kings Valley South and Kings Valley North resources (2,499,000 short tons at 0.076 weight percent U3O8), Aurora resource (76,390,000 short tons at 248 ppm U3O8), and Moonlight Mine resource (479,000 short tons at 0.108 percent U3O8), are active exploration projects (table 14). . . . The mercury and gallium resources at the Cordero (McDermitt) Mine are outside the proposed withdrawal area and are inside the USGS study area boundary. The Kings Valley South and Kings Valley North uranium resources are outside the proposed withdrawal area. . . .Several plans of operations and notices of mineral exploration for lithium, clays, and gemstones have been authorized, are pending, or are active, indicating recent and active mineral exploration in the study area (fig. 20; tables 12, 13). . . .Within the study area, a lithium resource of 823 million short tons at 0.30 percent lithium (Kings Valley Lithium; table 14) comprises five deposits that have been defined by drilling. The Stage I deposit, 374,443,027 short tons at 0.292 percent lithium occurs outside the proposed withdrawal area and within the USGS study area boundary. The Stage II, Stage III, Stage IV, and Stage V deposits have a combined resource of 449,528,206 short tons at 0.304 percent lithium (Fernette and others, 2016a).”

MERCURY MINES

Cordero mine

First discovered and claimed in 1929 (Fisk 1961), the Cordero cinnabar deposit lies 11 miles (18 km) southwest of McDermitt, Humboldt County, Nevada, near the Nevada-Oregon boundary. The Cordero mine is located about 13 miles (21 km) southwest of McDermitt, on the north end of a low range of hills which lie on the east side of the Quinn River Valley in Sec. 33, R37E, T42N. The original locators did only scattered surface exploration, but in 1935 the property was leased by the Bradley Mining Company, who sank a 50-foot (15 meter) shaft and drove several hundred feet (many tens of meters) of underground workings. However, only 45 flasks of mercury were recovered from several pockets of rich ore in the workings. They soon gave up their lease (U. S. Bureau of Mines Staff 1965).

The name “Cordero” means “little lamb” in the Castilian Spanish language and symbolizes the fact that the first mercury ore specimen was found during the lambing season. The Bradley Mining Company held the property for several years during the early 1930s, but the property remained idle until 1940, when it was leased by the Cordero Mining Company, a subsidiary of Sun Oil Company. The company, then known as Horse Heaven Mines, Inc., conducted preliminary work in 1940 which proved enough near-surface ore to warrant the construction of a mill during the following year. The company installed a 14-foot (4.3 meter) 12-hearth Herreshoff furnace in 1941 and became the largest mercury producer in Nevada between 1941 and 1943. By 1943, the Cordero ore was being rapidly depleted. Nevertheless, deeper churn drilling intersected a large underground orebody that was still being mined in 1968 (Fisk 1968). In 1970 the mine was permanently closed after a fire in the deeper underground levels.

The mine workings consist of six open pits and about 3000 feet (1000 m) of underground workings accessed by an inclined shaft. Most of the ore bodies were first found by surface drilling, then explored by underground workings, and finally mined by open-pit methods. Cinnabar was the only commercially important ore mineral, but liquid mercury and oxychlorides are locally abundant. For the most part, the cinnabar occurs as disseminated crystals and masses in altered volcanic rocks or in “opalite” (silicified tuff and fault rocks: Hetherington and Cheney (1985)), but a small amount is found as veinlets or solid masses. The associated minerals are quartz, chalcedony, opal, pyrite, hematite and other iron oxides, jarosite, alunite, and clays. Fluorite and heulandite have been found in some of the more altered rocks (Bailey and Phoenix 1944).

The following pages provide selected photographs, a vicinity map, and examples of records from the Cordero mine.

Figure 9. *View of the Cordero mine Brown shaft head frame and buildings.*

Figure 10. *Map showing the proximity of the Cordero and McDermitt mines with dumps and tailing ponds. (after Rytuba and Glanzman 1979).*

Figure 11. *Looking roughly north from the Brown shaft of the Cordero mine and burnt ore calcines pile in the middle distance. The southwest corner of the McDermitt mine pit is just to the right of the calcines pile.*

Figure 12. *G-Pit of the Cordero mine looking SW. Note underground exposed tunnels at arrows. Brown shaft headframe is visible in the background (see Figure 9). Footwall rhyolite of Fisk (1968) to left and opalite after tuffaceous sediment to right. The pit is centered on a caldera ring fracture called the M-fault.*

Figure 13, left. *Stacks of Silver Predator corporation drilling core samples at the old Cordero mine building (after Blumenfeld 2014).*

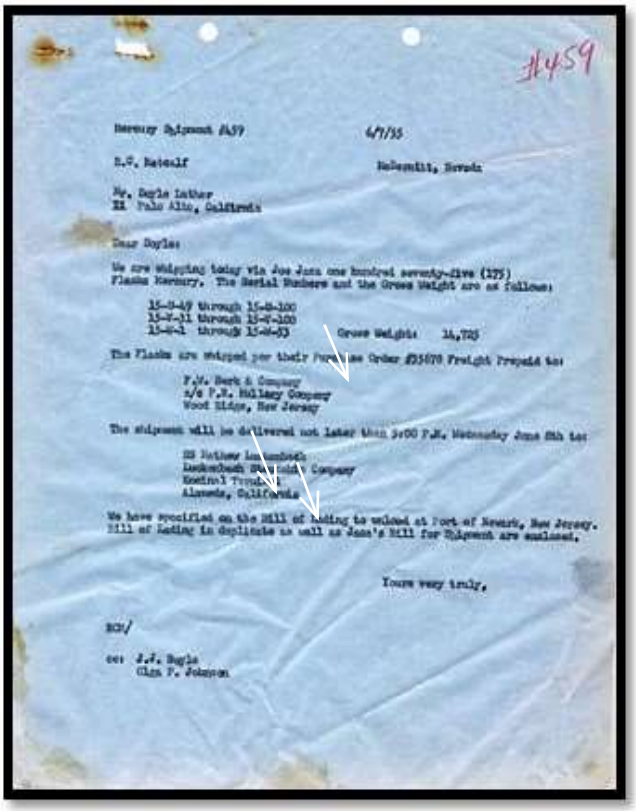

Mercury Shipment #459 4/7/55

R.G. Metcalf McDermitt, Nevada

Mr. Doyle Luther
Palo Alto, California

Dear Doyle:

We are shipping today via Joe Jans one hundred seventy-five (175) Flasks Mercury. The Serial Numbers and the Gross Weight are as follows:

15-M-49 through 15-M-100
15-M-11 through 15-M-100
15-M-1 through 15-M-53 Gross Weight 14,725

The Flasks are shipped per their Purchase Order #35078 Freight Prepaid to:

F.W. Berk & Company
c/o P.E. Hallery Company
Wood Ridge, New Jersey

The shipment will be delivered not later than 3:00 P.M. Wednesday June 8th to:

SS Nathaw Luckenbach
Luckenbach Steamship Company
Central Terminal
Alameda, California

We have specified on the Bill of Lading to unload at Port of Newark, New Jersey. Bill of Lading in duplicate as well as Jans's Bill for Shipment are enclosed.

Yours very truly,

RCH/

cc: J.J. Bugle
Olga P. Johnson

Figure 14. *1955 letter listing the shipment of 175 flasks of mercury to F.W. Berk & Co. via Alameda, CA.*

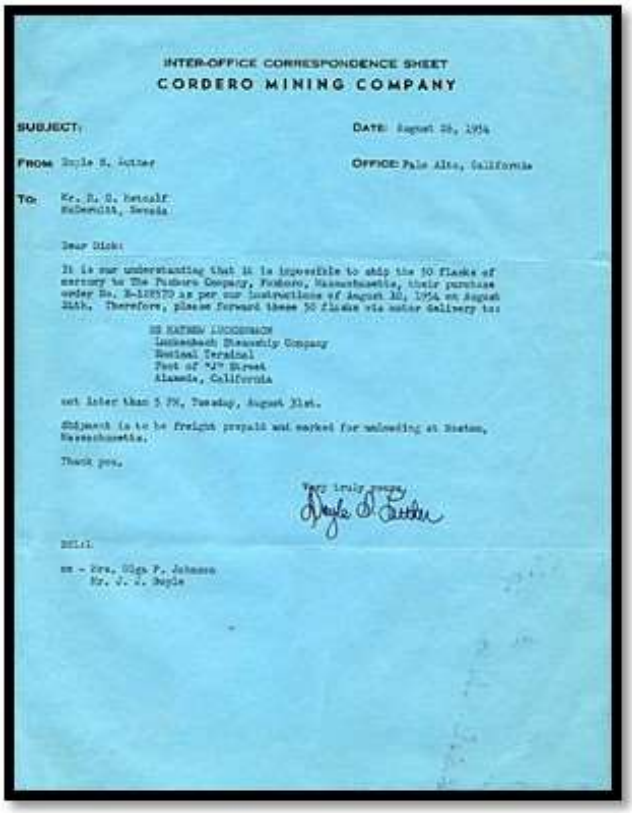

INTER-OFFICE CORRESPONDENCE SHEET
CORDERO MINING COMPANY

SUBJECT: DATE: August 26, 1954

FROM: Doyle H. Luther OFFICE: Palo Alto, California

TO: Mr. R. G. Metcalf
McDermitt, Nevada

Dear Dick:

It is our understanding that it is impossible to ship the 50 flasks of mercury to The Foxboro Company, Foxboro, Massachusetts, their purchase order No. B-128570 as per our instructions of August 20, 1954 on August 24th. Therefore, please forward these 50 flasks via motor delivery to:

SS NATHAW LUCKENBACH
Luckenbach Steamship Company
Central Terminal
Foot of "J" Street
Alameda, California

not later than 5 PM, Tuesday, August 31st.

Shipment is to be freight prepaid and marked for unloading at Boston, Massachusetts.

Thank you.

Very truly yours,
Doyle H. Luther

DHL:ll

cc - Mrs. Olga P. Johnson
Mr. J. J. Bugle

Figure 15. *1954 letter changing 50 flask mercury shipment from Foxboro, Mass. to a receiving port in Alameda, CA.*

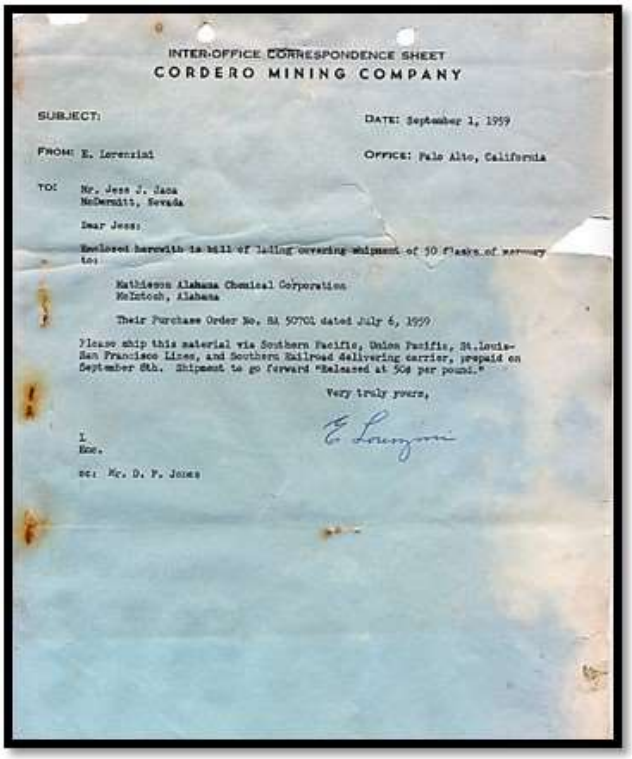

INTER-OFFICE CORRESPONDENCE SHEET
CORDERO MINING COMPANY

SUBJECT: DATE: September 1, 1959

FROM: E. Lorenzini OFFICE: Palo Alto, California

TO: Mr. Jess J. Jans
McDermitt, Nevada

Dear Jess:

Enclosed herewith is bill of lading covering shipment of 50 flasks of mercury to:

Mathieson Alabama Chemical Corporation
McIntosh, Alabama

Their Purchase Order No. BA 50701 dated July 6, 1959

Please ship this material via Southern Pacific, Union Pacific, St.Louis-San Francisco Lines, and Southern Railroad delivering carrier, prepaid on September 8th. Shipment to go forward "Released at 50¢ per pound."

Very truly yours,

E. Lorenzini

1
Enc.

cc: Mr. D. F. Jones

Figure 16. *1959 Bill of Lading covering shipment of 50 flasks of mercury to the Mathison Alabama Chemical Corporation, McIntosh, AL to McDermitt, NV.*

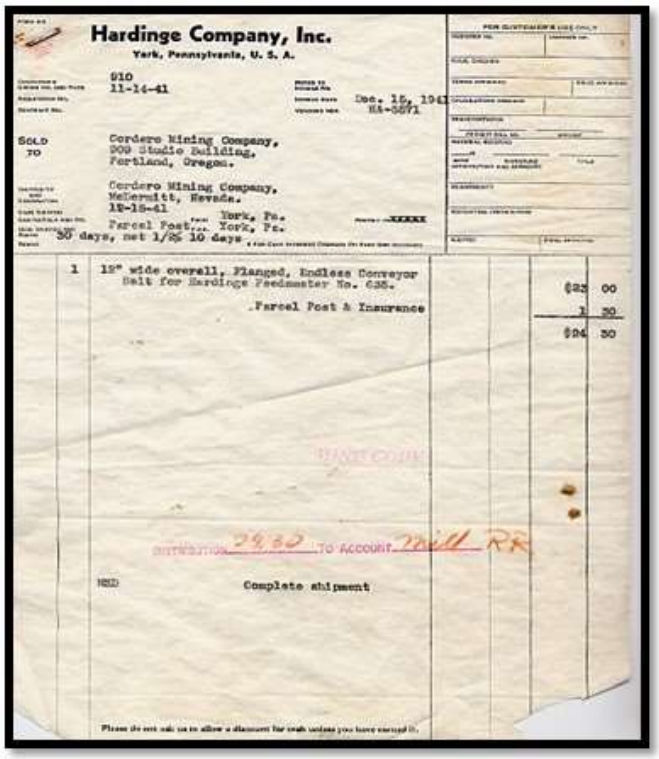

Hardinge Company, Inc.
York, Pennsylvania, U. S. A.

910
11-14-41

Dec. 16, 1941
HA-6671

SOLD TO
Cordero Mining Company,
909 Studio Building,
Portland, Oregon.

Cordero Mining Company,
McDermitt, Nevada.
12-16-41
Parcel Post... York, Pa.
30 days, net 1/2% 10 days

1 12" wide overall, Flanged, Endless Conveyor Belt for Hardinge Feedometer No. 635. $25 00
Parcel Post & Insurance 1 30
$94 30

DISTRIBUTION 2930 TO ACCOUNT 2111 RR

HOLD Complete shipment

Figure 17. *1941 order for a 12-in. flanged conveyer belt for Hardinge Feedometer No. 635 via York, PA to McDermitt, NV.*

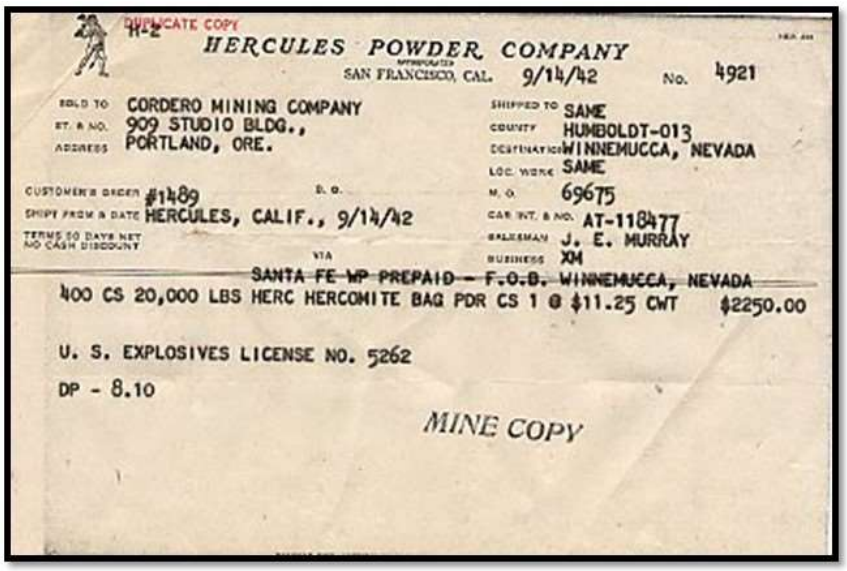

DUPLICATE COPY

H-2

HERCULES POWDER COMPANY

SAN FRANCISCO, CAL. 9/14/42 No. 4921

SOLD TO CORDERO MINING COMPANY
ST. & NO. 909 STUDIO BLDG.,
ADDRESS PORTLAND, ORE.

SHIPPED TO SAME
COUNTY HUMBOLDT-013
DESTINATION WINNEMUCCA, NEVADA
LOC. WORK SAME
M. O. 69675
CAR INT. & NO. AT-118477
SALESMAN J. E. MURRAY
BUSINESS XM

CUSTOMER'S ORDER #1489 D. O.
SHIPP FROM & DATE HERCULES, CALIF., 9/14/42
TERMS 30 DAYS NET NO CASH DISCOUNT
VIA SANTA FE WP PREPAID - F.O.B. WINNEMUCCA, NEVADA

400 CS 20,000 LBS HERC HERCOMITE BAG PDR CS 1 @ $11.25 CWT $2250.00

U. S. EXPLOSIVES LICENSE NO. 5262

DP - 8.10

MINE COPY

Figure 18. *1942 shipping receipt for 400 cases of Hercomite explosives to Cordero Mining Company F.O.B. Winnemucca, NV from the Hercules Powder Company Hercules, CA via Santa Fe Western Pacific railroad. Hercomite was an economy dynamite for dry rock conditions sold in water resistant fiber/asphalt bags packed in 50-lb. wood boxes holding 50 sticks of powder per box. By 1945, the wood box was replaced by heavy water-proofed corrugated fiberboard carton (cardboard). The order weight should be 2,000 lbs, not 20,000 lbs.*

Corderito, Crofoot, Ruja, Lenway Shaft, and Josefa Lenway, Mines

The Corderito mine is an open pit mine in surface exposures of mineralized volcanic sediments (opalite) about 1,000 feet (300 meters) north 55 degrees east of the Cordero mine Brown shaft. The Crofoot project mine was a 1960s inclined shaft to attempt to reach drilled ore targets in volcanic sediments at a depth of about 250 feet (80 meters) at the Josefa Lenway mine. The Crofoot project site is about 2,400 feet (730 meters) north 60 degrees east of the Brown shaft. The Josefa mine is about 2,100 feet (640 meters) north 74 degrees east from the shaft. The Lenway shaft, put down in the 1950s or 1960s, also explores tuffaceous sediments and is about 2,600 feet (790 meters) north 69 degrees east of the Brown shaft. The Ruja mine is about 2,300 feet (700 meters) north 95 degrees east of the Brown shaft and developed ore in basaltic rhyolite rocks similar to the Cordero mine. Nearby is Blackey's shaft, located 2,600 feet (790 meters) north 84 degrees east of the Brown shaft and appears to explore shallow tuffaceous sediments. The mineralogy of these smaller mines has not yet been investigated but is presumably the same as the shallow tuffaceous ores and deeper rhyolite-hosted ores at the Cordero mine. At the Cordero mine, just east of the Brown shaft, there are several pits in tuffaceous sediments and along faults named B, C, D, F. and G; also there are three named shafts (Blackey's, Bradley, and Brown) and two unnamed shafts (Yates 1942; Bailey and Phoenix 1944; Curry 1960; Fisk 1968; Speer 1977; McCormack et al. 1991; Tewalt and Carrington 2001).

Figure 19. *Furnace condensers and retort remains at the Ruja mine (after Blumenfeld 2014)*

Figure 20. *Deep pit at the Lenway mine (after Rytuba and Glanzman 1979).*

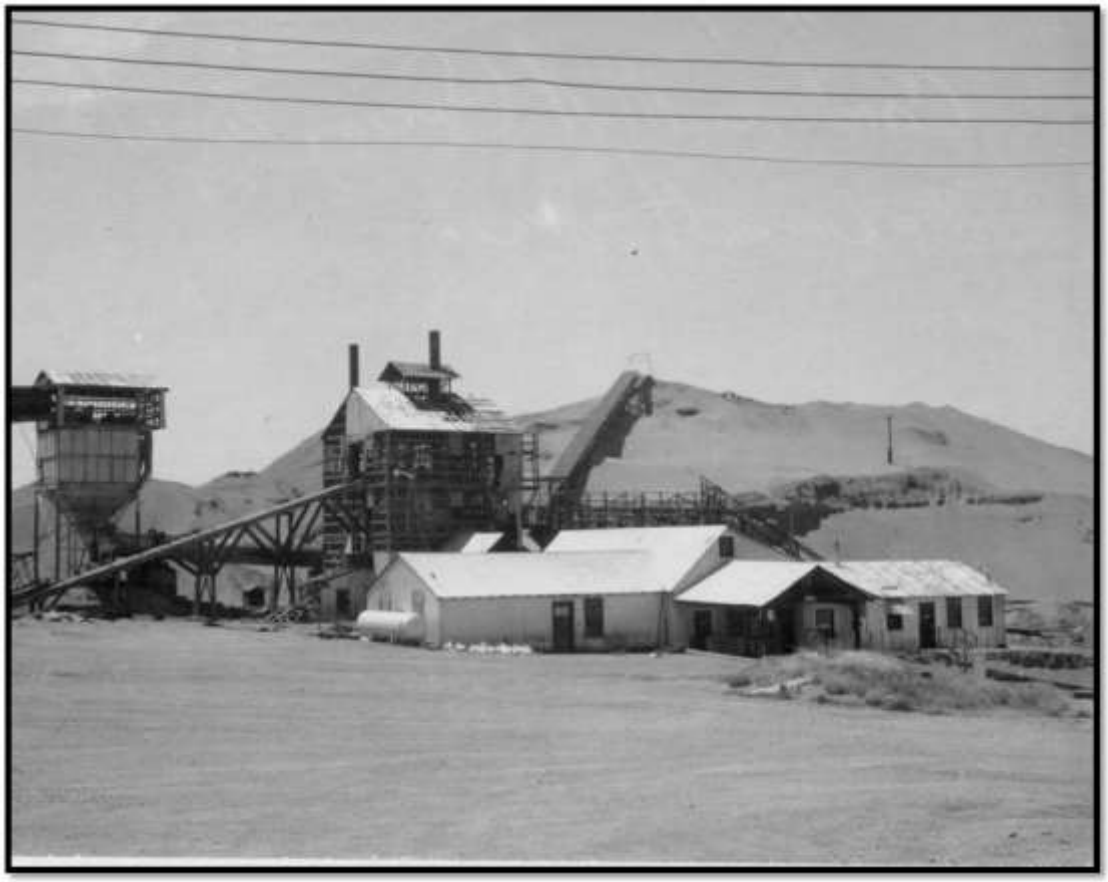

Figure 21. *Abandoned Cordero mine processing facility in about 1980 (Placer Amex Staff circa 1980). The tall structure at center housed a Herrschoff multiple-hearth furnace. In 2011, following a site closure and cleanup project, all that remained on site was the calcines pile and the cylindrical body of the multiple-hearth furnace.*

McDermitt mine

The McDermitt mine was discovered as a separate mercury ore-bearing occurrence approximately 1000 feet (300 m) northeasterly and in a different geologic setting from the old Cordero mine, which had been the district's major producer. The Cordero mining property was under lease by Sierra Mineral Management from the owner Fred H. Lenway in February 1971, when the property was brought to the attention of Placer Amex, Incorporated. The property was first examined by Amex geologists in the spring of 1971, who reported favorably on the project. During that year, Sierra Minerals Management had retained Dr. Larry Walters as a consultant. He proceeded to drill test mercury soils anomalies which he had found northeast of the old Cordero mine, in an area overlain by recent alluvium and gravel. A site known as the "D area" was subsequently blocked out and ascribed a tonnage of about 200,000 tons, which occurs in the vicinity of the eastern edge of the currently defined McDermitt ore body. This mineralization was found in flat-lying mercury-bearing lakebeds, quite unlike the steep, structurally controlled ore which was mined in the old Cordero mine (Storey 1985).

It became apparent to Placer Amex that since the chances of much more extensive ore were good in such a geologic environment, additional exploration was warranted. A joint venture was formed in October 1972 between American Exploration and Mining Co. and Sierra Mineral Management, to further explore the Cordero property. Sampling began by Placer Amex in the D area, where an open trench had exposed the lakebed ore. Visible cinnabar could not account for the high-grade mercury assays taken from the trench, and an unknown mercury mineral was suspected. Subsequent work established the presence of a chloride-bearing mercury sulfide which may have enriched the lakebeds as a secondary supergene mineral (Placer Amex staff 1980). Early identification of the new mercury-bearing mineral corderoite by Foord et al. (1974) aided in the geological interpretation of the ore occurrence and was helpful in exploring for the expansion of the D area. Corderoite was found occurring with cinnabar in the lakebeds, and in places it is a major component. Step-out drilling from the D area encountered extensive flat-lying lakebed ore (Storey 1985).

The McDermitt ore body, as subsequently defined by drilling, was found to contain 3 million tons of open-pittable ore, containing about 10 lbs./ton (0.5 wt. %) Hg. The ore body gently dips to the north and is found lying mainly in clay beds just above an opalite breccia blanket, which in turn overlies the earlier volcanic rocks. Some ore is also found in the opalite breccia. Production from the McDermitt open pit began in June 1975 at the rate of 20,000 flasks per year (Storey 1985). Estimated reserves at that time were 400,000 flasks (Hetherington and Cheney 1985). The McDermitt mine was the largest mercury mine in the United States when production ceased in 1990. Sisselman (1975) provides a detailed summary of the McDermitt mine opening and technical details concerning its early operation.

Figure 22. *Top: Placer Amex 1979 photograph looking west. The Cordero mine calcines pile is visible at the far left, below the left edge of the clouds. Bottom: McDermitt mine pit looking northwest from the center of the eastern cut face. Note automobiles at far right.*

Figure 23. *View of the southwest corner and former access ramp to the extensive McDermitt mine pit area (after Blumenfeld 2014).*

Figure 24. *Southeastern top edge of the McDermitt pit, looking roughly west, with scattered residual ore rocks.*

Figure 25. *Specimen collecting by F. Cureton and J. Marty at one of the rock piles within the McDermitt mine area.*

Figure 26. *View looking southwest from the McDermitt pit floor.*

Bretz mine

Cinnabar was first discovered in July 1917 by William S. Bretz, at what is now called the Bretz mine. The mine is in Malheur County, Oregon, in the northernmost portion of the McDermitt caldera, along the contact between rhyolite and tuffaceous sediments. It is about 7 miles (11 km) due east of the Opalite mine and 16 miles (26 km) northwest of McDermitt, Nevada, the nearest town. The U.S. Bureau of Mines Staff (1965) gives an account of the Bretz mining operations (Dadoly 2001), from which the description below is taken.

Following discovery in 1917, work was confined to exploration of the low-grade mineralized opalite exposed at the surface. In 1931 Mr. Bretz discovered high-grade cinnabar ore in the unsilicified lake beds near his original discovery and soon leased the property to the Bradley Mining Company, who at the time, was operating the Opalite mine about 11 miles (18 km) to the northwest. The ore was mined by open pit methods and trucked to the Opalite furnace plant. From 1931 to 1936, a total of 50,500 tones were mined resulting in nearly 10,000 flasks of mercury. In 1940 a new discovery was made about 2000 feet (610 m) northwest of the former workings. This period of mining activity lasted until 1944, when operations ceased. The mine was idle between 1944 and 1955 when in 1956 a third period of mining was begun, which lasted until 1961. During this latter mining period,

about 25,000 tons of ore containing 3 to 4 lbs. of mercury per ton were stockpiled during strip-mining operations. Cinnabar is the only mercury ore mineral reported from this mine in a gangue of baryte, calcite, quartz, pyrite, marcasite, and chalcopyrite.

Figure 27. *View of the Bretz mine (Oregon) showing the extensive workings (after Anderson 2003).*

Figure 28. *View of the Bretz mine retort site (after Anderson 2003).*

Figure 29. *View of the Bretz mine retort configuration (after Anderson 2003).*

Figure 30. *View of one of the remaining structures at the Bretz mine (after Anderson 2003).*

Opalite mine

The Opalite mine is located in the northerly section of the McDermitt caldera in Malheur County, Oregon, about 17 miles (27 km) northwest of McDermitt, Nevada. This deposit was discovered in 1924 by William S. Bretz and his partner, Murphy. They sold the property to the Mercury Mining Syndicate organized by F. W. Bradley in 1925. A large furnace plant was completed late in 1926 and mining was begun in 1927. Operations continued with some interruption through 1944. The Mercury Syndicate was dissolved in about 1931 and the Bradley Mining Company continued as operator of the mine. Production during the 1927-1944 period exceeded 10,000 flasks of mercury. The U.S. Bureau of Mines Staff (1965) gives an account of the mining activities of the Bretz mining operations.

The cinnabar at the Opalite deposit occurs mixed with silica in brecciated zones of an opalite mass about 1,200 feet (360 m) long, 800 feet (240 m) wide, and a little more than 100 feet (30 m) thick. A minor amount of

cinnabar is also mixed within tuffaceous lake sediments below the opalite. Mineralization decreases toward the bottom of the opalite mass. The opalite may have been formed by silicification of the surrounding lake bed deposits by hydrothermal activity. The cinnabar mineralization is presumed to have taken place during the last stages of silicification. The deposit is considered to be of the hot spring type (Brooks 1959, 1963).

Figure 31. *View of the Opalite mine processing plant and burnt ore pile (after Anderson 2003).*

Figure 32. *View of one of several adits of the Opalite mine (after Anderson 2003)*

Figure 33. *View of remaining underground workings, Opalite mine (after Anderson 2003).*

URANIUM MINES

The western and northern regions surrounding the McDermitt Caldera Complex, both in Humboldt County, Nevada and Malheur County, Oregon, hosts several uranium mines. In particular, the Moonlight, Granite Point and Disaster Peak mines along the western margin of the complex were mined for their uranium content, which occurred as uraninite, coffinite and several secondary minerals.

Across the border in Malheur County, Oregon, are additional uranium mines that host both mercury and uranium minerals, including the Bretz mine and Aurora prospect, which are located along the northeastern ring-fracture system of the caldera complex. A series of block faults, constituting the ring-fracture system, divide the area into two contrasting terranes. The northern terrane includes a series of mafic to silicic lavas and rhyolite ash-flow tuff (Bretz series). Rocks of the southern terrane (Aurora series) represent infill of the caldera after collapse. Uranium concentrations occur along several horizons, including geologic contacts, unconformities, and redox boundaries in the Bretz series; a widespread horizon within the tuffaceous lake sediments; and potentially commercial deposits along flow boundaries and interflow breccia in the Aurora lavas (Wallace and Roper 1981).

Moonlight mine

The Moonlight mine and several unnamed uranium mines are located in the southern sector of the McDermitt Caldera Complex, about 28 miles (45 km) south of McDermitt. These deposits occur in rhyolite domes intruded along the southwestern ring fracture zone. These domes are faulted on the west by range faults bounding the Quinn River valley. The uranium ore is localized along a breccia zone that strikes northwards, dips 60^{o} to the east and parallels the flow foliation planes within the dome. The uranium minerals reported from this mine include autunite, coffinite, “gummite” (a mixture of boltwoodite, curite, kasolite, soddyite, uranophane, clarkeite, and uraninite, (Frondel, 1956)), meta-autunite, metazeunerite, torbernite, and uraninite in a gangue of quartz, fluorite, and pyrite. Studies of unaltered rhyolite from the dome show anomalously high uranium content and indicate, along with the high temperature of deposition, that the deposit is genetically related to the rhyolite intrusive (Garside 1973).

Granite Point mine

This uranium mine is situated about 2 miles (3.2 km) northwest of the Moonlight mine and explores several rhyolite domes. The geology and mineralogy of this property is assumed to be the same as that of the Moonlight mine. Recorded minerals from the mine include autunite, carnotite(?), “gummite”, torbernite, and uraninite(?).

No further information, including production figures, is known for this uranium mine. Castor et al. (1996) state that the uranium mineralization may be partly coeval with deposition of volcanogenic sediments in the caldera moat.

Disaster Peak mine

The Disaster Peak property is a group of nine claims located about 22 miles (35 km) west of McDermitt, near the base of Disaster Peak. The prospect was originally developed in 1940 and 1941 by S. Crutcharray and P. Apesteguy. Development in 1942 consisted of a northeasterly-trending 95-foot (29 meter) adit and a second 32-foot (9.8 meter) adit, lying about 25 feet (8 meters) above the former. The workings explored silicified volcanic rocks which contain some cinnabar. The uranium minerals uraninite and coffinite also have been recorded from the workings (Bailey and Phoenix 1944). Additional mineral resources of the area are recorded by Leszcykowski (1987).

Aurora prospect

The Aurora uranium prospect, drilled but not yet mined (Nash 2010), is located southwest of the Bretz mine and adjacent to the Cordex Syndicate uranium prospect, within the northern rim of the McDermitt caldera complex. Uranium mineralization occurs dominantly as very fine-grained uraninite and coffinite, localized in highly altered, vesicular to scoriaceous flow tops and breccia layers within a complex intermediate lava sequence. Mineralization was introduced by hydrothermal action which added uranium-bearing solutions along an arcuate, steeply dipping fracture system sub-parallel to the axis of the mineralized zone. Supergene action may then have spread the altering and mineralizing solutions laterally along the more permeable layers within the lava sequence (Roper and Wallace 1981). According to Ainsworth (2004), the Aurora uranium prospect was explored by Placer Amex in the period of 1973-1981, initially for mercury and later for uranium. Although drilled, the prospect is not yet mine (Nash 2010).

Minor prospects

In addition to the above major mines, there exist a number of minor prospects and mining developments in Malheur County, Oregon. These are: the Burnell-Larson occurrence (mercury), Sunset Mercury occurrence (mercury), and the Ben-Bret 1-15 occurrence (mercury, gold, uranium). This area also hosts more than twenty agate, petrified wood and stone claims (Nash 2010).

POST-MERCURY MINING CONDITIONS

Mining operations at the district mercury mines ceased by 1971, when growing environmental concerns caused a drop in the demand for mercury and its price fell. The McDermitt mine was able to operate until the year 2000 because of its comparatively low cost of production. The McDermitt mine waste dumps and tailings pond have been respectively graded and capped. The open cut was graded to smooth down vertical cut faces.

At the Cordero mine, a hoist facility and associated buildings still remain on site, as well as the shell of a Herreschoff furnace, but the rest of the ore processing equipment, including condensers, were removed pursuant to EPA cleanup demands. The calcines pile from ore roasting was graded and capped in 2018, again, pursuant to a U.S. EPA demand. Numerous bags of exploratory drill cuttings from an exploration program (see next section) are stored in a large warehouse on site. In the former hoist room, mining records are scattered across the floor and rotting. Openings to the underground workings have either collapsed, been buried, or have gated and locked closures installed.

At the Ruja mine, a rotary furnace plant and condensers, a battery of retorts, and a pile of wrecked condensers and mining equipment remain. A mine hoist at the nearby Lenway shaft was vandalized, the hoist building has collapsed, and an air compressor has been dragged some distance away from its former location.

Cleanup and hazard abatement actions driven by the U.S. EPA, B.L.M., and State of Oregon removed waste piles and abandoned mining equipment at the Bretz mine. Openings to the underground workings are collapsed or buried, and the open cuts have been regraded to control erosion.

The Opalite mine is the subject of a U.S. EPA abatement action, but still has exposed calcines and mining equipment ruins, as well as unabated mine openings.

RECENT EXPLORATION EFFORTS

In 2008, the Silver Predator Corporation conducted a drill program of 13 holes to a depth of 730 feet (220 m), just east of the Cordero property. Anomalous gold mineralization was encountered in all 13 holes.

Figure 34. *View of 2008 drilling rig near the Cordero mine (after Shutty 2015)*

The RC (reverse circulation) and core drill programs resulted in the discovery of a significant new Nevada gold-silver mineralized system at Cordero. The exploration results defined a 2,250-foot-long (680 m) structural corridor of significant gold mineralization of about 0.3 g/t, with coincident pathfinder element geochemical anomalies. The grade and persistence of the shallow oxide-gold mineralization suggests upside exploration potential for bulk mineable gold targets that are associated with the upper levels of some deeper precious-metal vein systems. Most importantly, the high-grade, vein-hosted gold intercept successfully demonstrates the viability of this high-priority target type (Childs 2007).

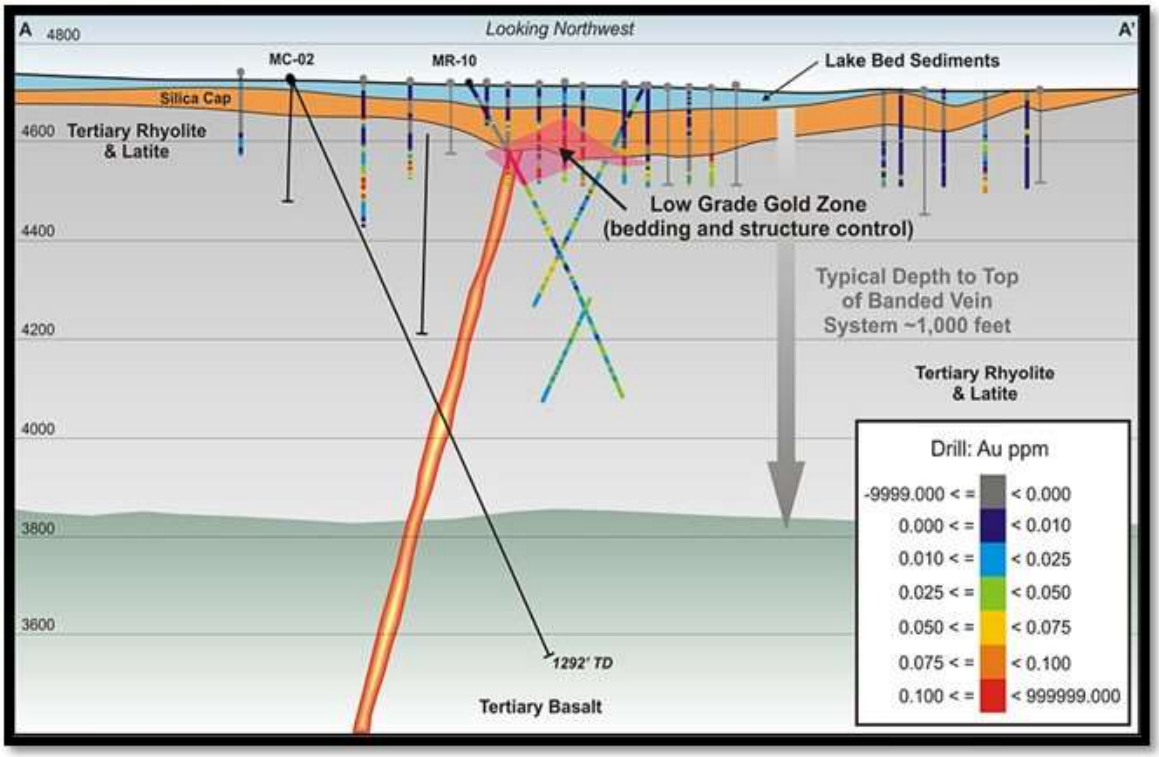

Figure 35. *Cross section view of drilling depths for gold (after Shutty 2015).*

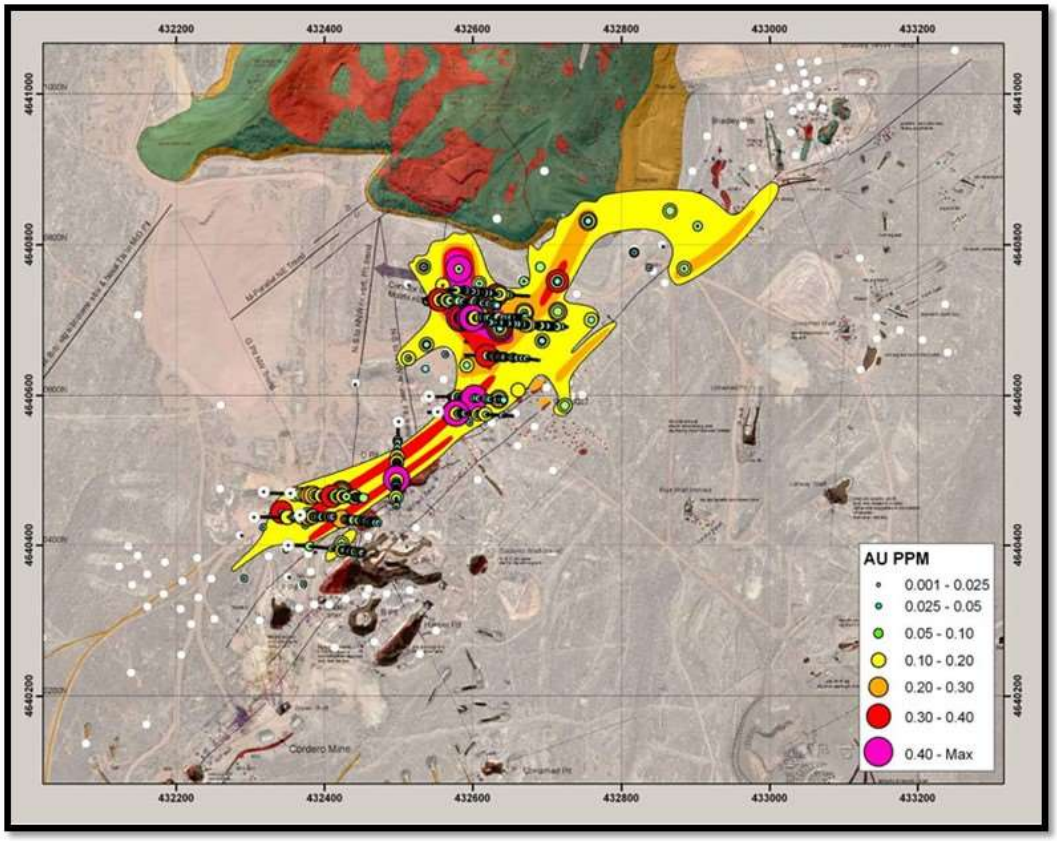

Figure 36. *Drill locations and gold levels at Cordero mine area (after Shutty 2015).*

MINERALOGY

MCDERMITT MINE

The abandoned McDermitt mine became a focus for field reconnaissance when a small cobble of float rock from the mine was found to contain scattered tiny pockets with microscopic cubic crystals that first were thought to be fluorite but were subsequently identified by powder X-ray diffraction (PXRD) as corderoite. Through careful inspection over many weeks of work spread over a three-year period, the abandoned mine proved to have a variety of interesting minerals, many of which were micro in size, including several uncharacterized mercury-bearing phases.

Rock exposures and mine spoils were examined to locate promising material for detailed microscopic evaluation. In the field, material was inspected using hand lenses for any visible unusual phases. Samples that showed unusual mineral forms, textures, and colors were bagged, labeled as to location and date, and held for later evaluation with a microscope. Promising material was found both in float rock and in-situ rock. There are large piles of cobbles and boulders scattered throughout the pit. When mining has first started, harder ore rocks were set aside because of the inability of the process equipment to reduce them for roasting. Later, the processing plant was modified to add crushing equipment, but the much harder rock was still pushed aside. Low-grade rock was sorted out and taken to the dump. Boulders with good ore were broken into smaller pieces prior to transport to the crushing equipment of the mill.

Through October 2018, six locations yielded specimens of interesting micro minerals. Four of these areas are near the center of the pit and two are toward the south (upslope) end of the pit as shown in Figure 37. In addition to the six primary areas, spot samples were obtained from numerous locations throughout the pit. Most samples produced only relatively common antimony and mercury-bearing minerals, such as small pockets of stibnite needles, stibiconite, massive cinnabar, massive corderoite, elemental mercury, calomel, and eglestonite. Occasionally a single pocked would reveal an unrecognized mineral that was designated as a potential unknown phase and given a specific code.

Figure 37. *Satellite photo showing the six primary locations of interest producing important micro-mineral specimens. Approximate outlines of each area are in red. Circular black targets are the Nevada State Plane coordinate system used by the mining company. The northern place mark pin is the thickest portion of a prominent opalite bed exposed by the north cut face and used therein as a reference point for collecting area locations. The red line is the approximate top edge of the open pit area. Aerial photography from Google Earth™, 22Jul2016. Note scale at the lower left.*

In all collecting areas the rocks containing disseminated colloidal cinnabar and corderoite are typically gray in color where exposed to the sun (Figure 38). When freshly broken, the most common color for ore rock is a light pink-vermillion to mottled red to red-brown color (Figure 39). The colloidal cinnabar and corderoite is typically in the finer-grain matrix surrounding clasts (lithic fragments) in the sedimentary and volcanic parent rocks. This accentuates the sedimentary and volcanic textures of the rocks. The ash-flow tuffs are often layered and/or banded (eutaxitic). Breccias are common and formed from volcanic eruptions, mass-wasting and erosion, and fault-related fracturing. Fragments range from lapilli to large boulders. Pebbly conglomerates are also common. Fill material along an ancient channel or channels may have later facilitated horizontal hydrothermal fluid migration from the southeast toward the northwest. Silicified beds are conformable to the stratigraphy, and the most prominent opalite beds appear thickest at the center of the pit, along a roughly north-south trend.

Figure 38. *Example showing a variety of textures and color of ore rock. The rock at the photo center has a layer with very little cinnabar and corderoite deposition in the matrix. The clastic nature of the parent rock is obvious*.

Figure 39. *An illustration of the typical darkening of rich ore in sunlight and the coloration of the rock matrix and distinct lithic clasts. The parent rock is probably a volcaniclastic wacke (mudflow?), described by Giraud (1986).*

Rocks rich in antimony are typically gray to nearly black (Figure 40). Weathering alters the pyrite to iron oxide, and the resulting iron-oxide staining also accentuates the texture of the parent rock (Figure 41).

Figure 40. *Massive stibnite with cinnabar (red) filling voids and fractures. Note the dark steel-gray matrix color, typical of rocks rich in stibnite.*

Figure 41. *Ash flow tuff with iron staining due to pyrite oxidation. The staining makes the texture obvious, which might be due to either post-depositional flow or fluvial reworking. Note the clast at the upper right side.*

Brown iron-oxide staining is prevalent along fractures and in open voids. Disseminated fine-grained pyrite is abundant and widespread in the silicified caldera rocks (personal observations). Speer (1977) found that pyrite in the vicinity of the mine pit has an extent that is some hundreds of feet (a few hundred meters) greater than the limits of the ore body as defined by drilling.

Interesting specimens of micro-minerals occur where the tuff is well silicified and has its original clastic texture preserved, with a matrix of colloidal cinnabar and corderoite in silica surrounding the clasts. Silicification is widespread and highly variable. In general, the best locations for collecting are where highly silicified ore-bearing rock transitions to softer and less-silicified volcaniclastic sediments. Additionally, many of the productive collecting areas seem to occur under clayey tuffaceous sediments capping structural highs in the volcaniclastic rocks. Fracture zones are also productive, but mainly for secondary minerals such as eglestonite, elemental mercury, and kleinite. Very productive rock often contains uniformly disseminated ore that is of medium-grade and scattered lapilli-sized voids lined with pure white microcrystalline quartz.

The ore-bearing tuff is light gray to dark grey in color on exposed surfaces, due to sunlight darkening of the cinnabar and corderoite in the siliceous matrix. Small areas of very rich ore are especially dark and often have schuetteite coatings. Upon breaking the surface with a hammer, the gray material is seen to be just a micron-thin surface coating on bright pink to vermillion and brownish-vermillion silicified tuff containing buff-colored angular clasts of tuff up to several inches (tens of cm) in size. The clasts are angular to rounded. Small vugs lined with clear to whitish tiny (drusy) quartz crystals are common. The ore replacement is pod-like and irregular, with small areas of significant enrichment normal bedding structures along which the silica fluids presumably migrated preferentially.

Except for kleinite, no significant samples of euhedral mineral crystals were found in rock that was not silicified or contained no ore. In Area 2, explained below, kleinite was often encountered as blebs and small clusters of crystals in clay-lined voids in weathered tuffaceous rock. Terlinguacreekite is associated with kleinite in many of the samples examined.

The presence of elemental mercury and yellow eglestonite warranted careful examination but did not always lead to useful samples of crystalline minerals. This was also the case for surface coatings of yellow schuetteite, which typically occurs on very high-grade ores or rocks that contain elemental mercury and often massive calomel. Searching by UV light for fluorescent minerals such as calomel, with its bright red-orange fluorescence, was somewhat useful, but sunlight and weathering has typically degraded the mercury minerals, and fluorescence is most useful only when dealing with freshly exposed surfaces. Late-stage bubbly chalcedony and hyalite, containing trace uranium with an associated bright green fluorescence under UV light, was useful for locating fractures that

warranted closer examination, especially within weathered rock containing kleinite in isolated pockets and fractures.

The area descriptions below provide locations relative to the thickest portion of the north wall chalcedony bed, located at 41.922330° by -117.811870° and at an elevation of about 4,557 feet (1,389 meters) AMSL. All latitude and longitude referenced in this paper is relative to the WGS-84 datum. Although the open cut work was irregular, the pit floor can be divided into five primary levels of ore stripping and benching, each separated by 24 feet (7.6 meters) of vertical elevation change. Two additional levels are related to overburden removal and are not counted here. The highest bench in ore-bearing rocks is at the south end of the pit, between 4,625 and 4,650 feet (1,410 meters and 1,417 meters) AMSL. This is stripping level one. The deepest portion of the pit floor is a broad flat area at the northwest corner of the pit and at an elevation of between 4,520 and 4,524 feet (1,378 meters and 1,379) AMSL. For this report, this is designated as the fifth stripping level.

Area 1 Description

The approximate center of the first collecting area is 1,083 feet (330 meters) and south 4.3° west from the thickest portion of the north wall opalite bed, specifically at 41.919359° by -117.812167° WGS-84 and at an elevation averaging about 4,595 feet (1,400 meters) AMSL. Area 1 is an irregular cut bench at the third-striping level. The pit floor to the northwest is striping level five. The Area 1 bench floor slopes northward and has several bulldozer trenches and pits at various angles. Figure 42 is a photograph of the area looking northwest. The primary collecting location is a small knob and trenching, about 2,700 square feet (250 square meters) in size.

Rocks in the area are thoroughly silicified interbedded tuffaceous fluvial and lacustrine sediments, probably including the volcanic wacke (mudflow) unit described by Giraud (1986). Lacustrine sediments that occurred on top of the fluvial rocks have been mostly stripped away in this area. The fluvial and lacustrine sediments overlie lithic tuff that is about 20 feet to 25 feet (6 meters to 8 meters) lower in elevation. Hetherington (1983 and 1985 with Cheney) describes the lithic tuff in detail. Area 1 has many interesting tuffaceous rocks with varying degrees of silicification and colloidal cinnabar and corderoite content, ranging from light pink to dark red to red brown in color.

The rocks are typically irregular in color, texture, hardness, and bedding due to variations in both the original rock and in the degree of replacement with silica and ore minerals. Weathering adds yet another variable, contributing iron staining and the breakdown of mineral grains into clays. Although rock here has vugs lined with small but exceptional euhedral crystals of jarosite, the area otherwise only yielded three significant finds. All three finds were in float cobbles of rock pushed around during mining, and an *in-situ* source for the material was not found.

Figure 42. *Collecting Area 1 looking northwest. The single cobble of rock containing corderoite crystals came from the toe of the pile of cut spoils to the left. The rock just to the right of the pile is grey due to sunlight-discolored disseminated cinnabar and corderoite.*

One of the significant finds was a small cobble of silicified fluvial tuffaceous rock collected from the eastern side of a low knob of blasted rock covered with open-cut spoils. Exceptional microscopic cubic corderoite crystals in small mm-sized vugs were recovered from the cobble. This find, in early 2015, prompted additional examination of the pit. Additional areas were found with noteworthy minerals and are described below.

The corderoite crystals of Area 1 occur where the rock has a uniform texture of evenly distributed small angular volcanic clasts and a uniform pink-vermillion coloration from colloidal cinnabar and corderoite. The field personnel call this texture "pudding stone." Despite thorough searching for similar rock over many days since the first find, no additional similarly-sized corderoite crystals were found. A cobble of grey-colored silicified fluvial rock, probably the volcanic wacke (mudflow) unit of Giraud (1986), contains noteworthy divergent clusters of millimeter-sized yellow fluorapatite crystals in large irregular vugs. The float cobble was collected from the top of the pile of cut spoils.

The silicified tuff exposures were followed east-to-west and upslope to the south for several hundred feet (around 100 meters). At this location, fluvial volcanic wacke grades into overlying bedded tuffaceous sandstone that has been stripped off most of the silicified layer. About 210 feet (65 meters) south 48° east of the knob, a third cobble was found with noteworthy micro minerals. The cobble is silicified tuffaceous sediment with the prerequisite pudding-stone texture and light-pink-to-vermillion color. One side of the cobble was finely interbedded tuffaceous shale to sandstone thoroughly replaced by silica. This portion of the rock has a mottled light-pink, pink-vermillion, and tan-white color due to varying content of colloidal cinnabar and corderoite in the matrix.

The cobble, which was broken up, contained small vugs, up to 0.4 inches (a centimeter) or so, and sometimes merging to form an area of several tenths of a square inch (several square centimeters). Vugs lined with a thin layer of white chalcedony or white microscopic drusy quartz contain plentiful but small cubic corderoite crystals. The crystals range from colorless to dark brown, almost black, and are generally less than 0.020 inch (0.5 mm) in size. Occurring with the corderoite are elongated light-tan-yellow tapering hexagonal crystals of unknown mineral MCDUK-3. These hexagonal crystal groups often have microscopic crystals of corderoite covering their surfaces. In addition, much larger corderoite crystals have been observed attached to the divergent crystals of MCDUK-3. Also in these rocks another unidentified mineral was noted (MCDUK-2) in small white lumps with micron-sized crystals. Only several small samples have ever been found.

Colorless crystals that have been tentatively identified by energy dispersive X-ray spectroscopy (EDS) as a possible mercury sulfide chloride occur in the Area 1 rocks. Subsequent X-ray structure data identified these prismatic crystals as kenhsuite. From other cavities, a very-light-yellow to cream-colored mineral in masses of acicular crystals was noted. An EDS of this mineral was identified as a possible mercury sulfate. Further examination of the rock samples revealed a gray coating on residual cinnabar. A PXRD examination of this gray coating revealed three mineral phases: (1) corderoite, (2) kenhsuite, and (3) the beta phase of $Hg_3S_2Cl_2$.

The following chart gives a probably mineral deposition and oxidation sequence for the minerals of Area 1. Because much of the surface rocks were not found within visible *in situ* layers, their original location is at best an educated guess.

Table 3. *Probable mineral deposition and oxidation sequence for mineral Area 1.*

SEQUENCE	PROBABLE EVENTS
1	Introduction of mercury sulfide solutions within the horizontal layers of host rock. Possible deposition of pyrite as well, although the pyrite is greater in extent than the mineral deposit (Speer, 1977) and may be an older mineral related to the ignimbrite host rocks.
2	Solutions rich in chloride invaded this host rock and partially altered the cinnabar to massive corderoite. Clay minerals are also formed.
3	Silica-rich solutions invaded the mercury-rich rock, with the formation of many cavities and vugs.
4	Specific ion-rich solutions, possibly derived from the initial corderoite-forming fluids formed (phase 1) a mercury-sulfide-molybdate, (phase 2) a mercury-sulfide-sulfate/molybdate, and (phase 3) cubic crystals showing edge modified edges {011} of corderoite following sequence (2). No time relationship was found between (1) and (2); the cubic corderoite crystals were found to be later than phase (2). Phase (2) shows a hexagonal outline with a dark-brown core. Minute corderoite crystals were identified coating these prisms.
5	Within small quartz-lined cavities/vugs in the corderoite-rich breccia, minute colorless acicular crystals

SEQUENCE	PROBABLE EVENTS
	had formed, identified as kenhsuite. These crystals formed on the prior quartz crystals. Again, no time relationship was found between the kenhsuite and the phases described under sequence 4.
6	Supergene oxidation and weathering of the deposit. Jarosite, hematite, limonite, and extensive clay minerals formed, although some of the jarosite may be related to event 4 or 5.

Area 2 Description

The approximate center of the second collecting area is 875 feet (270 meters) and south 15° west from the thickest portion of the north wall opalite bed, specifically at 41.919993° by -117.812708° WGS-84 and at an elevation averaging about 4,560 feet (1,390 meters) AMSL. Area 2 is a cut bench that covers roughly 10,700 square feet (1,000 square meters). It is the north-eastern portion of a larger roughly U-shaped cut that opens toward the north, (Figure 43). The bench has an access ramp that slopes east and then west down to the pit floor toward the north.

Area 2 is excavated in lacustrine tuffaceous sedimentary rocks over fluvial tuffaceous rock. The lacustrine rocks have been largely removed. The fluvial rock is mainly the volcanic wacke unit of Giraud (1986). The fluvial sediments overlie lithic vitric welded ash-flow tuff described by Hetherington (1983, 1984). The contact between the tuff and fluvial sediments appears conformable in some places and abrupt and non-conformable in other locations. It is likely the fluvial processes were scouring the top of the underlying lithic vitric ash-flow tuff. For convenience, these rocks are lumped together as “tuff” herein.

Area 2 contains significant kleinite, terlinguacreekite, and minor amounts of other mercury minerals, primarily calomel, eglestonite, and, an exceptionally rare mineral containing mercury and carbon, designated MCDUK-7. The most productive rock occurs in two places. Crumbly clayey tuff boulders pushed into a circular excavation about 10 feet (3 meters) deep in the center of the bench contain massive to crystalline kleinite and minor terlinguacreekite in scattered pockets and thin fractures. The boulders have been leached of silica and contain little of the colloidal cinnabar and corderoite that pervades the siliceous matrix of nearby silicified tuffaceous sediments. The degree of leaching versus silicification is irregular. The second area of productive rock are fractures in the buff-colored welded tuff exposed by the bench that surrounds the circular excavation, especially about 50 feet (15 meters) east, where small pits have been hand excavated.

Figure 43. *View of Area 2 looking east. The vegetation at the extreme right marks the edge of a circular pit about 10 feet (3 meters) deep, containing boulders of clayey tuff with blebs of crystalline kleinite. The small piles of broken rock delineate silicified fluvial and ash-flow tuff containing scattered pockets of kleinite, terlinguacreekite, and other minerals. The pickup truck is parked on the eastward-sloping portion of the access ramp.*

Well formed but small crystals of kleinite and terlinguacreekite occur in scattered mm to cm-sized vugs and along fractures in the *in-situ* rock. Some terlinguaite and liquid mercury are also found along thin fractures, as are thin fillings of massive kleinite. Fluorite, gypsum, hyalite opal, and bubbly massive chalcedony with trace uranium are common accessory minerals. The fractures are often deeply iron-stained.

In comparison to the overlying tuffs of the first collecting area, the rocks of Area 2 only contain enough colloidal cinnabar and corderoite to give the rock a pinkish cast, and in some layers and areas, there is no pinkish color other than from iron staining. The occurrence of good crystals in isolated voids seems to be inversely related to the degree of silicification, but rocks that are very clayey are not typically productive. Kleinite is especially enriched where less-silicified tuff occurs on top of dense and thoroughly silicified tuff.

Figure 44 shows one of the significant kleinite occurrences. The kleinite mineralization is clearly late in the mineral paragenesis and forms a distinct layer of dusty poorly-crystallized kleinite just above a dense highly-silicified tuff. Figures 45 & 46 show kleinite found along a fracture in a float bolder pushed aside during mining.

Figure 44. *Exposure of massive and fine-grained kleinite along a distinct upper horizon in a fracture zone on top of a dense gray tuff. The rock above appears to be the volcanic wacke (mudflow) of Giraud (1986) and might grade into the underlying lithic tuff unit of Hetherington (1983, 1984). There is obvious fluvial reworking of the clasts, and a chaotic mix and orientation of clast sizes. It is possible the rocks represent interfingered volcanic material from different local sources (air fall, flow, and erosion) reworked by subsequent fluvial runoff and in intermittent shallow water bogs and lakes. Iron staining coincident with the kleinite suggests deposition at a possible saturated and vadose zone interface, or where fluids were perched on the dense underlying silicified and welded tuff.*

Figure 45. *A boulder of tuff split in half along a fine fracture. Kleinite coats the fracture surface and a small aggregation of orange terlinguacreekite occurs on the roof of a small quartz-lined cavity at the center of the photo. The kleinite layer would have been horizontal when the rock was in-situ. A dense silicified tuff at the bottom grades into a weathered clayey volcanic wacke. A silicified layer of the wacke protrudes at the upper left corner. The kleinite coating is assuredly supergene. Iron-staining is more extensive than the kleinite and is likely a weathering feature.*

Figure 46. *The other half of the boulder in Figure 45 after exposure to sunlight for two days. The kleinite is fading and is barely visible. Interestingly, the exposure brought out a distinct band of iron staining that clearly shows an upward concentration to a very sharp top edge. This brown-colored band is slightly oblique to the kleinite layer. This suggests at least a fluctuating water surface or zone of concentration, if not a change in the orientation of the rock during different intervals of mineral deposition. It is also possible the staining represents what was a thin layer of meteoric water perched on top of the dense tuff after the kleinite had formed.*

In both the bleached and crumbly tuff, as well as the hard and dense silicified tuff, the crystals in the voids are often easily separated from the matrix and fall out when the rock is struck with a hammer. It is not obvious in the field why the crumbly bleached tuff should have more abundant and larger blebs and masses of primarily kleinite while the adjacent silicified tuff hosts less abundant scattered small patches of well-formed crystals of both kleinite and terlinguacreekite. Hetherington (1983, 1984) mapped a monoclinal structure cutting across Area 2 from west-northwest to east-southeast. This structure might be somehow related to the mineralization, perhaps by acting as a structural trap or zone of concentration. Dusty and massive kleinite occurs at distinctly sharp horizons above dense and hard silicified tuff.

The kleinite layers are overlain by very clayey and friable dregs of what was formerly tuffaceous rock. This suggests mineral precipitation at some sort of vadose zone and saturated zone interface. Mineral deposition and silica replacement occurred below the top of the saturated layer and intense alteration to clay minerals occurred above the saturated layer.

Table 4. *Probable mineral deposition and oxidation sequence for mineral Area 2*.

SEQUENCE	PROBABLE EVENTS
1	Silica deposition along permeable horizons of interlayered ignimbrite and sedimentary rocks, with minor pyrite and cinnabar, and partial alteration of the cinnabar to corderoite where the cinnabar was not fully encapsulated in silica. For the most part, the kleinite rock of Area 2 is notably devoid of significant cinnabar and corderoite.
2	Additional silicification, oxidation, and late deposition of kleinite and terlinguacreekite with associated minerals in a cream-colored to light gray rock. In decreasing order relative to abundance, the accessory minerals are: quartz, clay, chalcedony with trace uranium, iron hydroxides, hyalite, fluorite, calcite, calomel, and very minor elemental mercury. Iron hydroxides formed in thin bands parallel to bedding, possibly representing the vertical extent of saturated layers at the time. There is iron oxide encapsulated in silica, as well as kleinite and terlinguacreekite, so these must have formed prior to or along with some of the silicification. No evidence indicates that one or the other exclusively formed first, except that silica never encapsulates elemental mercury and rarely encapsulates calomel, therefore the minerals most likely formed during fluctuating conditions within the same time period.
3	Late-stage deposition of a bubbly massive chalcedony containing trace uranium and some massive kleinite, as well as gypsum. Usually, the late-stage dusty kleinite, and the chalcedony and gypsum, form a coating or filling in fractures and on top of earlier mineral surfaces.
4	Oxidation of the pyrite and development of oxide and hydroxide supergene minerals, clay minerals, iron-staining along fractures, and the filling of fractures with veins of satin-spar gypsum.

Area 3 Description

The approximate center of the third collecting area is about 935 feet (285 meters) and south 25.6° west from the thickest portion of the north wall opalite bed, specifically at 41.920003° by -117.813367° WGS-84 and at an elevation of about 4,560 feet (1,390 meters) AMSL. Area 3 is a pile of boulders pushed aside during mining and sitting on a narrow bench to the west of Area 2. Area 3 covers about 1,600 sq. feet (150 square meters). Some of the boulders contain low- to high-grade ore. One of these yielded massive and microcrystalline stibnite, cinnabar, corderoite, and secondary mercury minerals. Figure 47 is a photograph of the boulder pile looking west. Figure 48 is a photograph of the boulder that yielded many noteworthy minerals.

Table 5. *Probable mineral deposition and oxidation sequence for mineral Area 3.*

SEQUENCE	PROBABLE EVENTS
1	Introduction of antimony and mercury sulfide solutions within the horizontal layers of host rock. Possible deposition of pyrite as well, although the pyrite is greater in extent than the mineral deposit (Speer, 1977) and may be an older mineral related to the ignimbrite host rocks.
2	Solutions rich in chloride invaded this host rock and partially altered the cinnabar to massive corderoite.
3	Silica-rich solutions invaded this mercury-rich rock, with the formation of many cavities and vugs.
4	Specific ion-rich solutions, possibly derived from the initial corderoite-forming fluids and carrying oxygen due to meteoric water mixing, disproportionate the cinnabar and corderoite and deposit elemental mercury and secondary mercury minerals in vugs and along fractures, including calomel,

SEQUENCE	PROBABLE EVENTS
	eglestonite, and minor terlinguaite. Antimony oxidation minerals, such as stibiconite, are also formed, but except for stibiconite, these are rare and microscopic.
5	Late-stage deposition of a bubbly massive chalcedony containing trace uranium, as well as gypsum. The chalcedony and gypsum form a coating or filling in fractures and on top of earlier mineral surfaces.
6	Oxidation of pyrite and development of clay minerals, iron-staining along fractures, and filling of fractures with veins of satin-spar gypsum.

Figure 47. *Area 3 boulder pile looking southwest. The boulders are weathered tuff, mainly fluvial and lacustrine tuffaceous rocks, including shale, sandstone, conglomerate, and lithic vitric ash flow tuff. Grey and dark grey patches with white massive chalcedony are typically zones of mercury enrichment that include massive colloidal cinnabar and corderoite, but also sometimes host small pockets with microcrystals of antimony and mercury minerals and also scattered elemental mercury. A boulder rich in micro-minerals was found at the toe of the cut face at the left side of the photograph.*

Figure 48. *Enhanced color photo of a boulder of vuggy and clayey fluvial tuffaceous rock, probably from the volcanic wacke (mudflow) unit of Giraud (1986). Note the gray-blue surface coating formed on the cinnabar and corderoite ore from exposure to sunlight, and the freshly broken ore exposure to the right. The freshly exposed surface has small grey blebs and patches that are elemental mercury mixed with finely divided grey eglestonite. This boulder produced small pockets of microscopic stibnite needles and noteworthy mercury micro-minerals.*

Area 4 Description

Area 4 (Figure 49) is at the eastern edge of the deepest northwest corner of the pit, stripping level 5 in this report. The area is large and is comprised of many individual sampling points and three subareas, two of which are float boulder piles and one of which is an outcrop (see Figure 50). The entire area is about 37,000 square feet (3,450 square meters) of blasted, bulldozed, and in-situ highly variable silicified tuffaceous rock. The area has its approximate center about 620 feet (190 meters) and south 42° west from the thickest portion of the north wall opalite bed, specifically at 41.921057° by -117.813405° WGS-84. The average elevation is about 4,528 feet (1,380 meters) AMSL.

The outcrops of Area 4 are surrounded by recent sandy alluvium washed down from the higher elevations of the pit. Most of the exposed rock appears to be fluvial and lacustrine tuffaceous rocks, with some interlayered ignimbrite rock. Piles of boulders and exposed, blasted, and bulldozed rock have yielded massive and microcrystalline stibnite, cinnabar, corderoite, and secondary mercury and antimony minerals.

The first reconnaissance of the area was at its northern extent, where float boulders and exposed rock yielded many samples of elemental mercury, massive calomel, divergent groupings and steel-wool-like tufts of fine microscopic acicular stibnite, and massive to crystalline eglestonite. The minerals occur in small isolated pockets and along fine fractures. On a return visit in April 2016, a small but highly productive outcrop was located at the center of the southeast edge of the area. Although no similarly productive and mineralized rock was found elsewhere, the area is large and has not been thoroughly examined.

Figure 49. *Area 4 outline showing three subareas and individual sample collection points. Float means cobbles and boulders on the surface that were displaced by mining activity. Waste rock piles are large boulders pushed aside during mining. Outcrops are exposures of in-situ rock. The base aerial photo is from Google Earth™ imagery of 22July2016. A northing for the Nevada State Plane West Coordinate System was not within the area of the photograph. The text describes the location relative to an opalite bed landmark and provides WGS84 latitude and longitude in decimal degrees.*

The small but highly productive outcrop yielded exceptional examples of many minerals, including rare mercury and antimony minerals, such as shakhovite, valentinite, and tiny but visible crystals of terlinguaite. The minerals occur in dark-grey silicified zones in tuffaceous rock. The rock is a mixture of mainly fluvial and lacustrine deposits of reworked ignimbrite. Thin laminae of finer, silty material is interbedded with coarser tuff containing lithic fragments of yet more tuff. Mineralization occurs as pore-filling and crystallization in flattened pockets conformable to the bedding structures of the rock.

About 90 feet (27 meters) northwest of the exposure are large boulders of waste rock pushed aside during mining. Some of the boulders have yielded zones of mineralization like the productive outcrop. Elsewhere, at outcrops, productive grey silicified rock forms discontinuous and irregular lenses and pods of generally not more than several feet (a meter) in thickness and 10 feet or so (several meters) in extent. Many of the silicified horizons with rich ore are less than 1 foot (one-third of a meter) in thickness. The lenses and layers are normal to bedding that generally dips gently toward the north.

At the most productive outcrop (Figure 50), the degree of silicification varies considerably, but in general forms a layer about one foot (roughly 20-30 cm) thick. The silicified layer was found to contain veins of massive stibnite conformable to bedding structures and up to several inches (many centimeters) thick but limited in extent. Dispersed fine-grained cinnabar and stibnite also occur in layered zones, along with small isolated pockets and vugs of secondary oxide minerals. Better samples of micro-minerals were found in isolated vugs less than about 1/2 inch (1 centimeter) in diameter.

The collectible stibnite-cinnabar minerals did not persist through the silicified layer. Good specimens were most abundant in a small area lower down on the northeast side of the outcrop. It was also noted that the bottom of a distinct dark-grey silicified layer contained very large voids in a band of massive stibnite. The voids were lined with bubbly chalcedony, and the chalcedony often covers and is also coated by cinnabar (see Figure 51). The productive outcrop cannot be followed south due to a covering of fine sediment washing into this portion of the pit. Each large storm will no doubt add sediment until the outcrop is completely covered over. At times the exposure has been under water. Unconsolidated fine sand and silt are found in some of the voids.

Roots, plant fibers, and even spider webs and spider body parts were found in the largest of the voids in the veined rock exposure.

Figure 50. *Productive outcrop, looking west. Note rock hammer in front of a large iron-stained pocket. Several intersecting large and flattish voids occurred here that hosted significant micro-minerals, especially valentinite. The gray areas are zones of cinnabar enrichment. Notice the dome-like deformation of the subtle layers.*

Figure 51. *Portion of rock from the productive outcrop. Note the thick massive stibnite vein to the left. In places, this vein has pockets lined with iron-stained drusy quartz and clumps of acicular crystals of light-yellow stibiconite. To the right, the massive stibnite vein gives way to large iron-stained voids that are lined with quartz, chalcedony, and fine-grain cinnabar coating the quartz. The specimen is upside down relative to its in-situ position. The silica lining the large pocket fluoresces a bright green color under ultraviolet light. Horizontal FOV is 29-cm.*

The concentration of the sulfide minerals appears to be toward the top of the silicified layers in the outcrop and becomes much less pronounced in the lower portion. Where stibnite and quartz veins are well formed, the cinnabar occurs as veins surrounding orbicular stibnite and as thin crusts along the oxidized portion, with stibiconite pseudomorphs after stibnite. Cinnabar in the pit was stated by McCormack (1986) to have formed after the stibnite had precipitated, and pyrite appears to have formed contemporaneously with the stibnite.

The productive outcrop contains samples that have cinnabar on and after massive stibnite, and stibnite on quartz covering cinnabar. McCormack (1986) did not observe any cinnabar deposited with stibnite, nor have the authors of this paper. Botryoidal structures of what appears to be alternating layers of stibnite and cinnabar have been found, but the cinnabar is likely a later filling along voids and permeable horizons in the banded massive stibnite. There may be some minor secondary stibnite, in fine acicular needles, that is secondary and does occur on quartz that covers cinnabar. Figure 52 is an example.

Abundant cavities exist within the host rock containing quartz crystals. As mentioned, thin coatings of cinnabar occur on the quartz crystals. Also, within these cavities are abundant silica tubules, often colored yellow, probably by an oxide of stibnite. Along the veins of cinnabar there are veins of eglestonite replacing the former cinnabar. At times, mercury in fine globules adorn the silica-rich host rock. Rare terlinguaite crystals have been noted filling some cavities, but not directly associated with the eglestonite. Very rare shakhovite was identified within several quartz-lined cavities attached to crystals coated with iron oxide. The shakhovite is greenish-yellow and is prismatic in habit, with striation parallel to the c-axis.

Much of the chalcedony contains significant colloidal cinnabar and corderoite in the silica matrix and micro-crystalline secondary antimony and mercury oxide minerals in voids and fractures. Elemental mercury is by no means abundant but is often found in scattered patches along fine fractures and in isolated small vugs. The rock contains small voids that are not more than and inch (a few centimeters) or so in size, but one or two large voids 4 to 8 inches (10 to 20 centimeters) long by 2 to 6 inches (5 to 15 centimeters) wide by several inches (many centimeters) tall were encountered.

The voids are typically lined with well-crystalized drusy quartz and framboidal chalcedony and hyalite opal. Cinnabar in powdery microcrystalline layers often coats the silica minerals but is also enveloped within them. Some of the individual quartz crystals, albeit not more than 2.5-mm (a tenth of an inch) in size, had several

phases of growth, with cinnabar coating the faces of each phase and subsequently becoming enveloped. The mineral deposition sequence is further detailed in Table 6.

Figure 52. *Divergent stibnite needles on silicified tuff and surrounded by orbicular growths of drusy quartz covering cinnabar. Small water-clear double-terminated quartz crystals with valentinite associate with the areas of stibnite, but not the drusy quartz over cinnabar. To the right, out of view, is a dissolution void in a section of massive crystalline stibnite vein. Horizontal FOV is 19 mm.*

Table 6. *Probable mineral deposition and oxidation sequence of the stibnite-cinnabar host rock at Area 4.*

SEQUENCE	PROPOSED EVENTS
1	Introduction of antimony and iron sulfide and silica-rich solutions normal to bedding within the host rock.
2	Deposition of stibnite both as individual acicular crystals within quartz-lined cavities and along fracture as spherical and semi-spherical crystallized groups.
3	Introduction of mercury-bearing solutions along the previous channel bedding network.
4	Deposition of massive cinnabar along fracture surfaces and surrounding previously formed spherical and semi-spherical stibnite. Somewhat before this time, partial oxidation of selective stibnite produced stibiconite pseudomorphs, followed by precipitation of cinnabar along the individual replaced stibnite crystals. Some samples illustrated a combination of primary, unoxidized stibnite while just a few tens of mm away, complete oxidation of the stibnite is seen associated with slightly oxidized cinnabar.
5	Additional stibnite oxidation within the quartz-lined cavities formed valentinite crystals. Valentinite also formed within the host rock. Senarmontite is quite rare within the oxidation zone, with only a few minute octahedrons noted.
6	The upper portion of the outcrop received the most oxidation, producing much light yellow, powdery material consisting of antimony oxide(s) and goethite.
7	Cinnabar oxidation in the upper portion of the outcrop produced veins of eglestonite replacing the previous cinnabar. Calomel also formed during this period. Disproportionation of cinnabar and preexisting eglestonite formed isolated patches of minute globules of mercury. There is no evidence that mercury was introduced into the host rock as the native element either in the liquid form or as a vapor. Very rare montroydite with eglestonite replaced individual globules of mercury in a single sample.
8	Oxidation of both stibnite and cinnabar produced two very rare minerals within a confined environment. These include shakhovite and MCDUK-19, a mercury antimony oxide. Both formed on iron oxide coated

SEQUENCE	PROPOSED EVENTS
	quartz crystals. Also within this same host rock are greenish-yellow terlinguaite crystals, both as individual crystals and grains between quartz grains. Very rare kermesite formed within a cavity as delicate red prismatic crystals.
9	Oxidation of the cinnabar formed a number of secondary minerals including corderoite, MCDUK-17, 21, 23, 27, 28, 29, and 30. Basically, these unknowns contain Hg^{2+}-O-S-Cl in various amounts. Because of the dearth of material found, little is known with respect to the time relation between each phase.
10	Cryptocrystalline and amorphous silica in various forms were deposited along open cavities, at times covering preexisting cinnabar. Silica tubes are quite common on the host rock. Also, remobilized (?) cinnabar is seen coating both preexisting quartz crystals and silica tubes. The silica forming the innermost coating of larger vug typically fluoresces green under SWUV, suggesting the presence of trace amounts of uranium.

Areas 5 and 6 Descriptions

Areas 5 and 6 are described together because they are located close together and share similar geology and mineralogy. Figure 53 shows the areas in Google Earth™ and Figure 54 shows the areas on an image of Plate 2 from Hetherington (1983) a surface geology map of pit in 1981, also overlain on Google Earth™ air photo imagery (22Jul2016 imagery).

Area 5 is a roughly rectangular area, the approximate center of which is located 2,030 feet (630 meters) south 8.3 degrees west of the thickest portion of the opalite bed at the center of the north wall of the pit. The location is specifically at 41.916809° by -117.812967° WGS-84 datum. The average elevation is about 4,630 feet (1,410 meters) AMSL. The area covers about 6,200 square feet (580 square meters). This area is in the uppermost cut work (stripping level one) explored for this report.

Area 6 is trapezoidal, and its south edge is merely 15 feet (5 meters) from the north edge of Area 5. Its center is roughly 130 feet (40 meters) north twelve degrees east from the center of Area 5. Area 6 covers about 16,400 square feet (1,500 square meters). The main bench top of Area 6 is about 10 to 15 feet (3 to 4.6 meters) lower in elevation than that of Area 5, and Area 6 is mostly on stripping level two, at an elevation of about 4,615 feet (1,405 meters).

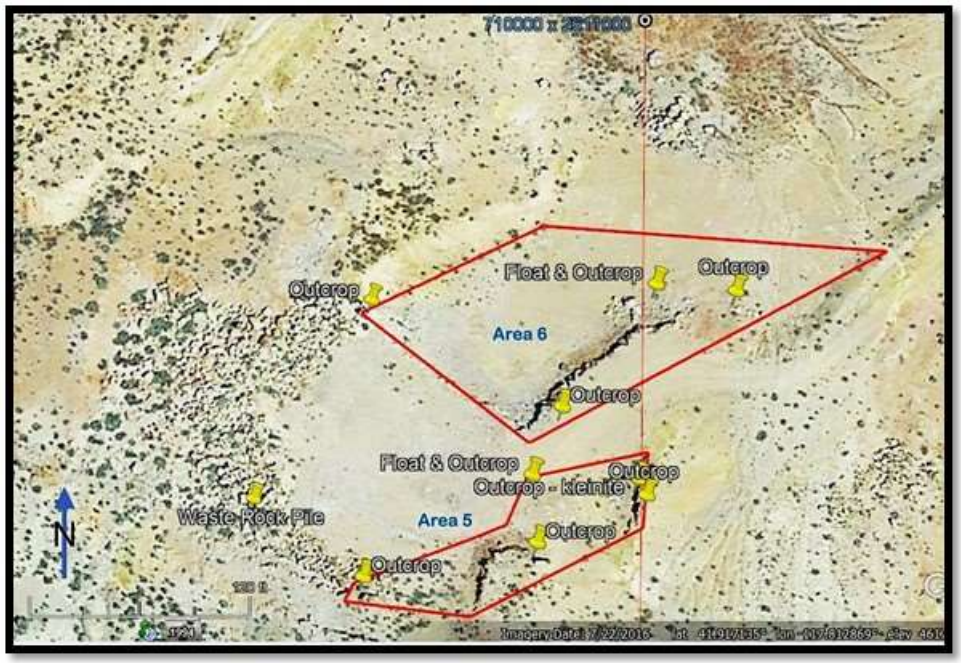

Figure 53. *Google Earth™ imagery with overlay outlining the areas 5 and 6 study zones*.

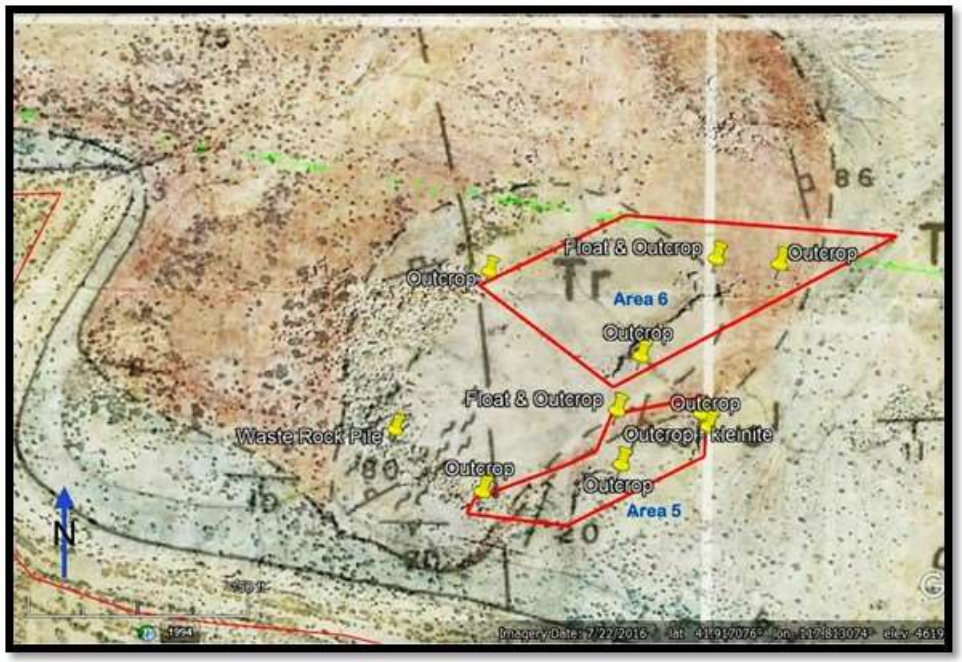

Figure 54. *Google Earth™ aerial photo imagery and outline of areas 5 and 6 overlain by Plate 2 from Hetherington (1983), a surface geology map of pit in 1981. 22Jul2016 imagery.*

Figure 55. *Panorama view of Area 5 looking from NE to SE. Scree covers a cut face in silicified interbedded lacustrine and fluvial tuffaceous rocks, including volcanic wacke, with minor siltstone, sandstone, and conglomerate. The matrix is rhyolite ash and clasts are also rhyolitic, ranging from pumice fragments to hard devitrified glass, but, for the most part, are pieces of tuffaceous rock. Rock hammer at the center is for scale. The cut face is about 10 to 15 feet high (3 to 4.6 meters). Bedding dips gently toward the northwest. The sediments at the top of the cut face are unconsolidated and ocherous.*

The rocks and noteworthy minerals of the out crop in Figure 55, from top to bottom, consist of:

1. Uppermost silicified fluvial conglomerate, possible channel fill, with angular to subangular clasts of rhyolite tuff. Two to three feet (0.6-0.9 meter) in thickness, lacking visible mercury mineralization.
2. Fine-grained rhyolitic ash and tuffaceous sediment. The layer is cut off to the north and pinches out to the south. Iron oxide staining and blackish fine-grained minerals, presumably goethite or other metal oxide, occur in fine strands and wisps conformable to bedding, with minor cinnabar and corderoite. Presumably, the iron oxide staining is later and from weathering, possibly after fine-grained disseminated pyrite.
3. Undifferentiated “basal opalite” of undefined thickness occupies the remaining exposed cut face. The opalite appears to grade conformably into the overlying unit 2, and the overlying unit 1 where unit 2 is absent. The top few feet (fractions of a meter) of the opalite produced frequent samples of liquid mercury and yellow mercury minerals along thin fractures. Some of the yellow material appears to be eglestonite,

but where the yellow color is very bright, the mineral blackens in sunlight very quickly, within seconds or minutes.

The darker layers of opalite at the center of the outcrop did not yield anything of significance mineralogically but were scarcely examined. The silicification of the opalite varies from slight to thorough. Where thorough, the rock texture and toughness is similar to quartzite and the original volcaniclastic textures are not recognizable. Silicification is normal to bedding.

Layers that are visibly darkened in the sunlight have a greater degree of silicification, and the darkest rock has the higher concentration of colloidal to micro-crystalline mercury minerals. This same observation lead McCormack (1986) to conclude that the mercury mineralization followed pathways of greater permeability within the volcaniclastic sediments and interbedded tuffs, and these same pathways were then followed by the siliceous fluids that formed the characteristic "opalite." The fluids may have been confined to a saturated zone, and tuffaceous sediments above the opalite remained soft, weathered substantially to clay, and were easily mined.

Adjacent to and on the west side of the areas, is a 13,200 square feet (1,200 square meters) dump of large waste rock boulders that were pushed aside during mining. Some attractive dusty cinnabar on drusy quartz in a couple of flattened and connected tennis-ball-sized vugs were found in one of the boulders during initial reconnaissance in 2015. At the same time, some schuetteite was found on loose rock at the north central edge of the Area 5 bench. The small cobble of float contained rich ore, massive calomel, and some scattered elemental mercury with eglestonite.

The geology from historical reports and theses were reviewed, and some spot visits were made in 2016. In 2017, a thorough search of the area was undertaken over several multi-day trips to the mine. The main reason was to examine Area 5, because it is the location of radtkeite reported by McCormack (1986). Dr. John McCormack (personal communication, 2017) reported that the radtkeite came from a single boulder loosened during mining in the mid-1980s. No additional material was discovered over many years of occasional searching, and the area was partially covered with waste spoils at some point after the initial find. Extensive searching by the authors in 2017 and 2018 also failed to uncover any radtkeite. An unusual occurrence of corderoite was discovered in rocks near the probable locality of radtkeite. A number of samples illustrated a dark orange, massive mineral forming from massive cinnabar. A PXRD of this mineral proved that it is massive corderoite and not radtkeite, as we first suspected.

The predominant rock types exposed in the area are the lithic tuff of Hetherington (1983) and the overlying volcanic wacke unit of Giraud (1986), which are mainly mudflows, but is layered and quite variable vertically and horizontally, with varying amounts of interfingered volcaniclastic sedimentary rocks of varying types, as well as tuff. Hetherington (1983, Figure 2) mapped an anticlinal structure bisecting the greater area roughly north to south. Area 5 and 6 are on the east-facing limb of the anticline, adjacent to the central axis.

Richer ore and more plentiful mineral samples seem to associate with the volcanic wacke. It is possible that a mudflow or lahar crossed the pit from roughly south to north and later, after being deeply buried, served as the primary pathway for hydrothermal fluid migration. Additionally, hydraulic pumping during hydrothermal alteration may have brecciated some of the layers and fattened up the volcaniclastic rocks along the axes of migration. In any case, the best collecting areas appear to be along the upper and lower surfaces of thicker layers of silicified tuffaceous rock along the eastern flank of the anticline. The western flank is largely buried under waste spoils and has not been thoroughly examined.

Significant examples of eglestonite, liquid mercury, and kleinite have been found here, primarily along fractures also lined with gypsum and occasional small crystals of colorless to pale-yellow fluorite. Material pulled out from the bench floor of Area 6, at the base of a ten-foot-high (3 meter) cut face in opalite, contained noteworthy well-crystallized, albeit small crystals of kleinite, sometimes in radiating groups, but both the crystals and their extent are small. Unlike Area 2, the Area 6 kleinite, albeit scarcely worked, has not been found with significant terlinguacreekite. Most of the kleinite pockets occur unexpectedly and randomly, with no associated feature to indicate their potential presence. The kleinite is found by breaking the rock into small pieces. This contrasts with Area 2, where both iron-staining and kleinite filling along thin fractures can be followed to find crystal pockets.

Compared to the rather uniform fine-grained tuffaceous rock of Area 2, where kleinite is also found, the Area 6 rock is more clastic and iron-stained, as well as tougher (more silicified) and more blackened in the sun owing

to a higher content of disseminated colloidal cinnabar and presumably corderoite. The Area 6 rock is extensively and irregularly fractured, probably from bench blasting. Where fine fractures related to the rock formation are present, breaking the rock along these fractures typically exposes liquid mercury, eglestonite, and thin coatings of unidentified yellow microcrystalline mineral phases, some of which darken very rapidly sunlight.

Table 7. *Probably mineral deposition and oxidation sequence of the Areas 5 & 6 minerals.*

SEQUENCE	PROBABLE EVENTS
1	Introduction of mercury sulfide solutions within the horizontal host rock
2	Solutions rich in chloride invaded this host rock and altered the deposited cinnabar in part to massive corderoite. In strongly acid conditions, oxidation of cinnabar would form sulfur and reaction with dissolved chloride would form corderoite, which is less stable under near-neutral conditions.
3	Silica-rich solutions then invaded this mercury-rich rock with the formation of many cavities and vugs.
4	Disproportionation of cinnabar produced liquid mercury. Eglestonite formed during this time.
5	Fluid action on either cinnabar or kenshuite produced another phase with a yellow orange color identified by PXRD methods as radtkeite.

Mineral Photos

Mineral photos are by Michael Cox and Gail Dunning, unless otherwise noted. Photos by Michael Cox were taken with plane-polarized 100-watt halogen lighting and/or electronic flash. A Sony™ A7R digital camera was used for the mineral photographs. Landscape photos were taken using an Olympus™ PEN E-PL1 digital camera with a M. Zuiko 14mm-42mm 1:3.5-5.6 lens fitted with a Tiffen 40.5mm UV filter. Photomicrographs were taken with either a Canon MP-E 65mm f/2.8 1-5x macro lens or a Leitz Orthoplan research compound microscope fitted with an Ultropak objective system, using objectives ranging in power from 3.2x to 22x. A variable effective magnification was obtained using a bellows system to vary the height of the camera sensor relative to the specimen. Each photomicrograph is a stacked composite of roughly 25 to 250 individual photographs, depending on the depth of field of the lens at the effective magnification. Staking was done electronically, using Zerene Stacker™ or CombineZP™. Photos by Gail Dunning were taken with either an Epson™ Perfection 1200U scanner (whole rock samples) or an iGaging 2MP USB microscope. SEM photos were provided by Anthony Kampf.

Calomel, Hg_2Cl_2

Calomel is uncommon in the mercury ores. It was found associated with cinnabar, eglestonite and liquid mercury at the McDermitt mine (Rytuba and Glanzman 1979; McCormack 1986), and with photosensitive cinnabar, terlinguaite and an Hg-S-Cl mineral, probably corderoite, at the Opalite mine (McCormack 2000). Recent discoveries of calomel crystals in silica-rich light gray rock associated with kleinite and terlinguacreekite presents an interesting association. Colorless calomel tetragonal crystals up to 0.5 mm cover older quartz.

Figure 56. *View of tetragonal calomel crystal on quartz in upper center. Smaller crystals are just to the left and a slightly larger one to the right. FOV = 2 mm.*

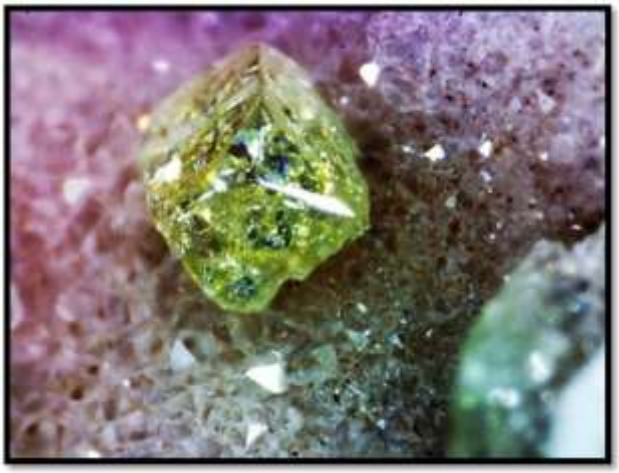

Figure 57. *Enlarged view of greenish-yellow calomel crystal. FOV = 0.3 mm.*

Figure 58. *Enlarged view of a colorless calomel crystal. FOV = 1 mm.*

Figure 59. *Scattered group of colorless calomel crystals on matrix. FOV = 2 mm.*

Figure 60. *Elongated calomel crystal showing a smooth surface on quartz. FOV = 1 mm.*

Figure 61. *A rotated view of the above calomel crystal. FOV = 1 mm.*

Figure 62. *A vertical view of the above calomel crystal. FOV = 2 mm. Dan Evanich photo.*

Cinnabar, HgS

The Cordero and McDermitt mines of the opalite district were the most productive Hg mining areas in Nevada. Here, cinnabar was found in small high-grade ore bodies under opalite blankets, disseminated in large ore bodies in altered volcanic rock, and in large low-grade bodies in opalite. Cinnabar is the most abundant Hg mineral and appears to have been the first formed. It was described as occurring in clusters of tiny crystals, veinlets, and rare twisted needles. Associated minerals included liquid mercury, mercury halides and oxychloride minerals, pyrite, hematite and other iron oxides, stibnite, fluorite, and heulandite (Bailey and Phoenix 1944; Fisk 1968). Photosensitive cinnabar has been noted from the Opalite deposit, Oregon, where it is often spatially associated with the mercury halide minerals terlinguaite, calomel, and probable corderoite. Photosensitive cinnabar also occurs at the McDermitt deposit, with corderoite, radtkeite, kenhsuite, calomel, kleinite, and eglestonite (McCormack 2000).

Figure 63. *Coating of cinnabar on silica rods with orbicular stibnite underneath. FOV = 60 mm.*

Figure 64. *Cavity containing minute cinnabar crystals. FOV = 12 mm*

Figure 65. *Irregular surface covered with cinnabar crystals. FOV = 20 mm.*

Figure 66. *Elongated cavity covered with cinnabar crystals. FOV = 20 mm.*

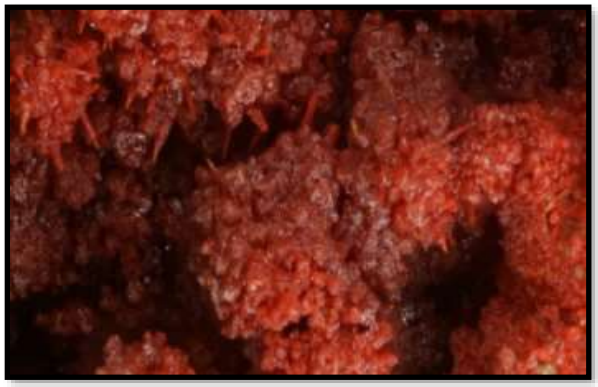

Figure 67. *Cinnabar coverage of micro crystals on quartz. Stephan Wolfsried photo. FOV = 2.5 mm.*

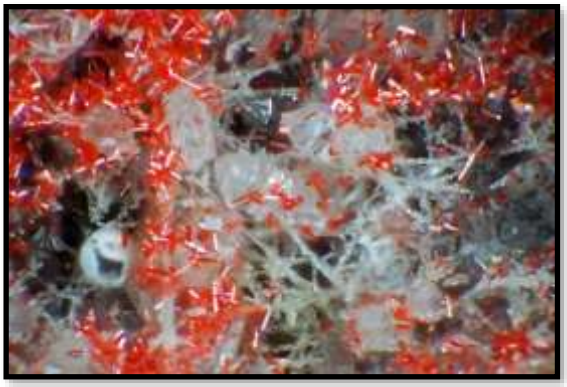

Figure 68. *Coverage of silica rods coated with cinnabar. FOV = 2 mm.*

Corderoite, α-$Hg_3S_2Cl_2$

Corderoite was discovered as a new mineral in 1973 by Dr. Eugene Foord in samples of mercury ore from the playa sediments adjoining the Cordero mercury deposit (Foord et al. 1974). A mercury compound of this composition was already known as a synthetic phase with three polymorphs distinguished by Greek letters α, β and γ (Puff and Küster 1962a, b, Carlson 1967). Corderoite corresponds to the cubic α polymorph (space group $I2_13$, a = 8.949 Å), whose crystal structure was refined by Frueh and Gray (1968). Detailed examination of residual mine rocks have yielded a few samples of a cubic mineral within individual cavities which were identified by PXRD methods as corderoite. These crystals exhibit {011} edge modifications and range in size from 25 to 50 um. Their color ranges from a dark brown to nearly jet black with an adamantine luster. Crystal intergrowths have been observed but are rare. Within the corderoite-rich breccia, cavities generally host cubic corderoite crystals associated with the Hg phase, MCDUK-3. Often cubic crystals of corderoite are observed attached to the surface of the above Hg phase.

The high-temperature β phase has also been found to be cubic (space group Pm-3n, a = 17.925 Å; Voroshilov et al. 1996). Recent examination of very fine-grained gray replacement products of cinnabar by PXRD methods have yielded diffraction lines of the three polymorphs of $Hg_3S_2Cl_2$, one of which is the beta polymorph, the first recorded occurrence in Nature. The metastable γ phase, monoclinic pseudo-orthorhombic, occurs as the mineral kenhsuite (see below).

At the McDermitt mine, corderoite is unusually abundant (~25% of the ore: McCormack 2000). It was determined to be a hypogene replacement of cinnabar, sometimes volume-for-volume, and its formation is likely due to a high activity of chloride in hydrothermal solutions (McCormack 1986). Corderoite occurs predominantly in Upper Miocene playa sediments, within a 5-7-meter-thick zone subparallel to bedding or as irregularly distributed discontinuous masses. Corderoite and cinnabar also occur within hydrothermally altered rhyolitic breccia, in the main Cordero mine and nearby underground workings and surface pits. Natural corderoite, when associated with cinnabar, occurs as grains less than 2 µm in diameter. These are light orange-pink when fresh, but upon exposure to sunlight, they become light gray to black.

Corderoite has also been noted as rhombic dodecahedra up to 5 µm across, with an unnamed Sb-Bi-Fe oxide, at the Paradise Peak mine in the Fairplay district, Nye County (Rytuba and Heropoulos 1992) and in the Gold Quarry mine in the Maggie Creek district, Eureka County, as globules coating a brecciated jasperoid with phosphate minerals such as variscite, and also intergrown with tiemannite as black spongy masses to 2 µm (Jensen et al. 1995). Other world localities for corderoite include France, Germany, Iran, Kyrgyzstan, Russia and Spain (Mindat.org).

Figure 69. *Typical example of freshly broken massive corderoite-bearing rock with high silica content and conchoidal fracture. FOV = 70 mm.*

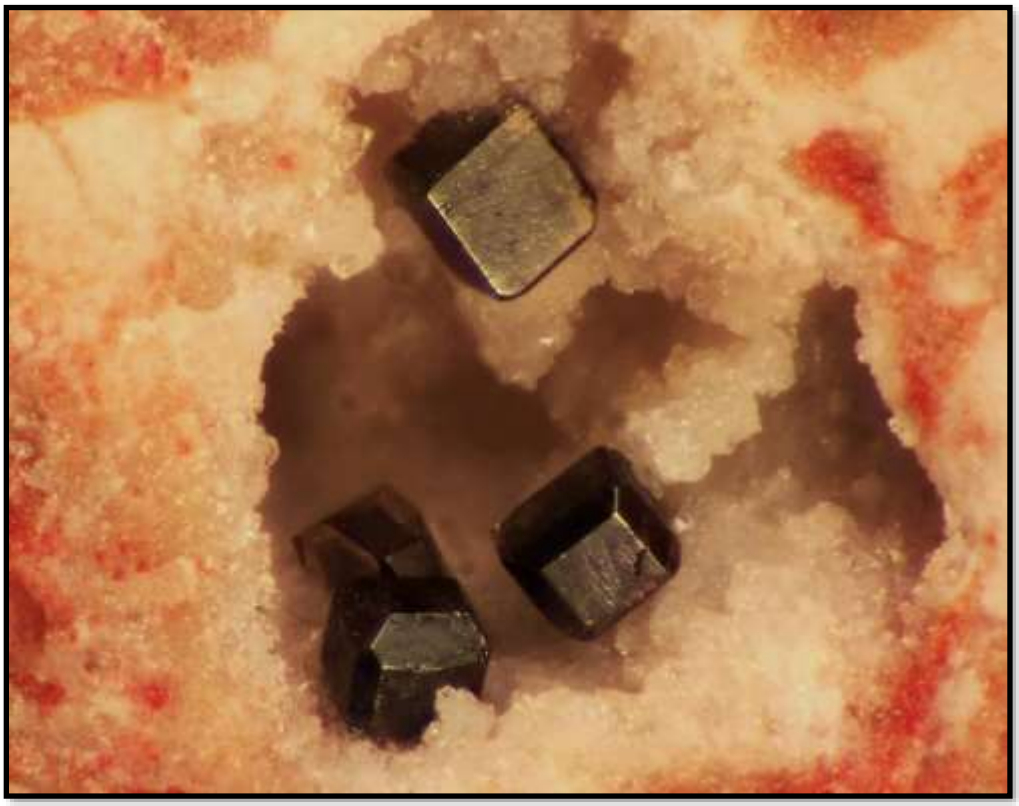

Figure 70. *Three modified cubes of corderoite within a cavity of silica. The {011} modifications can be seen on three of the crystals. FOV = 1 mm.*

Figure 71. *Massive, reddish-pink corderoite grains. FOV = 6 mm.*

Figure 72. *A group of dark brown modified corderoite crystals within a quartz-lined cavity. FOV = 2 mm.*

Figure 73. *Two larger modified dark brown corderoite crystals with about 20 lite brown smaller ones in the background. FOV = 2 mm.*

Figure 74. *Single cubic corderoite crystal in silica-lined cavity. Stephan Wolfsried photo. FOV = 2 mm.*

Figure 75. *Closeup of a single modified corderoite crystal in silica-lined cavity. Stephan Wolfsried photo. FOV = ~0.75 mm.*

Figure 76. *A group of prior cinnabar crystals replaced by corderoite on a quartz base. FOV = 1 mm. The crystals are coated (or replaced) with a dark gray/metallic phase have been identified as cinnabar. The core of these crystals are hollow with a highly reflective silvery phase, which was identified as corderoite. The crystals range in size from 0.5 to less than 0.1 mm. Some crystals show a pyramidal termination, while others show no crystal forms.*

Figure 77. *A single mass of minute cubic silvery corderoite crystals on quartz with a cinnabar substrate. FOV = 1 mm.*

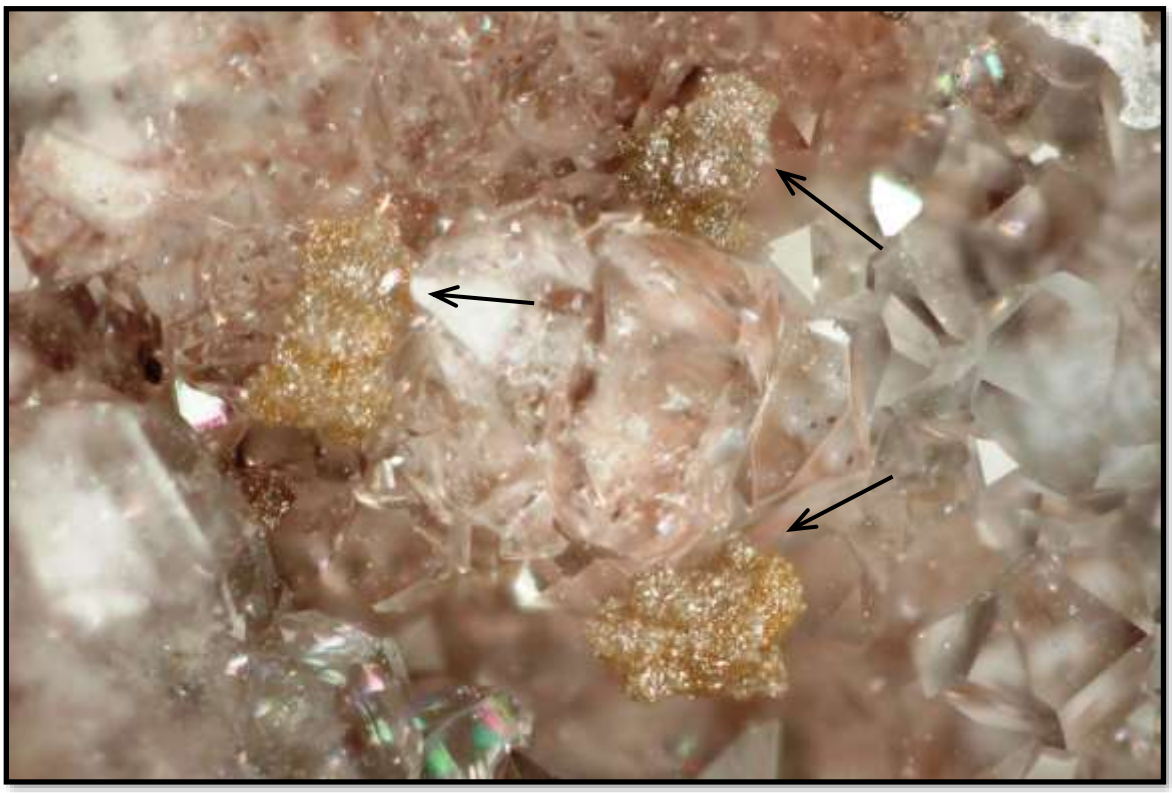

Figure 78. *Photo of three light tan groups of minute cubic corderoite crystals on quartz. FOV = 1 mm.*

Figure 79. *Elongated cavity hosting two red corderoite crystals. FOV = 2 mm.*

Figure 80. *View of a group of corderoite crystals with one attached to MCDUK-3. All of the corderoite crystals show the {011} edge faces. FOV = 2 mm.*

Figure 81. *View of both corderoite crystals and MCDUK-3 prisms. Note two corderoite crystals attached to individual MCDUK-3 prisms. Note one prism in upper right with a hexagonal outline at arrow. FOV = 2 mm.*

Figure 82. *A single corderoite crystal and two prisms of MCDUK-3 below it, on quartz. FOV = 1 mm.*

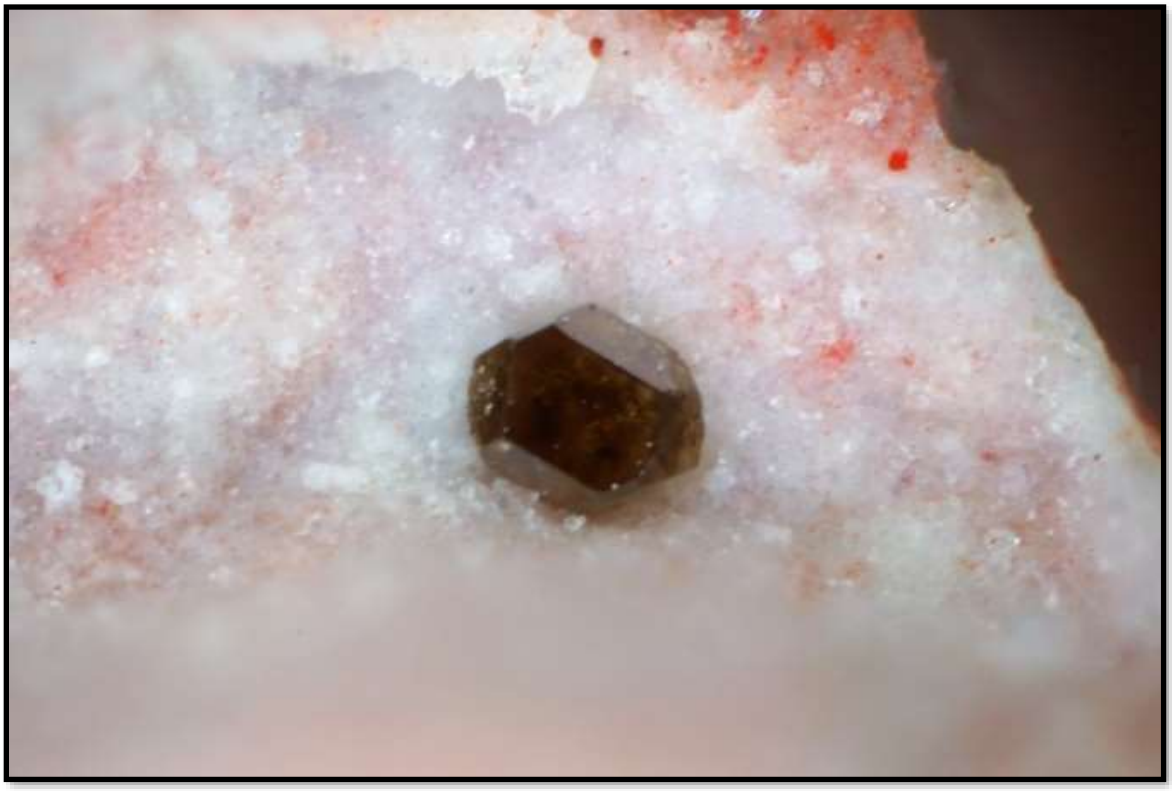

Figure 83. *A single corderoite crystal on quartz with {011} faces. FOV = 1 mm.*

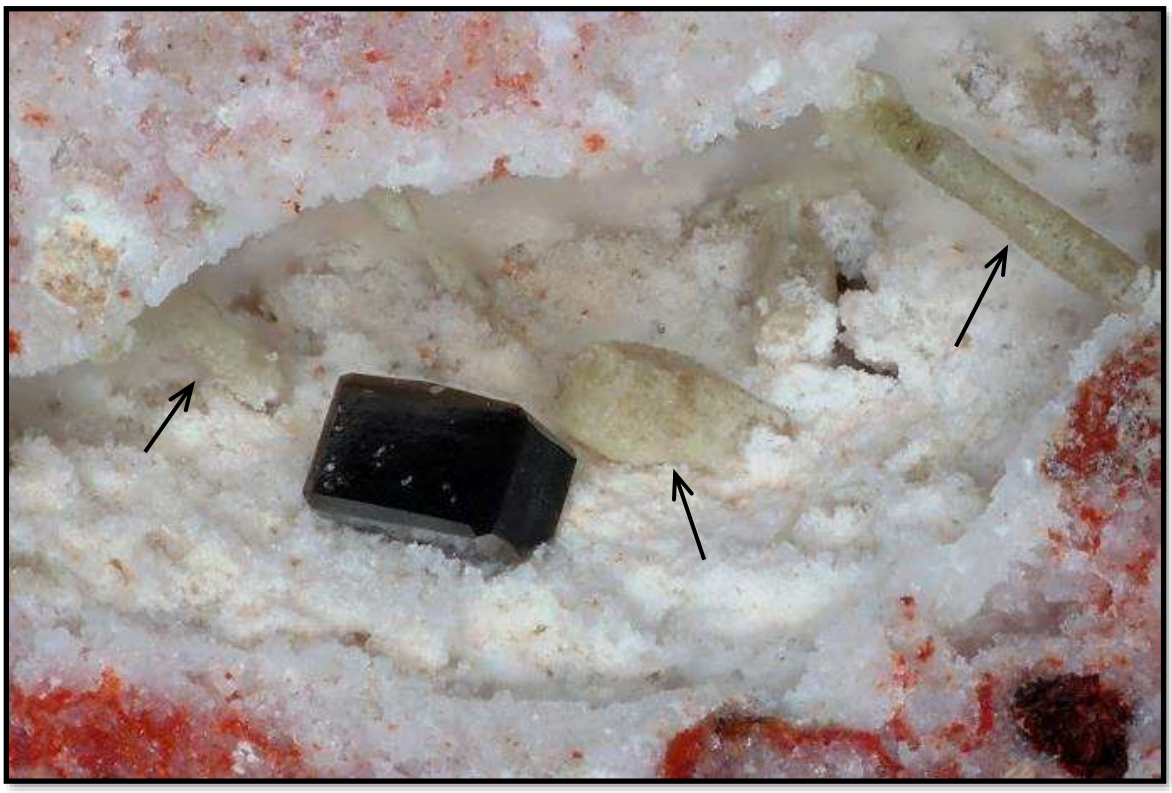

Figure 84. *Single modified dark brown corderoite crystal and three MCDUK-3 prisms. FOV = 2 mm.*

Figure 85. *View of single corderoite crystal and several MCDUK-3 prisms. Note the brown core of the prism at the arrow and the hexagonal outline. FOV = 2 mm.*

Figure 86. *View of a group of {011} modified corderoite crystals on quartz. FOV = 2 mm.*

Figure 87. *A single corderoite crystal on quartz showing {011} faces. FOV = 1 mm.*

Figure 88. *Silvery masses of minute corderoite crystals on quartz. FOV = 1 mm.*

Figure 89. *A closeup of the mass of individual corderoite crystals in Figure 77. FOV = 0.1 mm.*

Figure 90. *Three {011} modified corderoite crystals on quartz. FOV = 2 mm.*

Eglestonite, $Hg^{+}_{6}Cl_3O(OH)$

Very light yellow to water-clear eglestonite crystals up to several mm in size occur on rhyolite rock from the Cordero mine, associated with terlinguaite and calomel. It is also reported from the McDermitt mine associated with corderoite, cinnabar, liquid mercury and calomel (Yates 1942; McCormack 1986; Jenkins 1981). During our field studies, many additional samples were recovered containing veins and isolated masses of dark yellow eglestonite. Liquid mercury is often associated with the eglestonite as is MCDUK-17.

Figure 91. *Matrix sample showing black eglestonite. FOV = 30 mm.*

Figure 92. *Crystalline mass of eglestonite. FOV = 15 mm.*

Figure 93. *View of amorphous and crystal aggregates of eglestonite on quartz, especially upper right. FOV = 2 mm.*

Figure 94. *Surface coating of yellow eglestonite. FOV = 20 mm.*

Figure 95. *Surface coating of yellow eglestonite. FOV = 20 mm.*

Figure 96. *Black and yellow eglestonite. FOV = 2 mm.*

Kenhsuite, γ-$Hg_3S_2Cl_2$

Kenhsuite is the γ polymorph of $Hg_3S_2Cl_2$, and was already known as a synthetic phase (Carlson 1967). McCormack and Dickson (1998) recorded kenhsuite as orthorhombic with a *A*-centered lattice and *a* = 9.332, *b* = 16.82, *c* = 9.108 Å. However, (Ďurovič 1968) showed in his analysis of diffraction from γ-$Hg_3S_2Cl_2$ that the compound has a stacking-disordered intergrowth of two polytypes, both of which actually have monoclinic symmetry. One structure has space group (in standard setting) *C*2/*m*, *a* =16.82, *b* = 9.081, *c* = 9.328 Å, β ≈ 90°. The other polytype is *F*2/*m* with doubling of the 9.3 Å repeat. 'Compound I' (synthetic Br-rich kenhsuite) of Pervukhina et al. (2005) also has the pseudo-orthorhombic *C*2/*m* structure.

Kenhsuite was first described from the McDermitt mercury mine by McCormack and Dickson (1998) in small quantities from one location near the center of the open pit within montmorillonite and associated with cinnabar and corderoite. In addition, extremely fine grains of canary-yellow kenhsuite, with coarser cinnabar and corderoite, are dispersed in clay adjacent to fractures in argillized tuffaceous sedimentary rocks. Fibrous and bladed crystals 1 x 10 µm in length are typical.

Very fine grained kenhsuite was recently identified as a constituent of a gray replacement phase of cinnabar associated with equally fine grained corderoite and β-$Hg_3S_2Cl_2$ during this study. A single breccia rock sample from the surface area of the McDermitt mine was examined and found to contain multiple colorless prismatic crystals attached to quartz within several cavities. Cinnabar and corderoite was also noted within the rock. One sample was submitted for identification by PXRD. Due to the very small size of the individual crystals

(2µm × 80µm), no diffraction data was obtained. Single-crystal diffraction was also tried but, again, the resulting spots were not sufficient to obtain unit-cell data. EDS analysis of the crystals showed significant concentrations of Si, S, Cl, Hg and O. The Si was attributed to the underlying quartz matrix and ignored. Several samples were submitted for structure determination. The results indicated that these ultra-small crystals are indeed kenhsuite.

Excellent crystals of kenhsuite associated with corderoite have been recorded from the Oriental and San Francisco mines, El Hembrar, Chóvar, Castellón, Valencian Community, Spain (Vinals and Calvo 2007).

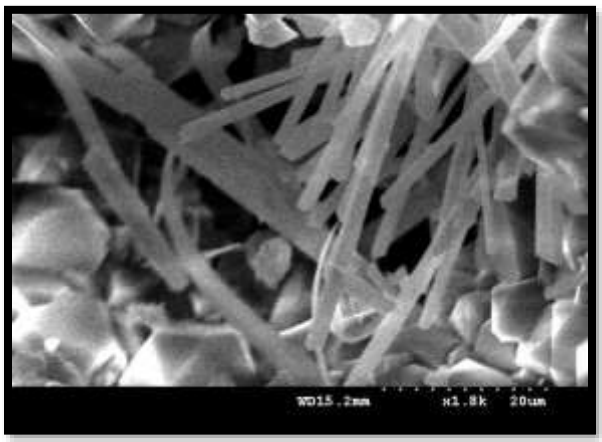

Figure 97. *SEM photo of colorless, acicular kenhsuite crystals within a quartz cavity in rock from Area 1.*

Figure 98. *Linear coverage of prismatic kenhsuite crystals. FOV = 2 mm.*

Figure 99. *Cavity containing acicular kenhsuite crystals on quartz. Stephan Wolfsried photo. FOV = 2 mm.*

Kleinite, $Hg_2N(Cl,SO_4)\cdot Nh_2O$

Kleinite has an unusual composition and structure in which a mercury nitride framework $[Hg_2N]^+$ with the topology of the high-tridymite form of SiO_2 is charge-balanced by 'zeolitic' anions (dominantly chloride) that occupy channels in the structure, along with some non-essential water molecules. The ideal formula is $[Hg_2N]Cl$; the more complex version above is from Giester et al. (1996).

Kleinite was discovered as fine, bright-yellow, hexagonal crystals in fractures in a light-brown opalite breccia, commonly associated with gypsum, from a small area in the southern part of the McDermitt pit and also the Cordero mine (McCormack 1986). The other nitride minerals terlinguacreekite and possible mosesite are also confined to the McDermitt mine, associated with kleinite and calomel. Coarse kleinite is sometimes overgrown by a second generation of platy kleinite crystals and/or terlinguacreekite (both identified by PXRD methods) in samples from the McDermitt mine.

Figure 100. *Surface covering of yellow-orange kleinite crystals on rhyolite. FOV = 40 mm.*

Figure 101. *Crystalline covering of orange-yellow kleinite. FOV = 30 mm.*

Figure 102. *Covering of yellow-orange kleinite on matrix. FOV = 30 mm.*

Figure 103. *Covering of delicate orange second-generation kleinite crystals. FOV = 3 mm.*

Figure 104. *Covering of orange and yellow kleinite crystals on dark matrix. FOV = 3 mm.*

Figure 105. *View of spherical groups of orange kleinite crystals. FOV = 2 mm.*

Figure 106. *Delicate array of fine colorless and scattered yellow-orange clusters of kleinite crystals. FOV = 3 mm.*

Figure 107. *Complex group of terminated light yellow kleinite crystals. FOV = 4 mm.*

Figure 108. *Group of kleinite crystals on quartz from the south end of pit. FOV = 16 mm.*

Figure 109. *A delicate group of kleinite with a "jackstraw" habit. FOV = 2 mm.*

Figure 110. Group of prismatic kleinite crystals on a calcite crystal. FOV = 2 mm.

Mercury, Hg

Liquid mercury occurs associated with cinnabar and with calomel and eglestonite in the deposit. It most likely formed from primary cinnabar by subsequent disproportionation. The reduction of Hg^{2+} to Hg^{o} is shown by the reaction: $HgS + 8OH^{-} \rightarrow Hg^{o} + SO_4^{2-} + 4H_2O + 6e^{-}$. It is recorded from the Cordero mine, associated with cinnabar and the mercury oxychlorides eglestonite and terlinguaite (Bailey and Phoenix 1944). Mercury occurs as isolated blebs, globules in extremely rich corderoite-cinnabar ore with calomel and eglestonite at the McDermitt mine and at the Cordero mine as tiny disseminated droplets with cinnabar and eglestonite (Fisk 1968; Roper 1976; McCormack 1986). Liquid mercury also occurs in association with both stibnite and cinnabar in isolated masses.

Figure 111. *Surface coating of mercury with cinnabar. FOV = 2 mm.*

Figure 112. *Coverage of mercury with cinnabar. FOV = 3 mm.*

Figure 113. *Droplets of liquid mercury on rock. FOV = 15 mm.*

Montroydite, HgO

Small acicular crystals of montroydite have been reported associated with liquid mercury in the ores of the McDermitt mine (Rytuba and Glanzman 1979). During our study of many samples containing mercury mineralization, a single sample was noted containing several spherical, hollow forms. Within these hollow forms are many prismatic reddish-brown crystals surrounded by crystals of eglestonite. No liquid mercury was observed in association with this find. Montroydite occurs as brownish-red, prismatic crystals within several hollow spheroids on a cavity lined with quartz crystals. Crystals of eglestonite occur surrounding each spheroid.

Figure 114. *View of a group of montroydite crystals on quartz. FOV = 2 mm.*

Figure 115. *Group of montroydite crystals surrounded by terlinguaite. FOV = 2 mm.*

Figure 116. *Group of montroydite crystals surrounded by terlinguaite. FOV = 1 mm.*

Mosesite, $Hg_2N(Cl,SO_4,MoO_4,CO_3)\cdot H_2O$

Mosesite is the cubic polymorph of kleinite, in which a framework $[Hg_2N]^+$ with the structure of the high-cristobalite form of SiO_2 is charge-balanced by 'zeolitic' anions (dominantly chloride) that occupy channels in the structure, along with some non-essential water molecules. The ideal formula is $[Hg_2N]Cl$; the more complex version above, showing non-essential components, is from Switzer et al. (1953).

Rytuba and Glanzman (1979) and McCormack (1986) tentatively identified mosesite from the ores of the McDermitt mine, associated with other secondary minerals such as calomel, eglestonite, and kleinite. No mosesite has been identified during this study of many samples collected at the mine and examined optically.

Radtkeite, $Hg_2S_2Cl(I)$

Radtkeite is an ordered chloride iodide sulfide of mercury, first found at the McDermitt deposit by McCormack et al. (1991). It was described by those authors as having a *F*-centered orthorhombic lattice. However, Pervukhina et al. (2004) refined the structure of synthetic radtkeite, and showed that it is in fact monoclinic pseudo-orthorhombic, with a crystal structure similar to that of the *F*2/*m* polytype of kenhsuite (see above).

Radtkeite occurs mostly as 2 µm grains and as finely dispersed grains, coatings, and prismatic crystals as long as 30 µm, some of which are hollow, in altered tuffaceous sediments (Figures 117, 118, 119). It was

discovered closely associated with quartz, cinnabar and corderoite at one location on the south margin of the present open McDermitt mine pit. Most commonly, radtkeite crystals are tabular prismatic, with combinations of orthorhombic pinacoids and prisms.

Radtkeite may have formed by the reaction of iodide-rich fluids with either kenhsuite or corderoite, as indicated by its common occurrence with corderoite (McCormack et al. 1991). Radtkeite darkens in sunlight to an orange-brown color and then to nearly black.

Samples of kleinite with an associated reddish-orange mineral have been erroneously identified as radtkeite. X-ray diffraction tests have shown that these reddish-orange grains are in fact the rare mineral terlinguacreekite. Many samples of yellow to orange kleinite have associated with a dull pale yellow phase that also has been erroneously identified as radtkeite. This pale yellow phase has been identified as a secondary generation kleinite. The probable location for radtkeite is known but it is covered with many tons of mine rock. It would take extensive work to uncover the zone where the radtkeite was first discovered. Radtkeite is extremely sensitive to UV light and turns from yellow to black within a short time period. This darkened phase could blend in with other black material common within the pit.

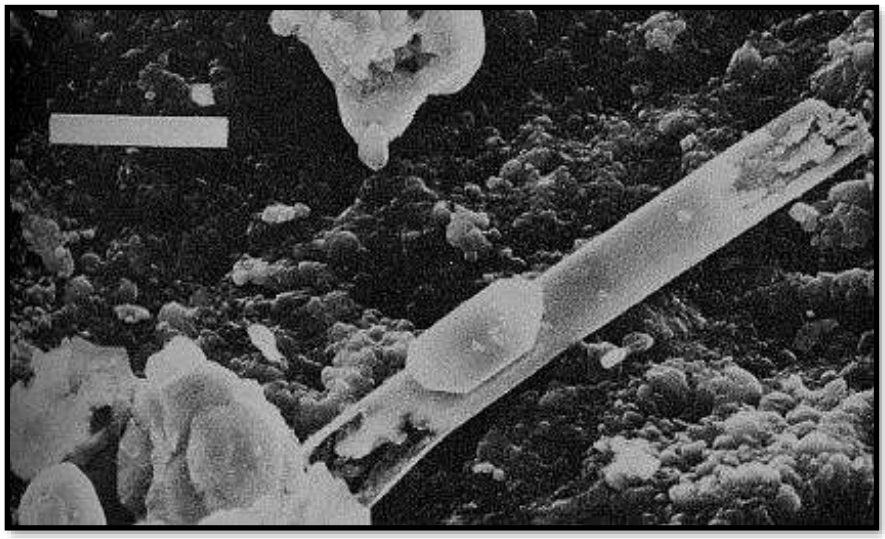

Figure 117. *SEM photo of prismatic radtkeite crystal with perched gypsum crystal. Bar scale = 10 microns. (after McCormick et al. 1991).*

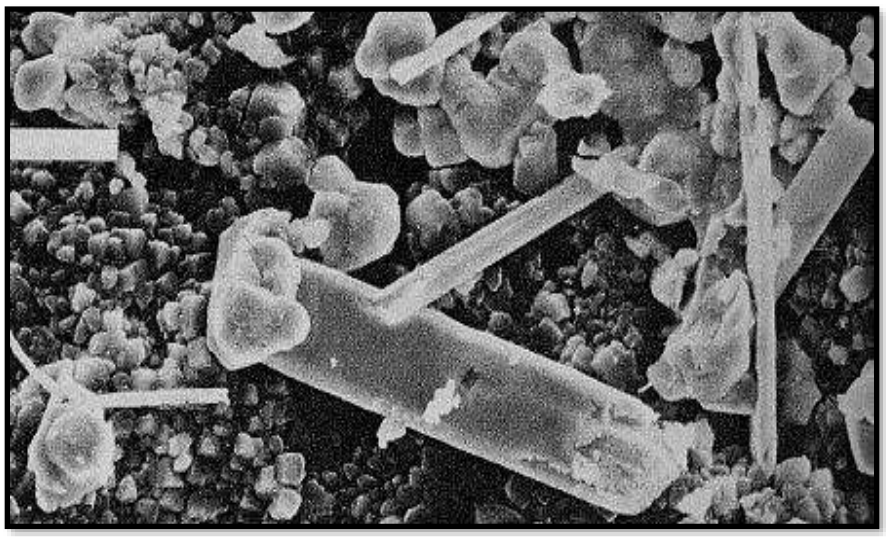

Figure 118. *SEM photo of prismatic radtkeite crystals and equant corderoite crystals on quartz matrix (after McCormack et al. 1991). Bar scale = 10 microns.*

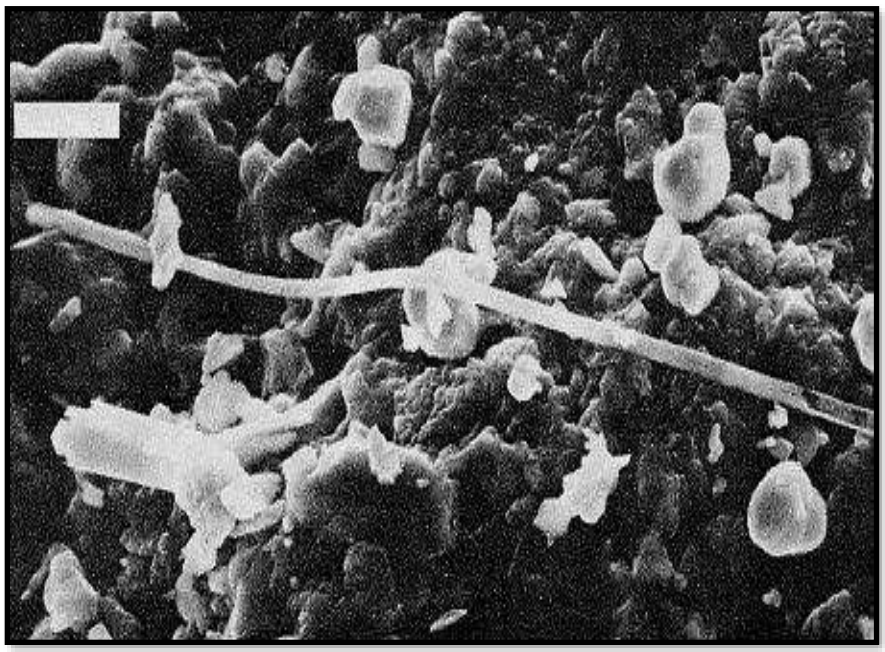

Figure 119. *SEM photo of tubular radtkeite crystal, capped on left end, on quartz matrix with equant white corderoite and prismatic radtkeite (after McCormack et al. 1991). Bar scale = 10 microns.*

Schuetteite, $Hg_3(SO_4)O_2$

Fine-grained yellow schuetteite has been reported as a coating on cinnabar from the Opalite mine as a coating on cinnabar, Malheur County, Oregon (Bailey et al. 1959; Jenkins 1981) and from the McDermitt mine as a light yellow, fine grained coating on a gray surface of breccia containing corderoite and cinnabar.

Figure 120. *Surface coating of fine-grained yellow schuetteite on cinnabar. FOV = 55 mm.*

Figure 121. *Surface coating of fine-grained yellow schuetteite on cinnabar. FOV = 35 mm.*

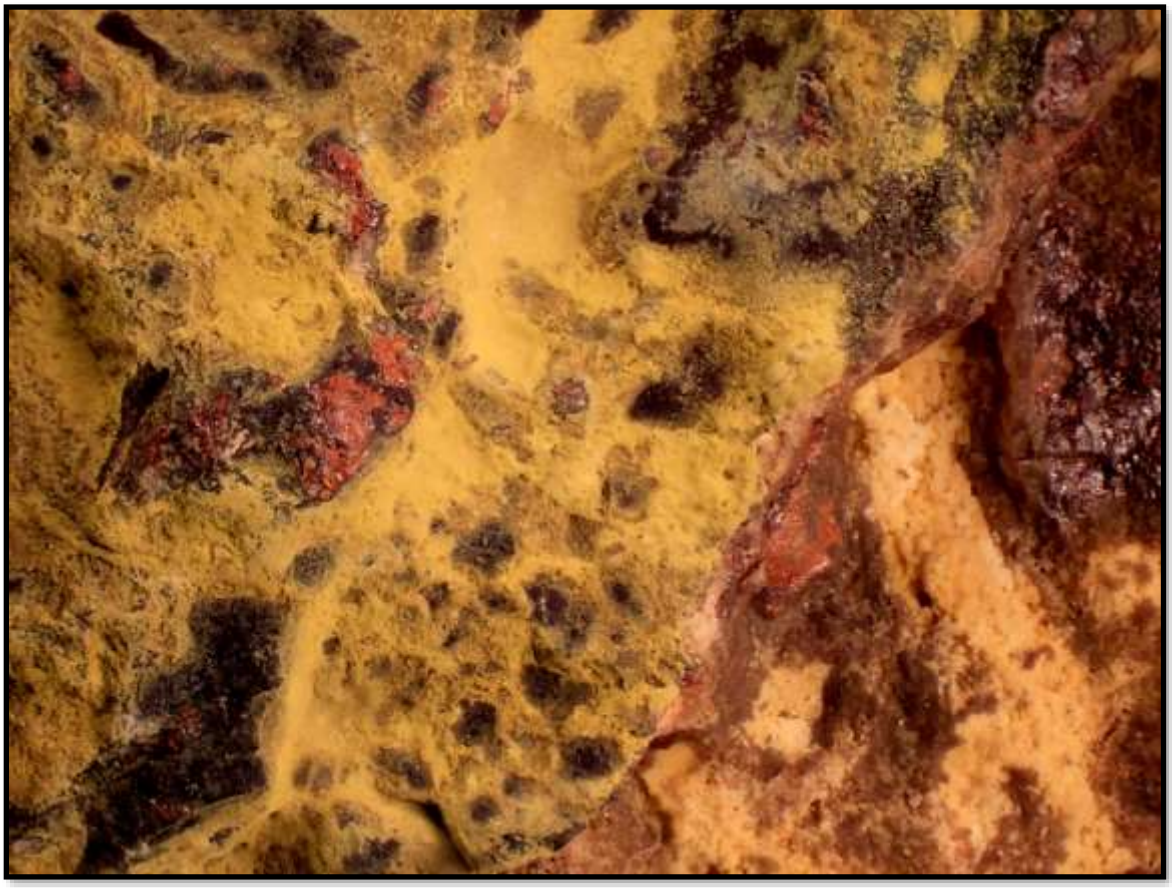

Figure 122. *Fine coating of yellow schuetteite on cinnabar. FOV = 3 mm.*

Figure 123. *Fine coating of yellow schuetteite on a silica hollow tube matrix. FOV = 6 mm.*

Shakhovite, $(Hg\text{-}Hg)^{2+}{}_2Sb^{5+}O_3(OH)_3$

This very rare mercury antimony oxide, verified by PXRD methods, was discovered in samples from a cinnabar-stibnite contact zone. Individual monoclinic crystals with an adamantine luster occur on quartz coated with an iron oxide (?). The crystals are emerald green with striations along the c axis. Associated with the shakhovite are abundant light brown rosettes of another similar phase, $(Hg\text{-}Hg)^{2+}{}_2Sb^{5+}{}_4O_{12}$, MCDUK-19, currently under study.

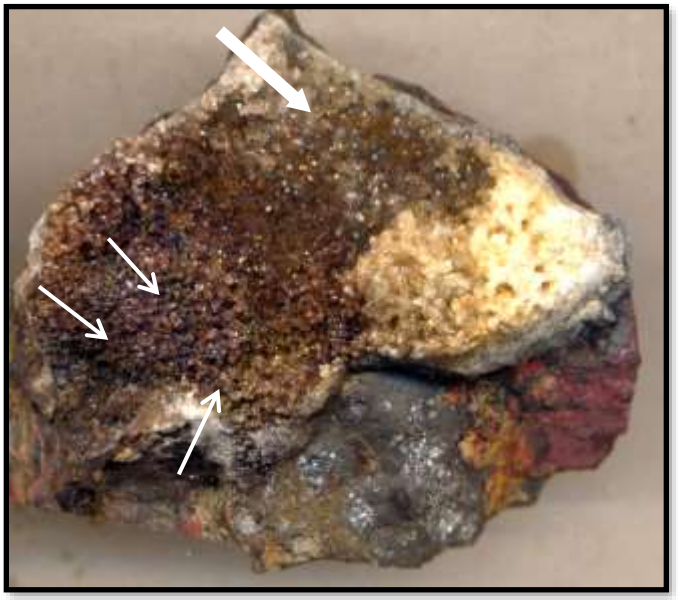

Figure 124. *Iron oxide coated quartz containing tiny multiple crystals of greenish-yellow shakhovite (not seen) at arrows. Area at upper block arrow contains multiple crystals of MCDUK-19. FOV = 45 mm.*

Figure 125. *Light greenish-yellow crystal of shakhovite on iron-coated quartz and silica tubes. FOV = 3 mm.*

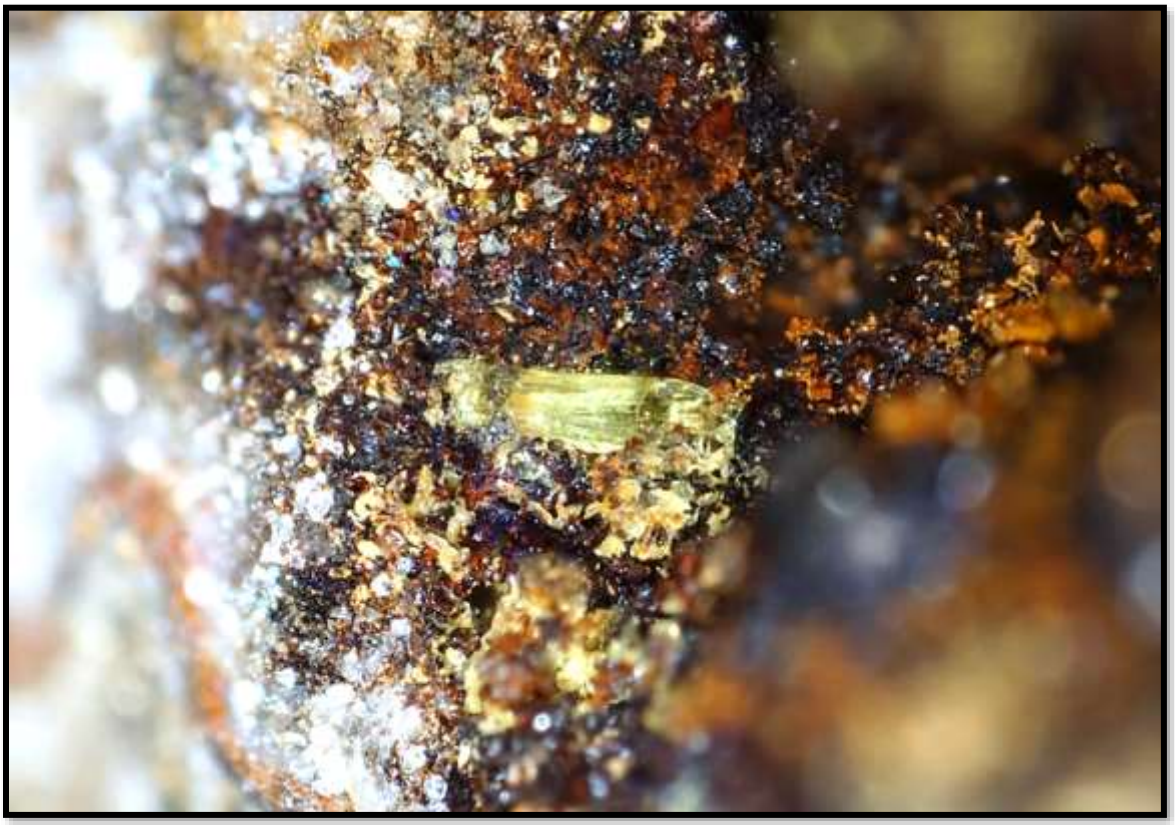

Figure 126. *Single crystal of light green shakhovite. FOV = 3 mm.*

Figure 127. *Multiple crystals yellow-green shakhovite on quartz. FOV = 2 mm.*

Figure 128. *Single crystal of shakhovite on quartz. FOV = 2 mm.*

Terlinguacreekite, $Hg^{2+}{}_3O_2Cl_2$

Rare terlinguacreekite, originally discovered at Terlingua, Texas, has been reported from the McDermitt mine, associated with kleinite and calomel in silicified volcanic rocks. It is photosensitive and changes from vivid orange to black in strong light, but this phenomenon is reversible. The color can vary from lemon yellow to dark orange to reddish orange. EDS tests show a small amount (< 3%) of Br in the analysis. Roberts et al. (2005) originally reported the formula of terlinguacreekite as $Hg^{2+}{}_3O_2Cl_2$, but preliminary Raman studies of terlinguacreekite suggest that it has nitrogen in the structure instead of oxygen, as is the case for comancheite (Cooper et al. 2013). Structure determination based on crystals of suitable quality (not twinned) will be

needed to establish the correct formula and structure for terlinguacreekite. So far attempts to find an un-twinned crystal to establish the formula have been unsuccessful.

Figure 129. *Cavity containing yellow kleinite and dark reddish-orange terlinguacreekite. FOV = 1 mm.*

Figure 130. *Group of dark reddish- orange terlinguacreekite crystals. FOV = 1 mm.*

Figure 131. *Red complex terlinguacreekite crystal and yellow kleinite crystals. FOV = 1 mm.*

Figure 132. *View of minute orange terlinguacreekite crystals. FOV = 3 mm.*

Figure 133. *Orange coating of terlinguacreekite on matrix. FOV = 3 mm.*

Figure 134. *Single reddish-orange terlinguacreekite crystal on quartz. FOV = 1 mm.*

Figure 135. *Terlinguacreekite beneath quartz. FOV = 1 mm.*

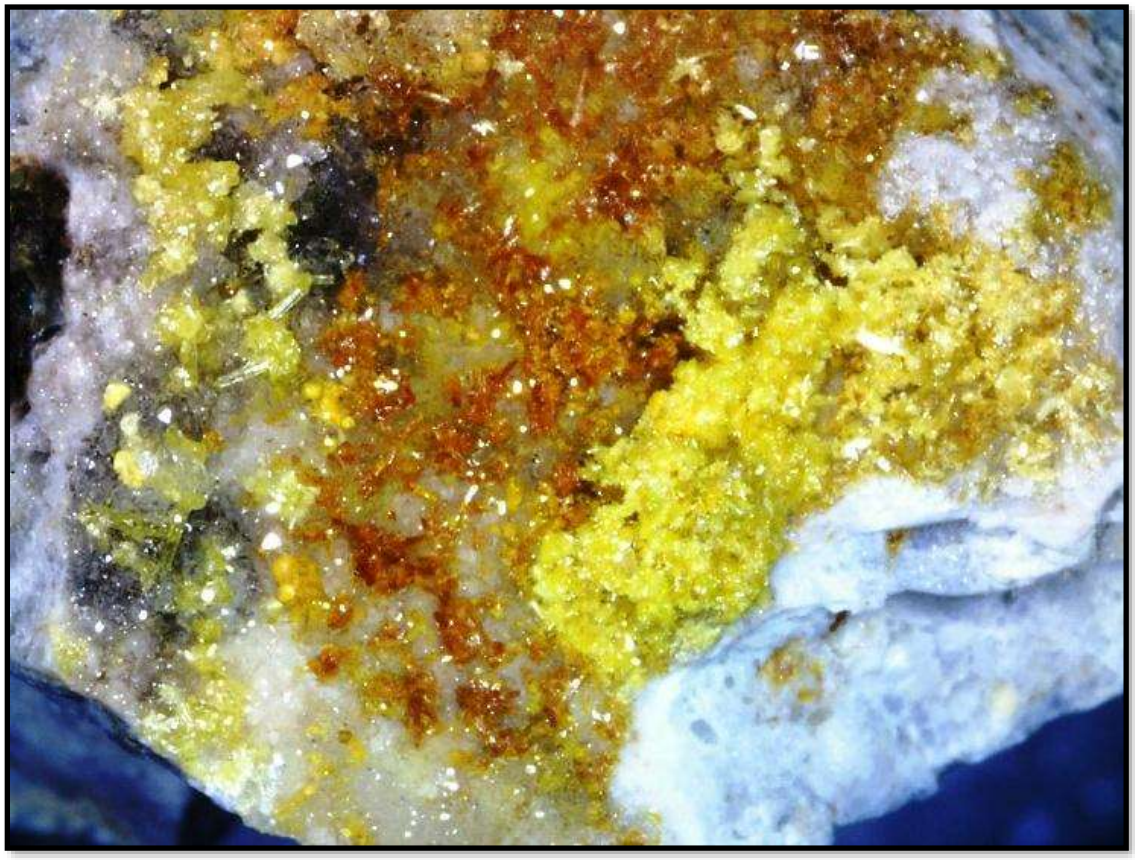

Figure 136. *View of yellow kleinite crystals and orange terlinguacreekite crystals on quartz. FOV = 4 mm.*

Figure 137. *A single orange terlinguacreekite crystal next to a long MCDUK-3 prism. FOV = 1 mm.*

Figure 138. *Coverage of terlinguacreekite crystals (orange) and kleinite (yellow) on quartz. Stephan Wolfsried photo. FOV = 2.5 mm.*

Figure 139. *Terlinguacreekite pseudomorph after kleinite on quartz. FOV = 1.3 mm.*

Figure 140. *Divergent group of terlinguacreekite pseudomorph after kleinite on quartz. FOV = 5mm.*

Figure 141. *Sample showing coverage of terlinguacreekite crystals. FOV = 45 mm.*

Figure 142. *Sample showing grouping of terlinguacreekite crystals on matrix. FOV = 15 mm.*

Figure 143. *Terlinguacreekite pseudomorphs after kleinite on calomel. FOV = 5 mm.*

Figure 144. *Higher magnification of above sample of terlinguacreekite crystal group. FOV = 25 mm.*

Figure 145. *Pocket containing multiple groups of terlinguacreekite crystals on amorphous calomel on drusy quartz. FOV = 65 mm.*

Terlinguaite, $[Hg_3]^{4+}Hg^{2+}O_2Cl_2$

Terlinguaite is a mixed-valence mercury oxychloride containing unusual triangular clusters of mercury atoms $[Hg_3]^{4+}$ (Brodersen et al. 1989). It has been noted with eglestonite, cinnabar and Hg in ore in tuffaceous sedimentary rocks at the McDermitt and Cordero mines (Jenkins 1981; F. Cureton pers. comm. 1999). Terlinguaite occurs with liquid mercury at the Opalite mine, as canary-yellow powder which rapidly turns green and then black (Yates 1942). It also occurs with photosensitive cinnabar, calomel and an Hg-S-Cl mineral, probably corderoite, at the Opalite mine (McCormack 2000).

Recently, greenish-yellow grains of terlinguaite were noted associated with quartz in the contact zone of cinnabar and stibnite. The terlinguaite was identified by PXRD as 0.1 mm grains embedded between quartz crystals associated with rare green shakhovite crystals and several other phases not immediately identified. Additional samples were recovered which showed abundant coverage of terlinguaite crystals within cavities. These crystals exhibited multiple forms and elongated along [010]. Colorless cubic interpenetrating crystals of fluorite were confirmed coating some of the terlinguaite crystals. Samples of terlinguaite associated with eglestonite are very rare.

Figure 146. *Terlinguaite crystals covering iron-stained cavity. FOV = 40 mm.*

Figure 147. *Covering of terlinguaite crystals on quartz-cinnabar matrix. FOV = 45 mm.*

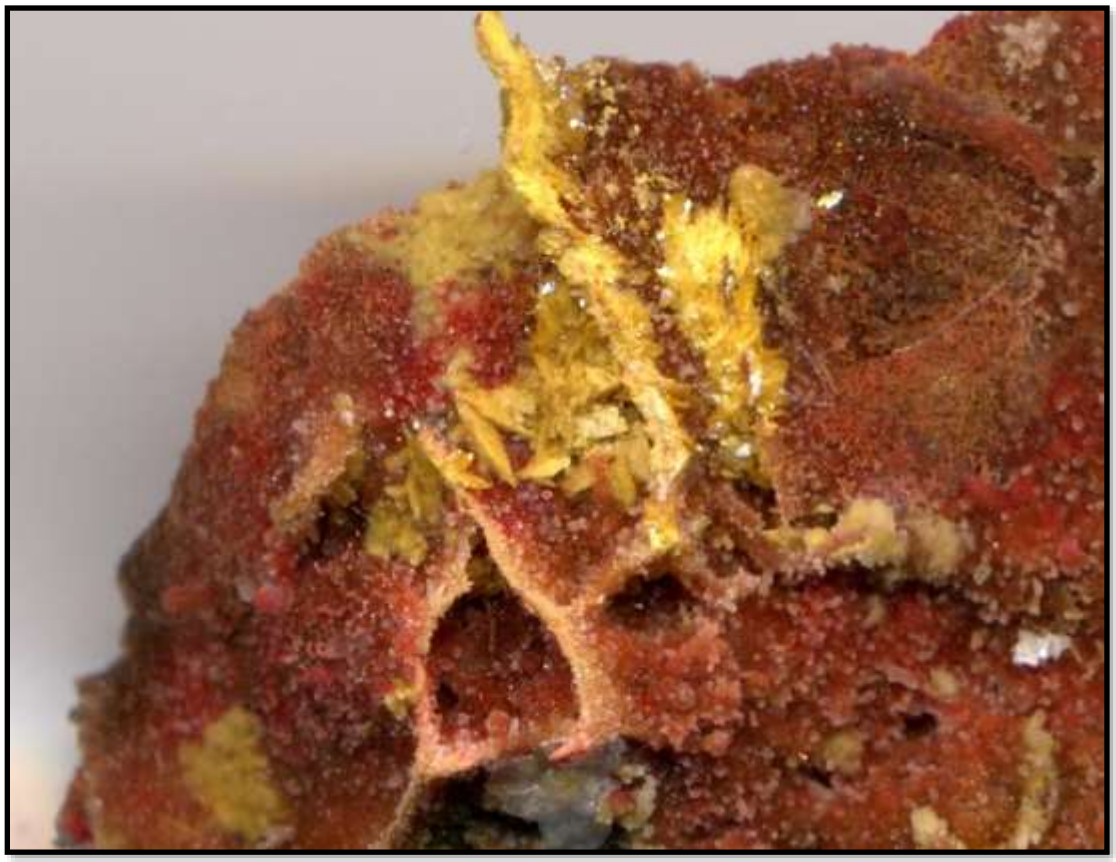

Figure 148. *Parallel groups of terlinguaite crystals on quartz matrix. FOV = 15 mm.*

Figure 149. *Covering of complex terlinguaite crystals on quartz matrix. FOV = 30 mm.*

Figure 150. *Coverage of terlinguaite crystals on iron-stained quartz. Note groups of white fluorite crystals in upper center. FOV = 50 mm.*

Figure 151. *Terlinguaite crystals, LED light, false color. FOV = 4 mm. Photo taken with Keyence VHX-5000 digital microscope, courtesy of Keyence Corp. and Chris DeRenzi. Compare to Figure 153.*

Figure 152. *Blade-like terlinguaite crystals. FOV = 4 mm.*

Figure 153. *Green-yellow crystals of terlinguaite. FOV = 4 mm.*

Figure 154. *Group of blocky terlinguaite crystals on quartz. FOV = 2 mm.*

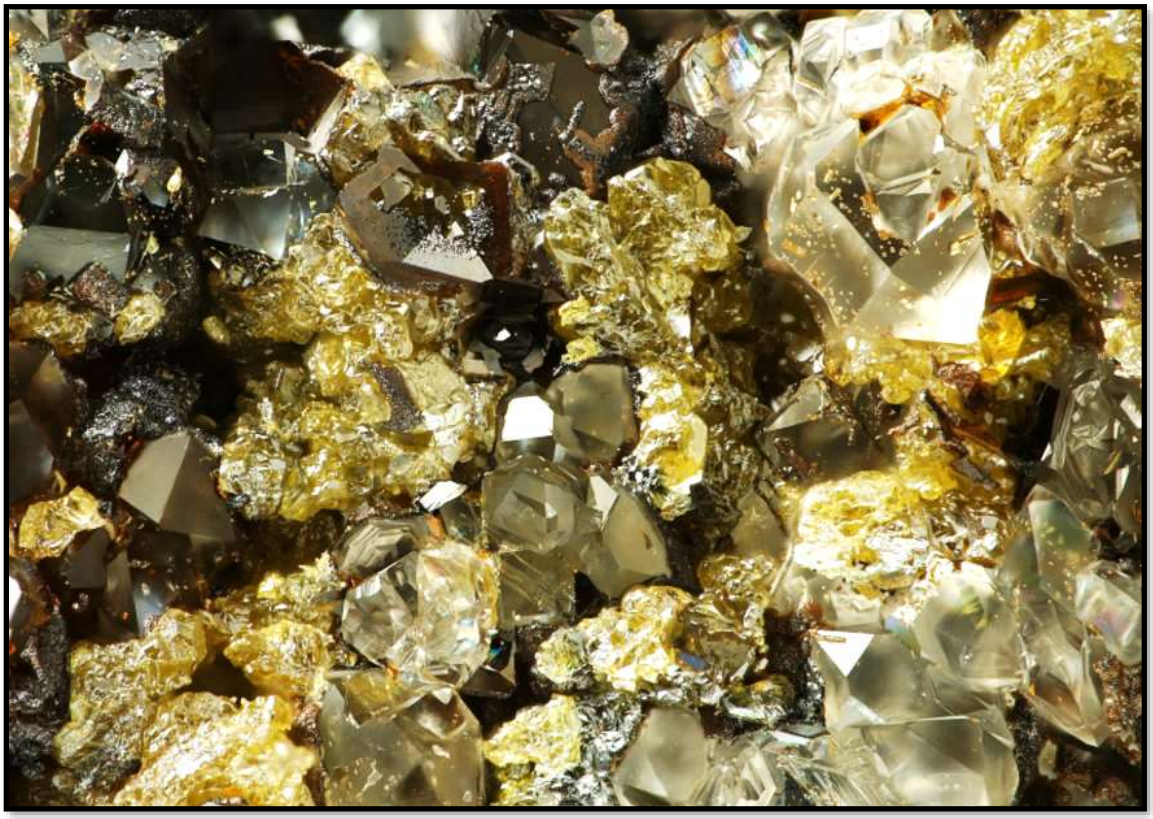

Figure 155. *Scattered grains of dark yellow terlinguaite on quartz. Stephan Wolfsried photo. FOV = 2.5 mm.*

Figure 156. *Scattered grains of dark yellow terlinguaite on quartz. Stephan Wolfsried photo. FOV = 2.5 mm.*

Figure 157. Greenish-yellow equidimensional group of terlinguaite crystals on quartz. FOV = 2 mm.

Unknown Phases

The following unknown phases are listed in order as they were observed during the examination process of mine samples. Sample photographs were made of each phase as appropriate and then submitted for further testing. Depending on the physical condition of the specific phase, descriptive data was obtained and recorded. A number of these phases have been determined to be known minerals and are so designated below.

MCDUK-1 = Kenhsuite

MCDUK-2, $(Hg^{2+})_3S^{2-}{}_2(MoO_4)$

Several dull cream-colored micro crystal groups were noted within quartz-lined cavities in a cinnabar and corderoite-rich breccia collected from Area 1. A PXRD of this crystal group did not match any known phase. An EDS of a crystal group gave major Hg, S and oxygen with values of 71.57% HgO and 28.43% SO_3, giving $HgSO_4$. Subsequent structure analysis has indicated that Mo occurs in the structure and the formula has been revised to reflect the Mo. This same phase was noted filling micro voids within the same breccia. A SEM photomicrograph of these groups revealed they are compose of a mass of elongated crystals with sloped terminations. The crystals have average dimensions of 10um x 1um x 0.05um. Figures 158 through 161 illustrate this new mercury phase.

A preliminary structure determination of a single crystal (R=3%) gave an orthorhombic-P cell in space group Pmnb with a = 6.97Å, b = 8.03Å, c = 12.97Å. Z = 4.

Figure 158. *A white mass of MCDUK-2 crystals attached to quartz. FOV = 1 mm.*

Figure 159. *A white mass of MCDUK-2 crystals on quartz. FOV = 1 mm.*

Figure 160. *A white mass of very fine, acicular crystals of MCDUK-2 attached to quartz. FOV = 1 mm.*

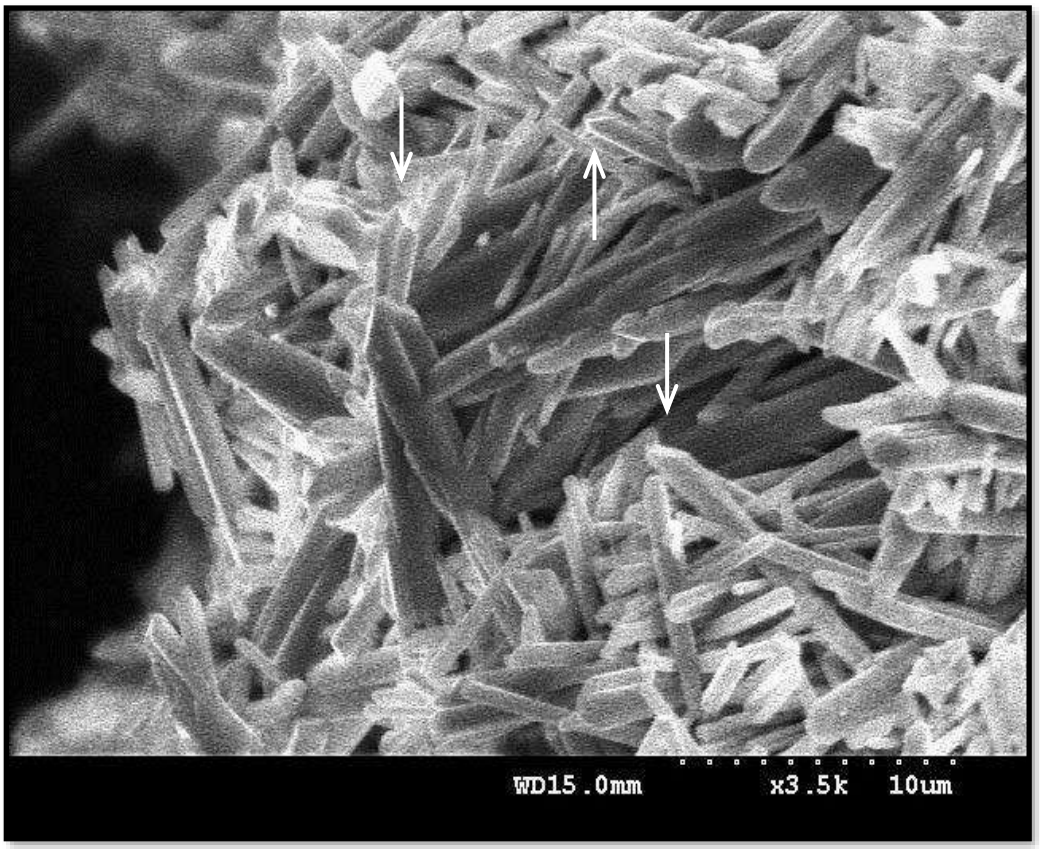

Figure 161. *SEM photo of MCDUK-2 showing the prismatic habit and end termination (arrows).*

MCDUK-3, $Hg^{2+}_3S_2(SO_4,MoO_4)$

Many of the fine-grained quartz-lined cavities in the corderoite-quartz breccia contain greenish-yellow, pseudo hexagonal prisms. These prisms extend from the cavity surface outward or along the cavity surface. Color variations are evident ranging from a greenish-yellow to red to black. The surfaces of these prisms are covered with minute corderoite crystals that are responsible for the change in color when exposed to light. When broken, a dark brown core is revealed. Branching is common among the prisms. The preliminary cell is monoclinic twinned with beta of 120o in P2 about a 2-fold axis. Cell data is: a=12.6406Å, b=7.7455Å, c=12.6383Å, beta=120.004o, V=1071.57Å3. No structure details have been established to date.

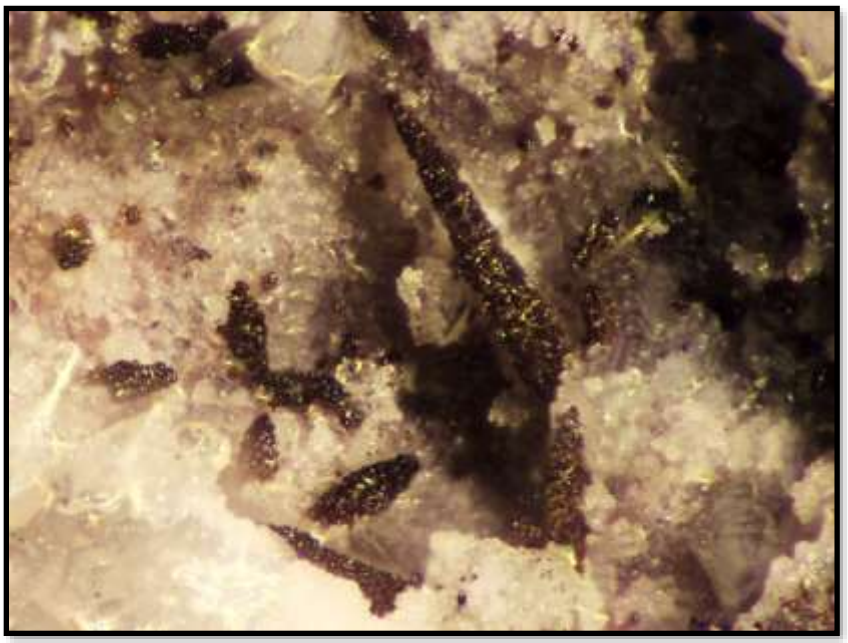

Figure 162. *Group of dark brown MCDUK-3 prisms on quartz covered with minute corderoite crystals. FOV = 1 mm.*

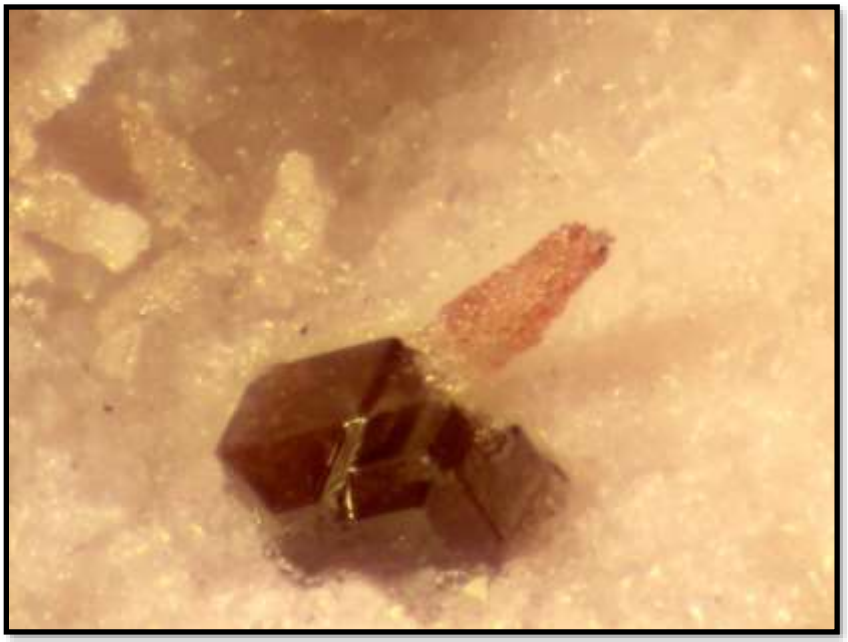

Figure 163. *Multiple crystals of corderoite attached to prism of MCDUK-3 on quartz; other colorless prisms in background FOV = 1 mm.*

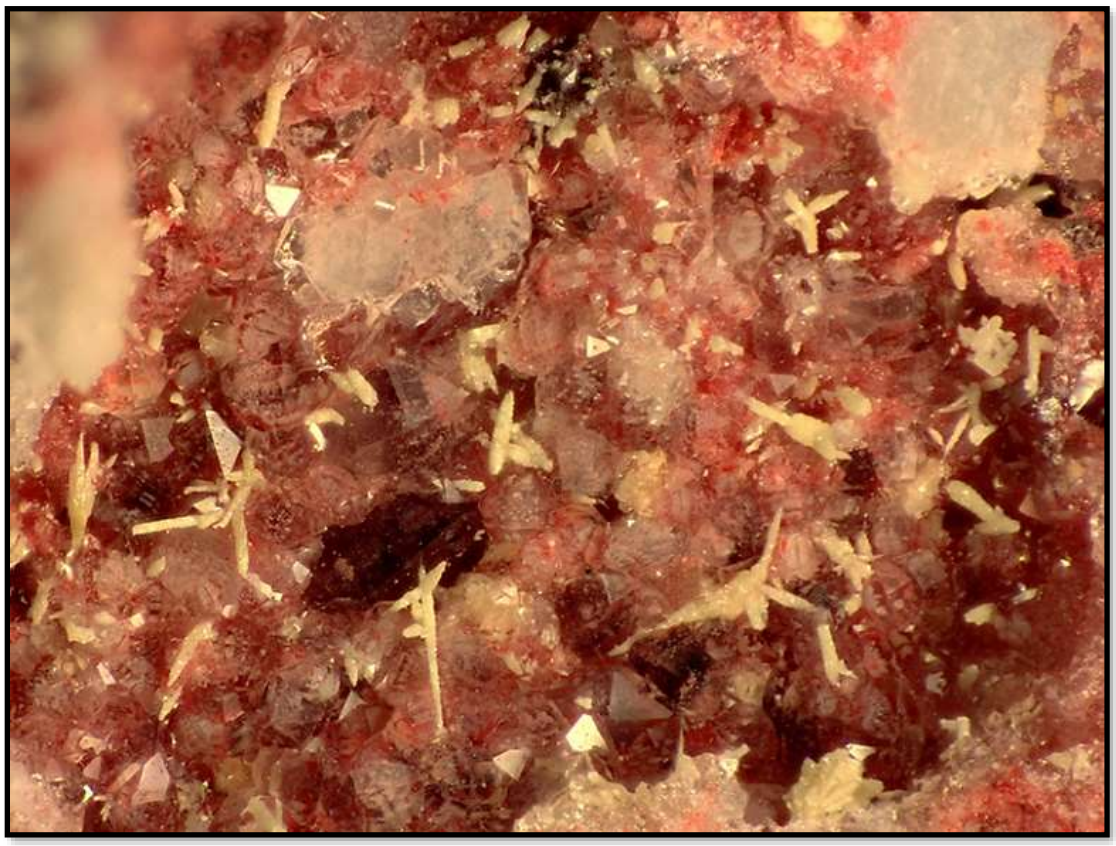

Figure 164. *Group of divergent MCDUK-3 prisms on quartz with underlying cinnabar. FOV = 1 mm.*

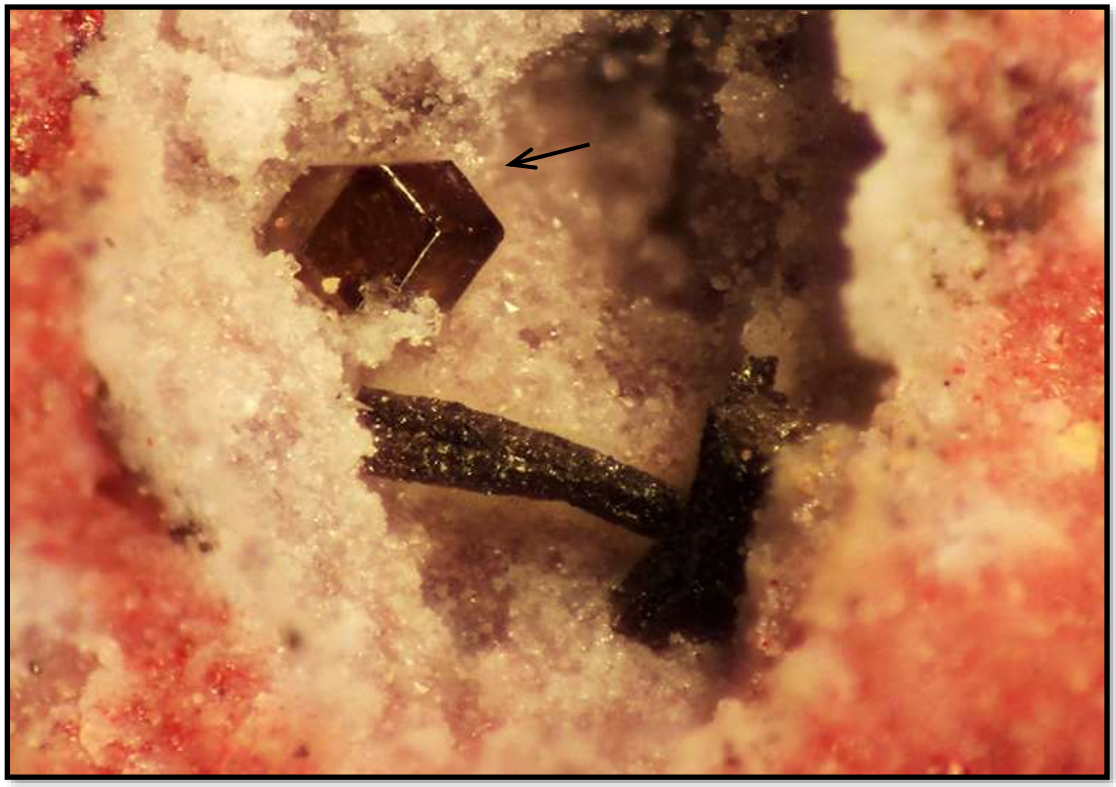

Figure 165. *Two prisms of MCDUK-3 with a single cubic corderoite crystal (arrow). FOV = 1 mm.*

Figure 166. *Several prisms of MCDUK-3 on quartz. Note dark zones along the prism length and deep red tip on one prism (arrow). FOV = 1 mm.*

Figure 167. *Single yellow prism of MCDUK-3 on quartz. FOV = 1 mm.*

Figure 168. *Large group of MCDUK-3 prisms with black tips on quartz with cinnabar. FOV = 2 mm.*

Figure 169. *Quartz surface showing prisms of MCDUK-3 with red corderoite coatings. Some have turned black. Note the off-white prisms of MCDUK-3 at arrow. FOV = 1 mm.*

Figure 170. *Quartz surface showing red coating of corderoite over prisms of MCDUK-3. FOV = 2 mm.*

Figure 171. *View of a group of greenish-gray MCDUK-3 prisms with a hexagonal outline showing a dark brown core (arrow) with a single dark brown corderoite crystal (arrow). FOV = 2 mm.*

Figure 172. *Several MCDUK-3 prisms, one showing dark brown core. FOV = 2 mm.*

MCDUK-4 = Corderoite

MCDUK-5 = Lithiophorite

MCDUK-6 = Corderoite

MCDUK-7 = $C[Hg^{2+}]_4OCl_2$

A single sample was identified from Area 2 containing a vug that hosted several black, highly reflective prismatic, bladed crystals. The host rock may be characterized as a very fine, light brown associated with a light pink fine-grained phase, possibly corderoite. Within this rock type are cavities hosting crystals of orange terlinguacreekite. The new phase is in intimate contact with the terlinguacreekite but the time position is not clear. Both phases show no sign of surface attack or alteration. Kleinite in massive, fine-grained layers also occurs within this rock type. This host rock suggests that it formed along the border between the typical corderoite breccia and a lighter silica rock rich in terlinguacreekite and kleinite.

The size of this new phase is less than 0.1 x 0.05 mm. Structure X-ray data suggests that this phase is a complex organometallic mineral. This is the first organometallic phase observed from this deposit and in nature with a single carbon in the structure. This phase has been identified as a derivative of Hofmann's Base [$CHg_4O(OH)_2OH_2$] and may have been formed by the action of Hg^{2+} ions on an earlier unknown aliphatic organic compound. No evidence has so far been noted on the original organic phase. (Breitinger et al. 1983; Grdenić et al. 1974, 1996; Kapustin 2010; Milić et al. 2009; Miles et al. 1968).

The new natural organometallic phase is monoclinic, space group $P2_1/n$. a=10.164Å, b=10.490Å, c=6.547Å, beta = 90.037°. It is a near merohedral twin emulating orthorhombic at R = 1.8%. The basic structure shows that oxygen is 3-coordinated and only half of the Cl ions are part of the structural unit. The highly corrugated layers, in which Hg atoms are bridges in a honeycomb net of 3-connected alternating C and O anions. This structure description is the first experimental confirmation of the existence of the layer topology predicted for Hofmann's base by Milić et al. (2009). Also, this is the first evidence that Hg^{2+} in nature can react with aliphatic organics, cleaving C-C bonds to produce Hg-C bonds. Figures 173 through 177 illustrate this new mercury phase.

Figure 173. *Single sample showing two very small crystal groups of black MCDUK-7 (arrows) associated with orange terlinguacreekite. FOV = 10 mm.*

Figure 174. *View of several black prismatic crystals of MCDUK-7. FOV = 1 mm.*

Figure 175. *A group of prismatic MCDUK-7 crystals.*

Figure 176. *Depression showing several complex crystals of MCDUK-7.*

Figure 177. *Group of prismatic MCDUK-7 crystals in depression.*

MCDUK-8 = Lithiophorite

MCDUK-9 = Corderoite + fluorite

MCDUK-10 = Corderoite

MCDUK-11 = Kleinite

MCDUK-12 = Corderoite

MCDUK-13 = Conichalcite

MCDUK-14 = Cryptomelane

MCDUK-15 = Valentinite

MCDUK-16

A single sample was recovered from Area 3 containing a pocket lined with quartz druse. The surface hosts several groups of very small divergent yellow prismatic crystals associated tiny colorless cubic corderoite crystals. No analysis has been performed on this phase.

Figure 178. *Scattering of divergent groups of MCDUK-16 crystals on quartz and with colorless cubic corderoite. FOV = 1 mm.*

MCDUK-17

Several samples from the stibnite vein (Area 4) show a bright yellow, platy mineral resembling orpiment. It is associated with cinnabar, eglestonite and mercury. Preliminary data gives a hexagonal cell with a = 5.84 and c = 29.08 A. A single sample was extracted from a group of rocks representing a segment of the stibnite/cinnabar locality. EDS shows a new phase containing Hg-S-O. Specifically, the sample is a highly silicified vein rock with massive cinnabar and cavities hosting quartz crystals. Within several of these cavities are brilliant yellow-orange platy crystals, many standing up. Some have a red color near the top termination. The habit and color resembles MCDUK-17, but are of a much better quality and size. Also within this sample are blebs of liquid mercury and massive yellow eglestonite.

Figure 179. *A mass of hexagonal MCDUK-17 crystals. FOV = 2 mm.*

MCDUK-18 = Shakhovite

MCDUK-19

Initial EDS and structure data show a new phase, $(Hg\text{-}Hg)^{2+}{}_2Sb^{5+}{}_4O_{12}$. On a single sample containing a surface of quartz crystals, many minute crystals with a hexagonal outline occur associated with shakhovite.

These minute crystals are light tan in color and occur as rosettes. Preliminary cell data gives a = 5.27Å, c = 14.97Å with a structure in hex-P at R = 4%. Structure shows Hg+ with Sb^{5+} octahedrally coordinated. The Hg-Hg units have displayed 3 medium distances O atoms off the Hg ends rather than the more typical near linear O-Hg-Hg-O connectivity. The variable Hg-Hg spacing of the Hg^{+}-Hg^{+} dimers may be responsible for the cell c-axis doubling.

Figure 180. *A large group of hexagonal, light tan MCDUK-19 crystals on quartz associated with shakhovite on the same sample. FOV = 2 mm.*

MCDUK-20 = Terlinguaite

MCDUK-21

No PXRD match was found for this mineral. EDS shows Hg-S-O. On a single sample a light gray-green phase was noted with some crystalline features. Preliminary cell data gives a = 9.68, b = 9.98, c = 17.14 in an orthorhombic setting. Only three samples found, one is remaining. No further work has been done on this sample.

Figure 181. *Gray-green mass of MCDUK-21 at arrows. FOV = 0.5 mm.*

MCDUK-22 = Terlinguaite

MCDUK-23

This unknown mercury-bearing phase was first noted in samples from Area 4, where rich samples of cinnabar, stibnite, and pyrite were recovered. A region of this site has been subjected to local oxidation by fluids, resulting in several new mercury phases, this being one of them. This phase is currently under study in Spain.

Refinement of the structure is essentially complete at R=4.6% in Fmmm and supports simple $Hg_3S_2Cl_2$ formula. Note that the Hg6 and Hg7 sites are each half-occupied. Also, the Hg4 and Hg5 sites were originally held on special positions 16k and 16j respectively, but showed greater ADP behavior; therefore, we relaxed these positions as disordered general positions [i.e. local Hg4,5 ordering about S2]. The reflections 004, 022 and 111 are suppressed as they partially hide behind the beam stop and have Fo way too low in relation to Fc. The refinement files are Fmmm [.lst .res .cif]. The single-crystal raw data frames were combined into precession slices to provide a good visual rendering of all diffraction; i.e. what lies between integrated diffraction maxima). The included 3KL slice shows streaking along c*, and presumably this streaking and half-occupied Hg sites are a similar OD behavior also observed for syn-kenhsuite structure.

Figure 182. *Colorless to pale yellow MCDUK-23 crystal groups on quartz. FOV = 2 mm.*

Figure 183. *Colorless to pale yellow MCDUK-23 crystal groups. FOV = 2 mm.*

Figure 184. *Group of pale yellow MCDUK-23 crystals. FOV = 3 mm.*

Figure 185. *Side view of MCDUK-23 crystals on matrix. FOV = 3 mm.*

Figure 186. *Surface covering of MCDUK-23 crystals on matrix and small orb of an unknown mineral. FOV = 3 mm.*

Figure 187. *Surface coating of minute colorless corderoite crystals with a cinnabar under coating. MCDUK-23 was identified on the same sample. FOV = 2 mm.*

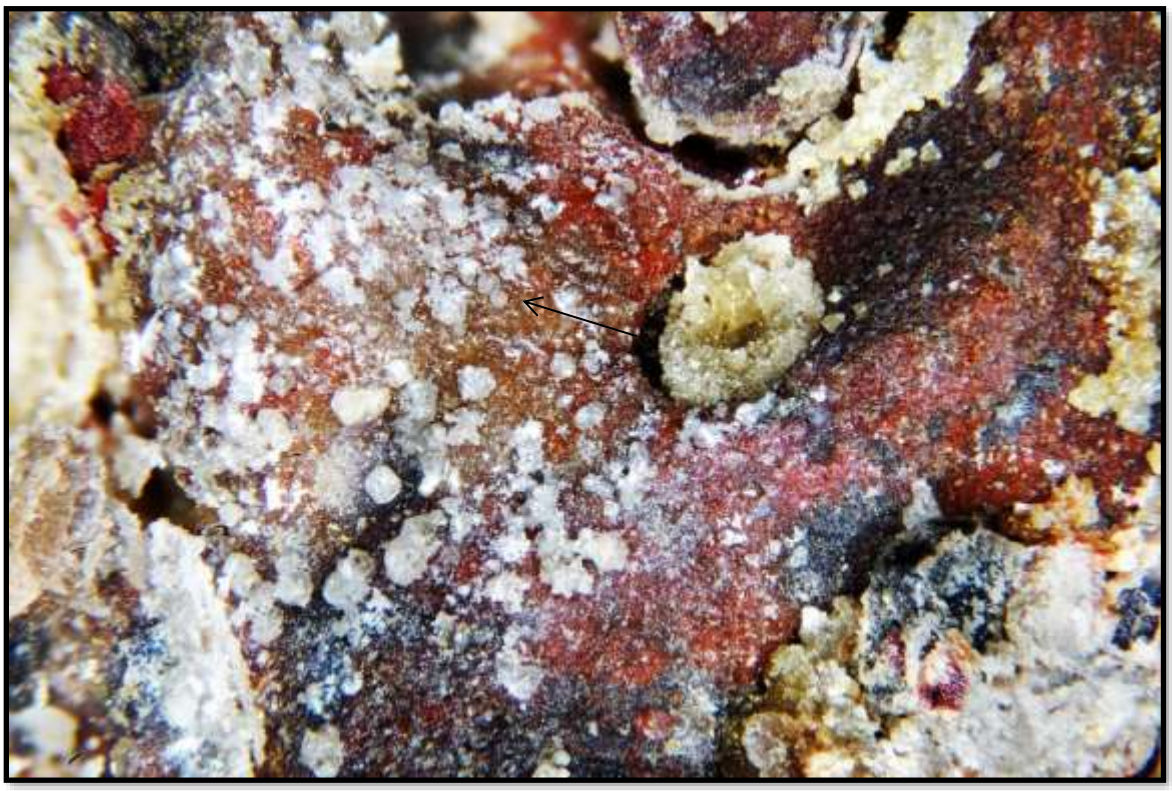

Figure 188. *Close up of left side of Figure 187. Surface covering of minute colorless corderoite crystals associated with MCDUK-23. FOV = 1 mm.*

MCDUK-24 = Corderoite

MCDUK-25 = Kermesite

MCDUK-26 = Cinnabar

MCDUK-27

Occurs as black to dark brown radiating, acicular crystals on a light tan, orbicular surface. Black eglestonite occurs associated with this unknown.

Figure 189. *Individual sprays of prismatic crystals of MCDUK-27 associated with eglestonite. FOV = 3 mm.*

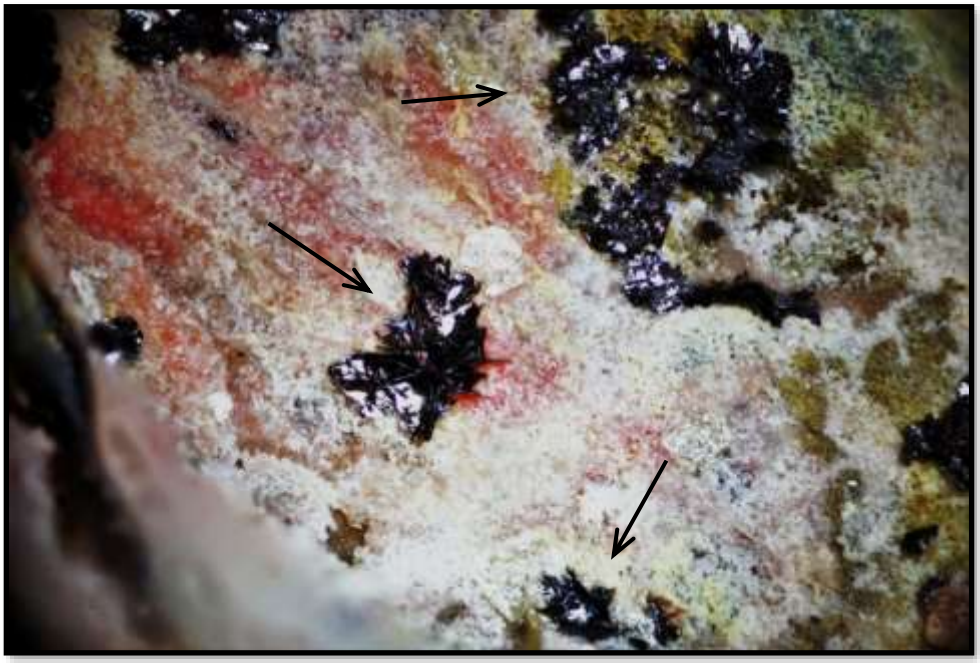

Figure 190. *Divergent groups of acicular MCDUK-27 crystals on matrix. FOV = 1 mm.*

MCDUK-28

Occurs as bright yellow-orange fan-shaped, radiating crystal groups associated with MCDUK-17, native mercury and eglestonite. No additional data has been determined for this phase.

Figure 191. *Radiating spray of MCDUK-28 crystals on matrix with orange-yellow eglestonite to left. FOV = 3 mm.*

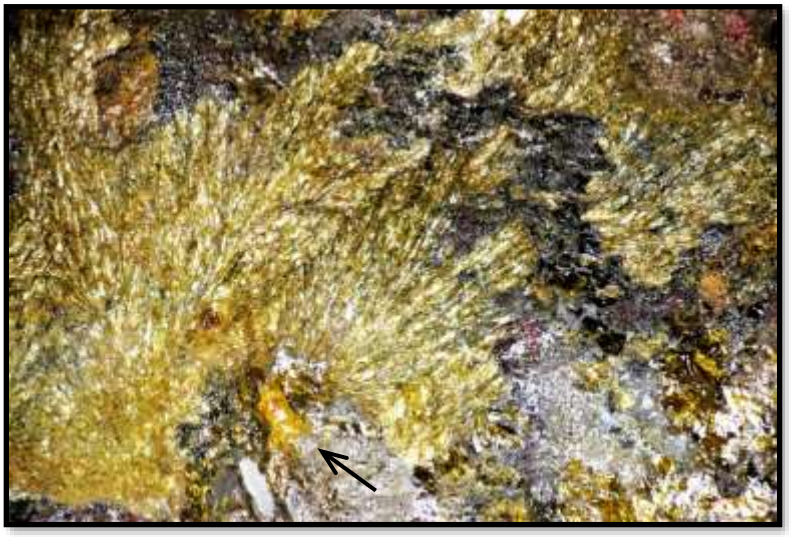

Figure 192. *Close up of Figure 191 and possible eglestonite crystal (arrow) adjacent to spray of MCDUK-28 crystals on matrix. FOV = 2 mm.*

MCDUK-29

Occurs as colorless complex crystals in cavity. No further work has been done on this phase

MCDUK-30

Occurs as white, acicular sprays on quartz surface with cinnabar beneath. Structure data suggests that it is a $Hg^{2+}_3SO(SO_4)$ phase. Unit cell is in the orthorhombic setting with a = 28.574Å, b = 12.556Å, c = 7.234Å, space group Fdd2. Volume = 2595 $Å^3$. Individual crystals are flattened, rectangular prisms with elongation along [100] and flattened on (100). The likely structure shows a similarity with the edoylerite structure, $Hg^{2+}_3S_2(CrO_4)$, where SO_4 has replaced CrO_4 and one of the S^{2-} atoms has been replaced by O^{2-}.

Although MCDUK-30 has the same formula structure as edoylerite, the connectivity is quite different. MCDUK-30 structure is based on Hg_3OS sheets, whereas edoylerite is based on Hg_3S_2 ladders. For both, the $X^{6+}O_4$ tetrahedra are inserted with longer bonds from the O vertices to neighboring Hg atoms.

MCDUK-30 has a very interesting relation to schuetteite, $Hg^{2+}_3O_2(SO_4)$. For both, the Hg-anion nets have the same topology, and similar (SO_4) insertion into the central "hole" in the net. We regard MCDUK-30 as a S^{2-} substituted schuetteite, where ½ of the net O atoms are replaced by S^{2-} in MCDUK-30.

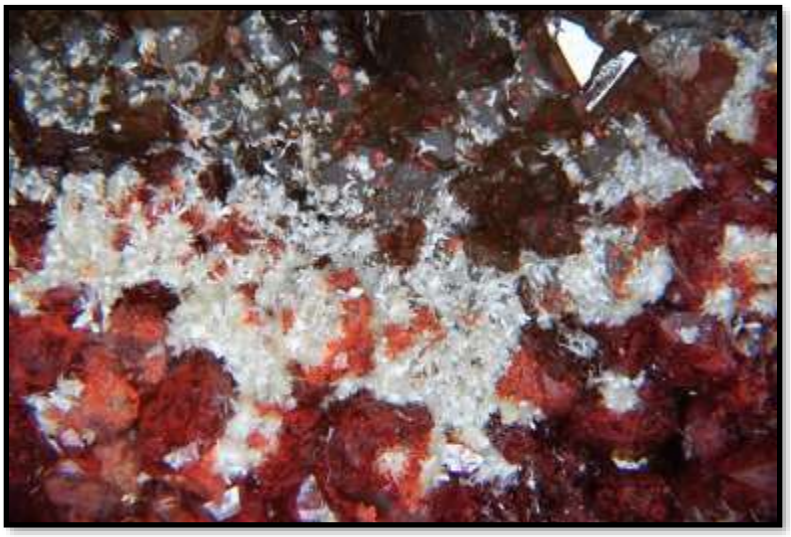

Figure 193. *Exceptional coverage of MCDUK-30 (white, acicular) on quartz over cinnabar and corderoite. FOV = 1.6 mm*

Figure 194. *Closeup of exceptional coverage of acicular MCDUK-30 crystal groups. FOV = 0.4 mm.*

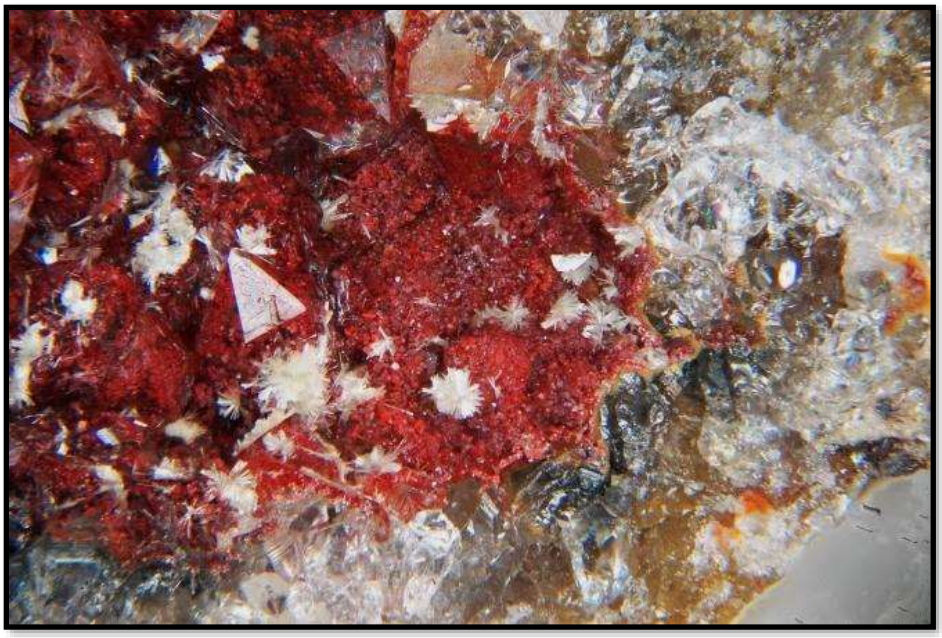

Figure 195. *Individual groups of acicular crystals of MCDUK-30 on cinnabar. FOV = 4.1 mm.*

MCDUK-31

Occurs as near black flat radiating sprays on a light yellow background. Only one sample known. Associated with MCDUK-17.

MCDUK-32 = Quintinite-2H

MCDUK-33

Occurs as off-white to light yellow crystalline masses on a quartz base. Associations include cinnabar and eglestonite. No additional work has been done on this phase.

MCDUK-34 = Montroydite

MCDUK-35 = Kenhsuite

MCDUK-36

Occurs as moderate yellow-orange, flat, divergent to radiating crystal groups on micro crystalline cinnabar. These crystals give poor optical extinction and diffraction smears. No unit cell data could be obtained from this phase. This sample was destroyed during testing.

MCDUK-37 = Goethite

MCDUK-38

Occurs as thin, white crystals on quartz. Three samples known. May be some form of silica.

MCDUK-39 = Corderoite

Occurs as yellow-orange direct replacement of cinnabar at Area 5 (south end of pit). Associated with eglestonite and mercury.

MCDUK-40 = Kleinite

MCDUK-44 = corderoite

MCDUK-45

A deep blue phase occurs on the surface of a sample of silica containing many hematite spheres. No such phase has been observed before. A PXRD test was conducted on the material but gave only very week quartz peaks. There was not enough material remaining to perform EDS.

MCDUK-46

This phase occurs associated with terlinguacreekite in samples collected in June 2018. It is greenish-gray and in groups of crystals. No testing has been done but the phase is under study.

Figure 196. *Unknown phase, MCDUK-46, associated with kleinite. FOV = 1.3 mm.*

Figure 197. *Unknown phase, MCDUK-46, as triangular crystals. FOV = 1.3 mm.*

Unnamed, β-$Hg_3S_2Cl_2$

A sample of cinnabar from the McDermitt mine was found coated by a very thin fine-grained gray material (see under corderoite) that was identified by PXRD as a mixture of corderoite, kenhsuite and β-$Hg_3S_2Cl_2$. This discovery completes the three known series discovered at this mine. The identification of this phase is the first observed in Nature.

Figure 198. Fine gray replacement product of cinnabar containing minute crystals of corderoite, kenhsuite and β-$Hg_3S_2Cl_2$. FOV = 2 mm.

Experiments conducted by McCormack and Dickson (1998) by reacting stoichiometric mixtures of HgS and $HgCl_2$ (2:1) in sealed evacuated glass tubes at 400°C produced a few mm-sized glassy crystals of ϒ-$Hg_3S_2Cl_2$ along with fine crystals of the cubic β-$Hg_3S_2Cl_2$ form. Crystals of ϒ-$Hg_3S_2Cl_2$ formed on the upper and slightly

cooler portions of tubes, separate from the β-$Hg_3S_2Cl_2$ form, which made up most of the synthetic product. Crystals of ϒ-$Hg_3S_2Cl_2$ and HgS, Hg_2Cl_2, $HgCl_2$, and α-$Hg_3S_2Cl_2$ were found to grow in evacuated tubes in which natural materials were heated in a thermal gradient from 350 to 25°C.

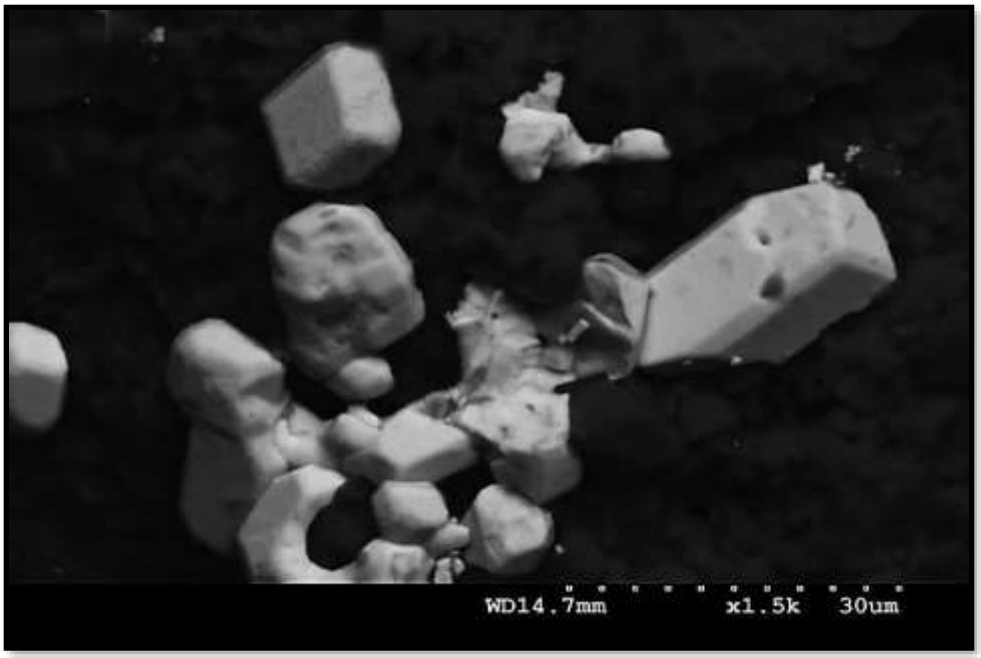

Figure 199. *SEM photo of crystals of cubic corderoite and β-$Hg_3S_2Cl_2$. Note edge modifications on many of the crystals.*

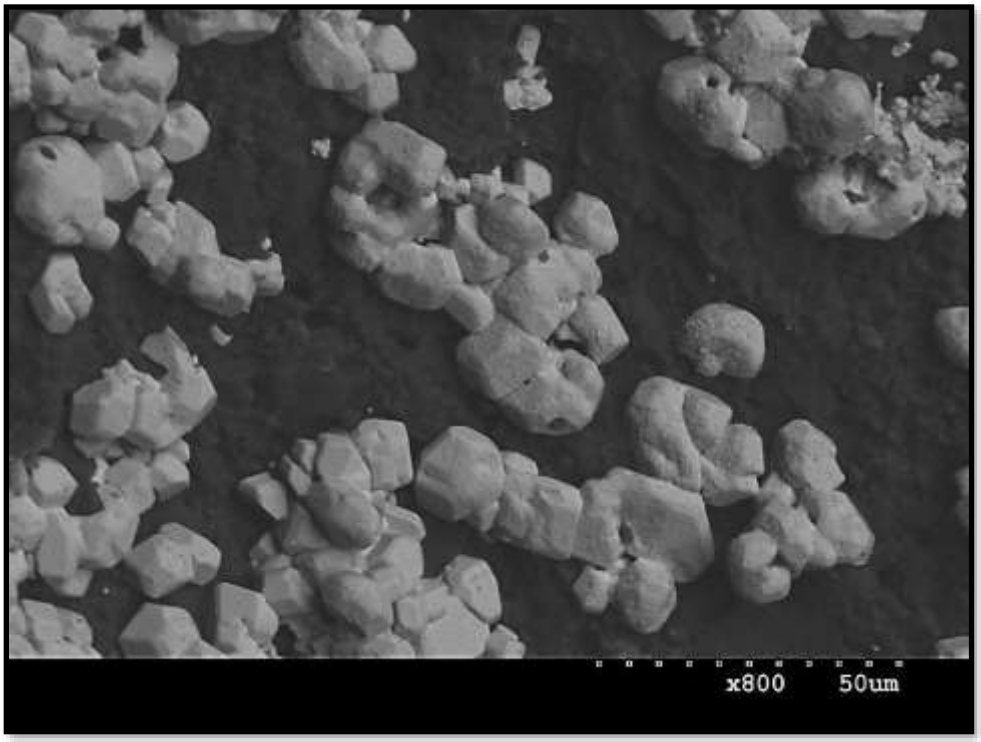

Figure 200. *SEM photomicrograph of individual corderoite, kenhsuite and β-$Hg_3S_2Cl_2$ crystals.*

Discredited minerals

Mcdermittite, $Hg_2(N,VO_4)(Cl,Br,VO_3,SO_4)\cdot xH_2O$ (?)

This now discredited mineral has a varied and confused history. Its original discovery may have been in the ores associated with kleinite at Terlingua, Texas or at the now closed McDermitt mine in Nevada. On line references state that (1) it was found together with tripuhyite at the McDermitt mine in Nevada but has been discredited. Another source (2) states that it was found together with kleinite at Terlingua, Texas and was called "an unknown species". However, none of the references actually provide what it is.

A note by Roper (1976) states that it is "a rarely observed, yellow photosensitive mineral with the above composition, tentatively named "Mcdermittite", has also been identified by Foord within the lakebed orebody. Occurrence of this mineral, as minute pseudo-hexagonal crystals lining vugs and fractures, and additional research by Foord suggest precipitation from a vapor phase."

Figure 201. *Kleinite formerly labeled as "mcdermittite". Photo by Joy Desor, Mineralanalytik, approximately 4 mm FOV. Downloaded July 2019 from: e-rocks.com, item jyj515450/kleinite.*

MERCURY MINERALOGY COMPARISON

The mercury mineralogy between the McDermitt mine Humboldt County, Nevada and that of the Clear Creek mine, San Benito County, California shows an amazing difference. Despite the extensive mercury-bearing phases discovered at each locality, only a select few phases are found at both localities. The following table illustrates this difference. Minerals in bold print indicate mercury phases found at both localities.

***Table 8**. Comparison of mercury-bearing phases between the McDermitt and the Clear Creek mines. Bold type indicates approved minerals that occur at both mines.*

Mineral	McDermitt mine, NV	Clear Creek mine, CA	Chemistry
Cinnabar	**x**	**x**	**HgS**
Donharrisite		x	$Ni_8Hg_3S_9$
Metacinnabar		x	HgS
Mercury	**x**	**x**	**Hg**
Wattersite		x	$Hg^{+}_4Hg^{2+}(CrO_4)O_2$
Edgarbaileyite		x	$Hg_6Si_2O_7$
Edoylerite		x	$Hg_3S_2(CrO_4)$
Deanesmithite		x	$Hg^{+}_2Hg^{2+}_3(CrO_4)OS_2$
Schuetteite	**x**	**x**	**$Hg_3O_2(SO_4)$**
Calomel	**x**	**x**	**Hg_2Cl_2**
Montroydite	**x**	**x**	**HgO**
Hanawaltite		x	$Hg^{+}_6Hg^{2+}[Cl,(OH)]_2O_3$
Terlinguaite	**x**	**x**	**$[Hg_3]HgO_2Cl_2$**
Eglestonite	**x**	**x**	**$Hg^{+}_6Cl_3O(OH)$**
Mosesite	**X?**	**x**	**$Hg_2NCl{\cdot}H_2O$?**
Gianellaite		x	$Hg^{2+}_4N_2(SO_4)$
Peterbaylissite		x	$Hg^{+}_3(CO_3)(OH){\cdot}2H_2O$
Szymanskiite		x	$Hg^{+}_{16}(Ni,Mg)_6(CO_3)_{12}(OH)_{12}(H_3O)^{+}_8{\cdot}3H_2O$
Clearcreekite		x	$Hg^{+}_3(CO_3)(OH){\cdot}2H_2O$
Tedhadleyite		x	$Hg^{+}_{10}Hg^{2+}O_4I_2(Cl_{1.2}Br_{0.8})$
Aurivilliusite		x	$Hg^{+}Hg^{2+}OI$
Vasilyevite		x	$Hg^{+}_{20}I_3O_6(Br_{1.6}Cl_{1.4})[(CO_3)_{0.8}S^{2-0.2}]$
CCUK-8		x	Hydrous mercury sulfide chromate
Gaildunningite		x	$Hg^{2+}_3\,[NHg^{2+}_2]_{18}(Cl,I,Br,S,OH)_{24}$
CCUK-12		x	Hg oxy halide
CCUK-13		x	Hg Silicate
CCUK-14		x	Hg Silicate
CCUK-15		x	$Hg^{+}_{10}Hg^{2+}_3O_6I_2(Cl,Br)_2$
CCUK-18		x	$Hg^{2+}_3N(I,Cl,Br).H_2O$
CCUK-19		x	Hg-N-Cl
Corderoite	x		$Hg_3S_2Cl_2$
Kenhsuite	x		$Hg_3S_2Cl_2$
Beta-$Hg_3S_2Cl_2$	x		$Hg_3S_2Cl_2$
Radtkeite	x		$Hg_3S_2Cl(I)$
Terlinguacreekite	x		Hg-N-(Cl,Br)
Kleinite	x		$Hg_2N(Cl,SO_4){\cdot}nH_2O$
MCDUK-2	x		$Hg_3S_2(MoO_4)$
MCDUK-3	x		$Hg_3S_2(SO_4/MoO_4)$
MCDUK-7	x		$[Hg_4C]OCl_2$
MCDUK-16	x		Mercury oxy sulfate?
MCDUK-17	x		Mercury sulfide oxide
MCDUK-19	x		$Hg_4Sb_4O_{12}$

Mineral	McDermitt mine, NV	Clear Creek mine, CA	Chemistry
MCDUK-21	x		Hg-S-oxide
MCDUK-23	x		$Hg_3S_2Cl_2$
MCDUK-27	x		?
MCDUK-28	x		?
MCDUK-29	x		?
MCDUK-30	x		$Hg_3OS(SO_4)$
MCDUK-31	x		Flat black xls w/ MCDUK-17
MCDUK-33	x		Off-white/yellow mass
MCDUK-46	x		?

A series of mercury phases were recognized during this study as having a common thread between them. Although their structures and cell data differ, a common substitution relationship was recognized. After an examination of the individual chemistries, a general chemical formula for this family of chemically-related mercury phases was created. Basically, different elements can be substituted into three positions within each compound. A general formula can be written as follows:

$Hg^{2+}{}_3(A_2)(X_2/(MO_4)$ where A = S, O, Te, Se or SO; X = Cl, Br, I, F and M = S, Cr, Mo, W

Three members of this chemical family are known from the Clear Creek mine, San Benito County, California (Dunning et al. 2002) as edoylerite, the sulfide-chromate member, CCUK-8, a hydrated mercury sulfide chromate and schuetteite, the oxy sulfate member. Schuetteite is known from a number of localities, especially in California and Nevada. Nine natural phases are known from the McDermitt mine. Grechishchevite, arkazite, and lavrentievite occur in the Tuva Republic, Eastern-Siberian Region, Russia. The following table compares the known natural (in bold) and synthetic members known to date, although others are certainly possible.

Table 9. *Comparison of known members of the substitutional family of mercury phases. Natural phases are in bold face.*

NATURAL (bold) AND SYNTHETIC PHASES	COMPOSITION	SITE A	SITE X/MO_4	REFERENCE
Edoylerite	$Hg_3S_2(CrO_4)$	S	Cr	Erd et al. (1993); Dunning et al. (2005)
Schuetteite	$Hg_3O_2(SO_4)$	O	S	Bailey et al. (1959); Weil (2001)
CCUK-8	$Hg\text{-}S\text{-}CrO_4{\cdot}xH_2O$	S	Cr	Dunning et al. (2005)
Corderoite	$\alpha\text{-}Hg_3S_2Cl_2$	S	Cl	Foord et al. (1974)
Unnamed β-phase	$\beta\text{-}Hg_3S_2Cl_2$	S	Cl	This study; Voroshilov et al. (1996)
Kenhsuite	$\gamma\text{-}Hg_3S_2Cl_2$	S	Cl	McCormack & Dickson (1998)
Radtkeite	$Hg_3S_2Cl(I)$	S	Cl,I	McCormack et al. (1991)
Grechishchevite	$Hg_3S_2(Br,Cl,I)_2$	S	Br,Cl,I	Vasil'ev et al. (1989)
Arkazite	$Hg_3S_2(Br,Cl)_2$	S	Br,Cl	Vasil'ev et al. (1984)
Laventievite	$Hg_3S_2(Cl,Br)_2$	S	Cl,Br	Vasil'ev et al. (1984)
MCDUK-2	$Hg_3S_2(MoO_4)$	S	Mo	This study
MCDUK-3	$Hg_3S_2(SO_4,MoO_4)$	S	S,Mo	This study
MCDUK-16	?	?	?	This study
MCDUK-23	$Hg_3S_2Cl_2$	S	Cl	This study
MCDUK-30	$Hg_3SO(SO_4)$	S,O	S	This study
$\beta\text{-}Hg_3S_2Cl_2$	$Hg_3S_2Cl_{1.5}Br_{0.5}$	S	Cl,Br	Borisov et al. (1999)
$\beta\text{-}Hg_3S_2Br_2$	$Hg_3S_2Br_{1.5}Cl_{0.5}$	S	Br,Cl	Borisov et al. (1999)
$Hg_3Te_2I_2$	$Hg_3Te_2I_2$	Te	I	Lyakhovitskaya et al. (1989)
$Hg_3Se_2I_2$	$Hg_3Se_2I_2$	Se	I	Beck & Hedderich (2000)
$Hg_3S_2I_2$	$Hg_3S_2I_2$	S	I	Beck & Hedderich (2000)

NATURAL (bold) AND SYNTHETIC PHASES	COMPOSITION	SITE A	SITE X/MO_4	REFERENCE
$Hg_3Se_2Cl_2$	$Hg_3Se_2Cl_2$	Se	Cl	Puff & Küster (1962a, b); Puff et al. (1966, 1968)
$Hg_3Te_2Cl_2$	$Hg_3Te_2Cl_2$	Te	Cl	Puff & Küster (1962a, b); Puff et al. (1966, 1968)
$Hg_3Te_2Br_2$	$Hg_3Te_2Br_2$	Te	Br	Puff & Küster (1962a, b); Puff et al. (1966, 1968)
$Hg_3S_2F_2$	$Hg_3S_2F_2$	S	F	Puff & Küster (1962a, b); Puff et al. (1966, 1968)
$Hg_3Se_2F_2$	$Hg_3Se_2F_2$	Se	F	Puff & Küster (1962a, b); Puff et al. (1966, 1968)
β-phase $Hg_3S_2Br_2$	$Hg_3S_2Br_2$	S	Br	Voroshilov et al. (1996a)
α-$Hg_3S_2Br_2$	$Hg_3S_2Br_2$	S	Br	Voroshilov et al. (1996a)
$Hg_3S_2Br_{1.0}Cl_{0.5}I_{0.5}$	$Hg_3S_2Br_{1.0}Cl_{0.5}I_{0.5}$	S	Br,Cl,I	Pervukhina et al. (2003)

Uranium minerals

The rhyolite domes intruded along the southwestern ring fracture zone of the McDermitt caldera host several uranium occurrences. The major uranium deposit is the Moonlight mine. The smaller Granite Point mine is located about 2.5 miles (4.0 km) to the northeast, in rhyolite. The dome in which the Moonlight deposit occurs is faulted on the west by range faults bounding the Quinn River valley, and the uranium ore is localized along a breccia zone that strikes northerly, dips 60° to the east and parallels the flow foliation planes within the dome. The uranium mineralization is genetically related to the rhyolite intrusion (Garside 1973; Rytuba 1976; Rytuba et al. 1979; Rytuba and Glanzman 1979; Castor et al. 1996).

Autunite, $Ca(UO_2)_2(PO_4)_2{\cdot}11H_2O$

Autunite, or more likely its common dehydration product, meta-autunite, has been reported with quartz, pyrite, fluorite and torbernite in a fault zone at the Moonlight and Granite Point mines in the Disaster district (Sharp 1955; Garside 1973; Dayvault et al. 1985).

Coffinite, $U(SiO_4)_{1-x}(OH)_{4x}$

Coffinite has been reported with uraninite at the Moonlight and Disaster Peak mines (Sharp 1955; Williams 1980). It also occurs in the Aurora prospect, Opalite district, Malheur County, Oregon (Roper and Wallace 1981).

"Gummite"

A mixture of boltwoodite, clarkeite, curite, kasolite, soddyite, and uranophane with uraninite (Frondel 1956). An orange, massive material identified as "gummite" has been reported with meta-autunite and metatorbernite at the Moonlight and Granite Point mines (Garside 1973).

Meta-autunite, $Ca(UO_2)_2(PO_4)_2{\cdot}6H_2O$

Meta-autunite has been reported from a number of claims in the Moonlight mine area including the Granite Point mine (Garside 1973).

Metazeunerite, $Cu(UO_2)_2(AsO_4)_2{\cdot}8H_2O$

Metazeunerite has been reported as green tetragonal dipyramids up to 1 mm across in cavities in partially to wholly oxidized breccia with uranium-rich zircon at the Moonlight mine (Castor et al. 1996).

Torbernite, $Cu(UO_2)_2(PO_4)_2{\cdot}12H_2O$

Torbernite, or more likely metatorbernite, has been reported with quartz, fluorite, pyrite and autunite at the Moonlight Uranium and Granite Point mines in the Disaster district (Sharp 1955; Taylor and Powers 1955; Garside 1973 and Dayvault et al. 1985).

Uraninite, UO_2

Fine-grained uraninite associated with coffinite occurs in all of the uranium mines and prospects in the area, including the Disaster Peak, Moonlight and Granite Point mines (Sharp 1955; Williams 1980). It also occurs in the Aurora prospect, Opalite district, Malheur County, Oregon (Roper and Wallace 1981).

Accessory Minerals

The mercury and uranium ore deposits of the McDermitt Caldera Complex host a number of gangue and secondary minerals. Some of these are primary products of the hydrothermal activity, others are replacements of pre-existing volcanic minerals and glass, and yet others are related to the near-surface oxidation of sulfide minerals.

Accessory sulfides associated with the mercury ore minerals include pyrite, marcasite, realgar, and stibnite. Gangue minerals not directly due to ore oxidation include alunite, baryte, cristobalite, fluorite, gypsum, lithiophorite, montmorillonite, opal, quartz, tridymite, and kaolinite. Secondary minerals resulting from the oxidation of primary sulfides include, copiapite, fibroferrite, goethite, hematite, jarosite, melanterite, and tripuhyite (Castor and Ferdock 2004). Zeolite minerals identified in the area include analcime, clinoptilolite, eronite, heulandite, and mordenite (Glanzman and Rytuba 1979).

Alunite, $KAl_3(SO_4)_2(OH)_6$

Alunite is locally abundant as very fine-grained, white, chalky material in the McDermitt mine, commonly in balls to 10 cm diameter; also as white masses at shallow levels in the Cordero mine (McCormack 1986; Fisk 1968) and as veins in the McDermitt mine (Rytuba and McKee 1984). It is likely to have formed by reaction of Al-rich materials such as feldspar, kaolinite and volcanic glass with acidic hydrothermal fluids rich in sulfate. Also found in the pit are unusual alunite "balls" described by McCormack (1986). The authors found alunite balls, distinctive piles of chips from disintegrating balls, and some alunite nodules in place in tuffaceous rock.

Figure 202. *Group of spherical alunite on quartz. FOV = 3 mm.*

Analcime, $NaAlSi_2O_6 \cdot H_2O$

A zeolite mineral formed from volcanic glass at the in the zones of more intense hydrothermal alteration of the volcaniclastic sediments. It can in turn be pseudomorphed by K-feldspar (Glanzman and Rytuba 1979; Rytuba and Glanzman 1979). It has been reported closely associated with hectorite in the interior portions of the McDermitt Caldera Complex.

Aragonite, $CaCO_3$

Aragonite occurs as invertebrate fossils in the volcaniclastic sediments, in the Bretz area (Glanzman and Rytuba 1979).

Baryte, $BaSO_4$

Baryte has been recorded as bladed crystals up to 6 mm long, perched on and containing cinnabar and marcasite inclusions, at the Cordero mine (Fisk 1968).

Buddingtonite, $(NH_4)AlSi_3O_8$

Buddingtonite is a rare ammonium feldspar, reported from the McDermitt mine by Castor and Ferdock (2004). It was presumably formed by ion exchange in alkali feldspars or devitrification of volcanic glass, due to attack by NH_4^+-rich fluids.

Calcite, $CaCO_3$

Calcite is common as a cement phase, nodules and veins in the altered tuffs (Glanzman and Rytuba 1979) and forms calcretes (cf. Yates 1941). It also occurs as prismatic crystals known as dogtooth spar.

Figure 203. *Group of calcite crystals on matrix at center of photo. FOV = 15 mm.*

Figure 204. *Group of scalenohedral calcite crystals with kleinite inclusions. FOV = 3 mm.*

Figure 205. *Group of colorless calcite crystals. FOV = 2 mm.*

Figure 206. *Group of calcite crystals on matrix. FOV = 4 mm.*

Chapmanite, $Sb^{3+}Fe^{3+}_2[Si_2O_5]O_3(OH)$

Chapmanite is an unusual layered silicate of iron and antimony, with a structure related to that of kaolinite (Zhukhlistov and Zvyagin 1977). It is reported to occur as a primary product. The mineral forms dull greenish-yellow micro granular bands and veinlets with cinnabar, stibnite, and pyrite (McCormack 1986).

Figure 207. *Cavity filling of yellow-green chapmanite on quartz. FOV = 9.5 mm. Photo by Mike Trebisky.*

Clinoptilolite, $(Na,K,Ca_{0.5})_6(Al_6Si_{30}O_{72})\cdot\sim 20H_2O$

One of the hydrothermal zeolite minerals formed from volcanic glass during diagenesis and hydrothermal alteration in the volcaniclastic sediments (Glanzman and Rytuba 1979). It disappears only in the most extensively altered rocks towards the southwest of the caldera complex. The clinoptilolite series of zeolites have the same structure as heulandite, but are richer in Si (Si/Al > 4) and concomitantly poorer in exchangeable alkali and alkaline earth cations (Coombs et al. 1997). It is not known which of the exchangeable cations Ca, Na or K is dominant.

Conichalcite, $CaCu^{2+}(AsO_4)(OH)$

Apple-green spheres of conichalcite on a white quartz base were discovered in rock samples from Area 2. All three spheres show slender acicular crystals protruding from the surfaces. The mineral was identified by PXRD methods.

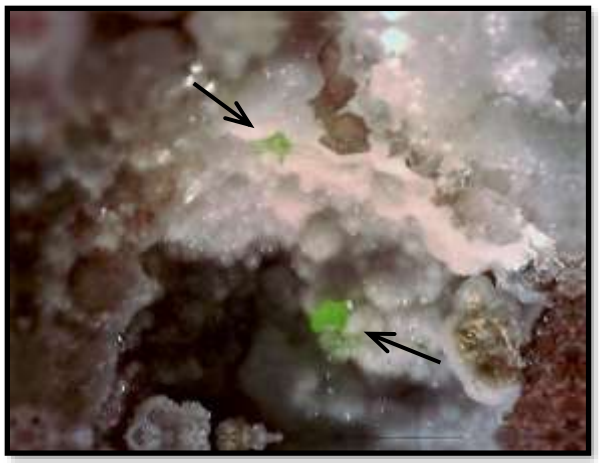

Figure 208. *Two groups of acicular crystals of green conichalcite on quartz. FOV = 4 mm.*

Figure 209. *Closeup of Individual group of acicular conichalcite crystals on quartz. FOV = 1 mm.*

Figure 210. *Closeup of group of acicular crystals of conichalcite on quartz. FOV = 0.6 mm.*

Copiapite, $Fe^{2+}Fe_4^{3+}(SO_4)_6(OH)_2 \cdot 20H_2O$

Copiapite was noted on the 700-foot level of the Cordero mine as yellowish crusts, which formed by rapid oxidation of melanterite (Fisk 1968).

Cristobalite, SiO_2

Cristobalite has been identified as a devitrification product of volcanic glass in the least-altered volcaniclastic sediments. It occurs adjacent to mercury and uranium deposits in the McDermitt caldera complex (Glanzman and Rytuba 1979; Rytuba and Glanzman 1979).

Cryptomelane, $K(Mn^{4+}_7Mn^{3+})O_{16}$

A group of black, acicular crystals in a light pink breccia cavity has been identified as cryptomelane by PXRD methods.

Figure 211. *Fine, acicular crystals of cryptomelane in a quartz cavity. FOV = 2 mm.*

Figure 212. *Fine, acicular crystals of cryptomelane in a quartz cavity. FOV = 2 mm.*

Dolomite, $CaMg(CO_3)_2$

Some dolomite occurs in the finer-grained (medial mudstone) facies of the volcaniclastic sediments (Glanzman and Rytuba 1979).

Erionite, $(Ca,Na_2,K_2)_5(Al_{10}Si_{26}O_{72})\cdot 30H_2O$

One of the zeolite minerals formed from volcanic glass during diagenesis and at the lowest grades of hydrothermal alteration in the upper and lower "sandstone" units of the volcaniclastic sediments (Glanzman and Rytuba 1979). It is not known which of the exchangeable cations Ca, Na or K is dominant.

Fayalite, $Fe^{2+}{}_2SiO_4$

Fayalite has been reported as phenocrysts in the peralkaline ash-flow stuff and intrusive rocks of the McDermitt caldera (Conrad, 1984; Rytuba and KcKee, 1984; Astor et al.,1996). During the examination of corderoite-rich samples from Area 1, several thin brown crystals of fayalite were noted in quartz-lined cavities. In several samples, light yellow cubes of corderoite were also found associated with the fayalite. The crystal habit of the fayalite matches the fayalite in obsedian from Coso Hot Springs, Inyo County, California. The fayalite appears to have formed first followed by quartz and then corderoite, and in some samples, MCDUK-3.

Figure 213. *Multiple parallel fayalite crystals in a quartz-lined vug. FOV = 1.3 mm.*

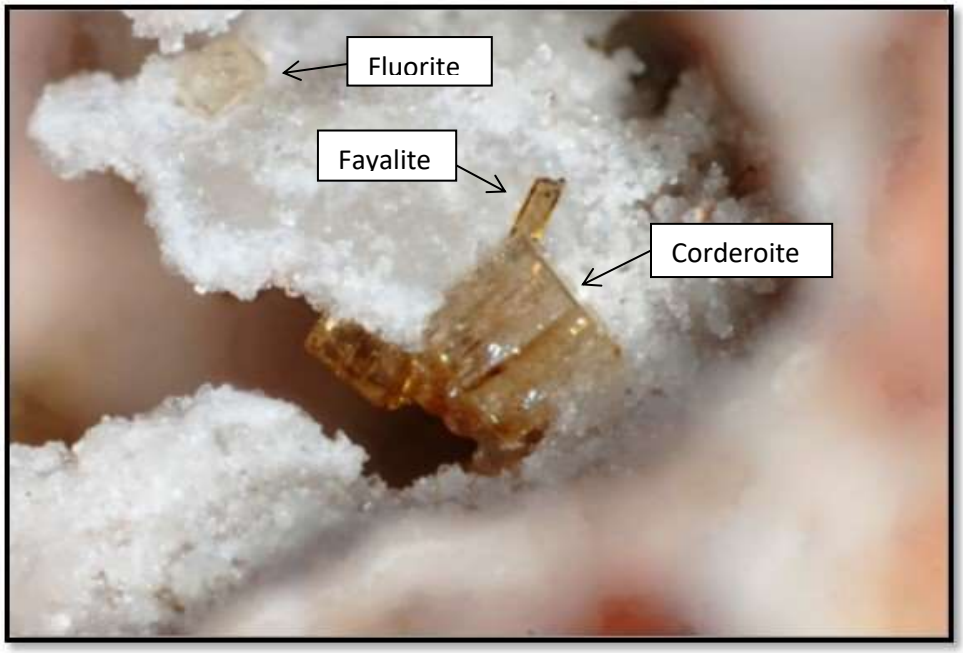

Figure 214. Quartz-lined cavity hosting a slender fayalite crystal at arrow, a light brown corderoite crystal below the fayalite and a smaller cubic, clear fluorite crystal in the upper left area with arrow. FOV = 2 mm.

Fibroferrite, $Fe(SO_4)(OH)\cdot 5H_2O$

Fibroferrite occurs as light-brown crystalline masses with copiapite, melanterite and other supergene iron minerals at the Cordero mine (Fisk 1968), and is formed by oxidation of iron sulfides.

Fluorapatite, $Ca_5(PO_4)_3F$

Divergent crystal groups of fluorapatite have been identified by PXRD methods from breccia samples at the McDermitt mine. These crystal groups generally occur within voids in the breccia. One sample was noted on quartz lining a void in breccia that has a coating of cinnabar beneath the quartz.

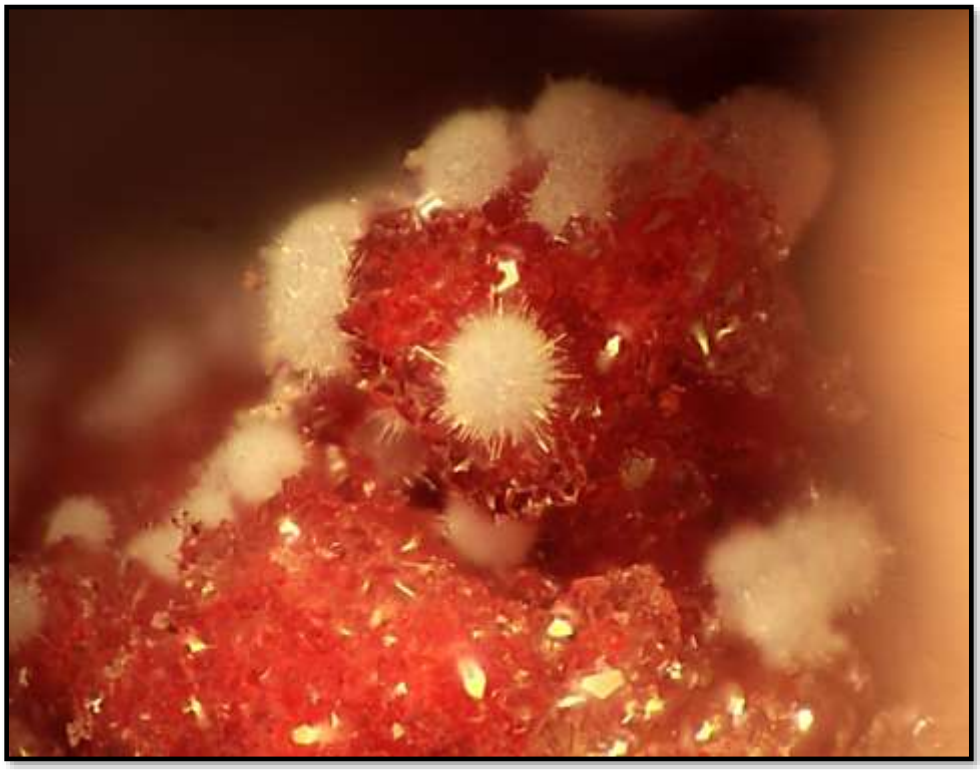

Figure 215. *Groups of fine, acicular crystals of fluorapatite on quartz. FOV = 2 mm.*

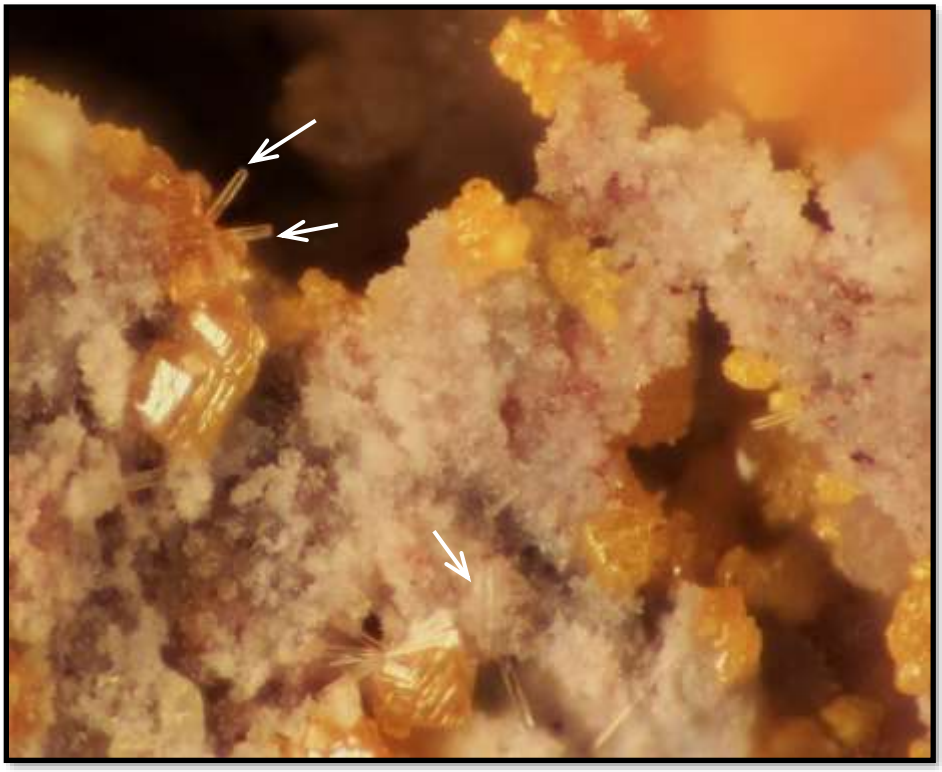

Figure 216. *Colorless crystals of fluorapatite plus yellow kleinite in silica. FOV = 1 mm.*

Figure 217. *Groups of colorless fluorapatite crystals. FOV = 1 mm.*

Figure 218. *Single hexagonal crystal of fluorapatite. FOV = 1 mm.*

Figure 219. *A triad of fluorapatite crystals. FOV = 1 mm.*

Fluorite, CaF_2

Rare fluorite has been identified from the Cordero mine (Bailey and Phoenix 1944). Exceptional clear cubic crystals of fluorite have been identified in cavities on quartz up to 1 mm on an edge during this study.

Figure 220. *Penetrating cubes of light-yellow fluorite in a quartz cavity. FOV = 2 mm.*

Goethite, α-$Fe^{3+}O(OH)$

Goethite is a common alteration product of marcasite at the Cordero mine (Fisk 1968), and occurs in the McDermitt mine as pervasive finely disseminated "limonite" to depths of 150-210 feet (45-65 m); Hetherington and Cheney (1985). Additional goethite samples have been identified in corderoite-quartz breccia as divergent sprays of crystals up to 1 mm.

Figure 221. *Hematite-lined cavity in corderoite-rich rock with several goethite crystals along the left edge. FOV = 4 mm.*

Figure 222. *Divergent group of goethite crystals. FOV = 1mm.*

Gold, Au

A small flake of leaf gold was identified on one sample of breccia containing kleinite and terlinguacreekite from the McDermitt mine. Gold has also been identified surrounding quartz crystals in a vug of high silica massive corderoite rock. Both gold and silver values have been reported from the several drill core samples made in the area.

Figure 223. *View of quartz crystals coated with gold. FOV = 2 mm.*

Gypsum, $CaSO_4 \cdot 2H_2O$

Gypsum occurs as rare, small, white tabular or needle-like crystals or fibrous bundles at the Cordero mine (Fisk 1968). More generally, it is a widespread accessory mineral in the clinoptilolite-zone altered volcaniclastic sediments of the caldera complex, particularly in the region of intense alteration surrounding the McDermitt mine, and is common as nodules, lenses and veins in the mudstone unit of the volcaniclastics near the Opalite mine (Glanzman and Rytuba 1979).

Figure 224. *Group of parallel gypsum crystals. FOV = 4 mm.*

Hematite, Fe_2O_3

Hematite is common as an oxidation product of marcasite at the Cordero mine (Fisk 1968). Minute black spheres of hematite have been observed on ore rock from the McDermitt mine during this study.

Figure 225. *Bright, black spheres of hematite on silica. FOV = 1 mm.*

Hectorite, $(Na,Ca)_x(Mg,Li)_3Si_4O_{10}(OH)_2.nH_2O$

Glanzman and Rytuba (1979) reported that in the "medial mudstone" units of the volcaniclastic sediments, diagenesis and hydrothermal alteration produced a high-lithium trioctahedral smectite (hectorite or Li-rich saponite) rather than low-Li dioctahedral smectite (montmorillonite). Rytuba and Glanzman (1979) identify the mineral as hectorite.

Heulandite, $(Ca,Na_2,K_2)_{4.5}(Al_9Si_{27}O_{72})\cdot 21\text{-}26H_2O$

A zeolite mineral reported form intensely altered rocks in the Cordero mine by Bailey and Phoenix (1944). It is possible that the mineral would now classify as clinoptilolite. The clinoptilolite series of zeolites have the same structure as heulandite but are richer in Al (Si/Al < 4) and concomitantly richer in exchangeable alkali and alkaline earth cations (Coombs et al. 1997). It is not known which of the exchangeable cations Ca, Na or K is dominant.

Jarosite, $KFe_3(SO_4)_2(OH)_6$

Jarosite is abundant as a cavity filling, on quartz as yellow-brown rhombs and plates at the Cordero mine and within surface rocks examined at the McDermitt mine pit. The specimens are quite attractive when perched on colorless quartz crystals.

Figure 226 (left) & 227 (right). *Coating of dark brown jarosite crystals on altered rock. FOV = 40 mm.*

Figure 228. *Surface coating of brown jarosite crystals. FOV = 15 mm.*

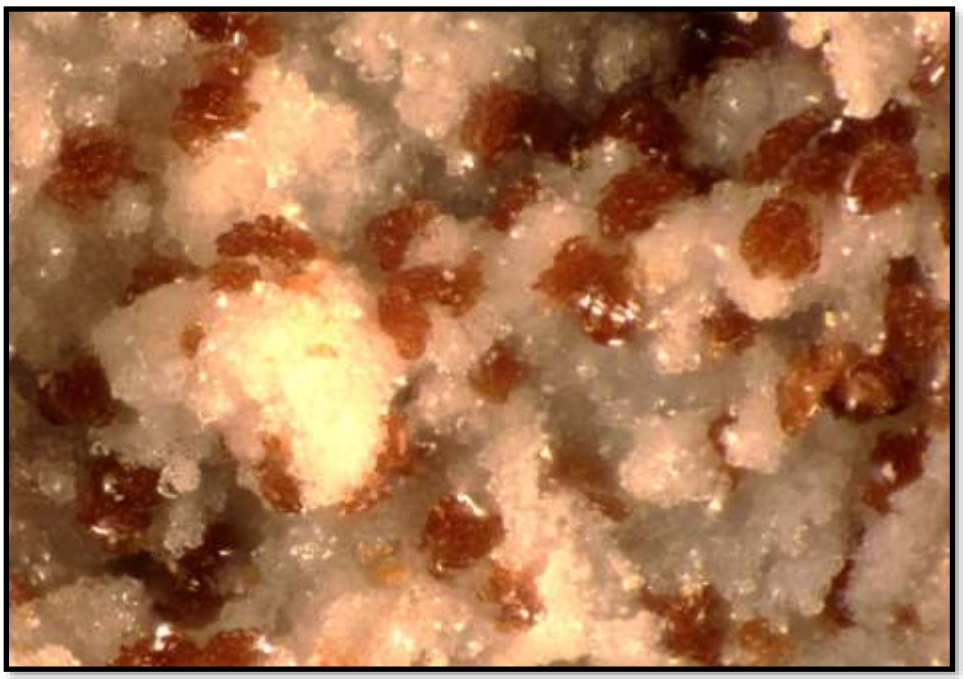

Figure 229. *Covering of brown jarosite crystals on quartz. FOV = 2 mm.*

Kaolinite, $Al_2Si_2O_5(OH)_4$

Kaolinite is the most common alteration mineral at the Cordero mine, produced during diagenesis and hydrothermal alteration of glass shards in volcaniclastic sediments (Glanzman and Rytuba 1979); it can occur in relatively pure veinlets (Fisk 1968).

Kermesite, Sb_2S_2O

Kermesite occurs as prismatic, acicular cherry-red crystals on a black crust in a stibnite-rich rock high in silica. The rock type is a high silica breccia. There is a thin vein of cinnabar on one end. Macroscopically, the red crystals resemble the mineral kermesite. If more material is found, a few crystals will be sent for cell data.

Figure 230. *Group of acicular, divergent kermesite crystals. FOV = 2 mm.*

Figure 231. *Linear groups of acicular kermesite crystals. FOV = 1 mm.*

Lithiophorite, $(Al,Li)Mn^{4+}O_2(OH)_2$

Massive to crystalline lithiophorite occurs associated with kleinite along fractures in a quartz-rich rock. It also occurs filling cavities in a light gray breccia rock as divergent groups of crystals.

Figure 232. *Jet black crystals of acicular lithiophorite. FOV = 2 mm.*

Marcasite, FeS_2

Marcasite is common as disseminated grains, crystals in vugs, and veins to 20 cm thick in rhyolite at the Cordero mine (Fisk 1968).

Melanophlogite, $46SiO_2{\cdot}6(N_2,CO_2){\cdot}2(CH_4,N_2)$

Minute cubic crystals of melanophlogite (or its possible chalcedony pseudomorphic equivalent) on quartz was noted in a single sample of light tan cinnabar-corderoite breccia from Area 1, a diverse collection of rocks left after mining operations ceased. The occurrence of melanophlogite at McDermitt would require some sort of stabilizing molecules such as CO_2, N_2, and CH_4 for its formation (Nakagawa et al. 2001). Since melanophlogite is very rare, the stabilizing volatiles may have been restricted in their occurrence and were available at lower temperatures after quartz had formed. No association of melanphlogite with opal has been observed in the deposit. Although minute, the complex intergrown crystals resemble those observed from the Borges quarry and the Vaughn mine, California (Dunning and Cooper 2002).

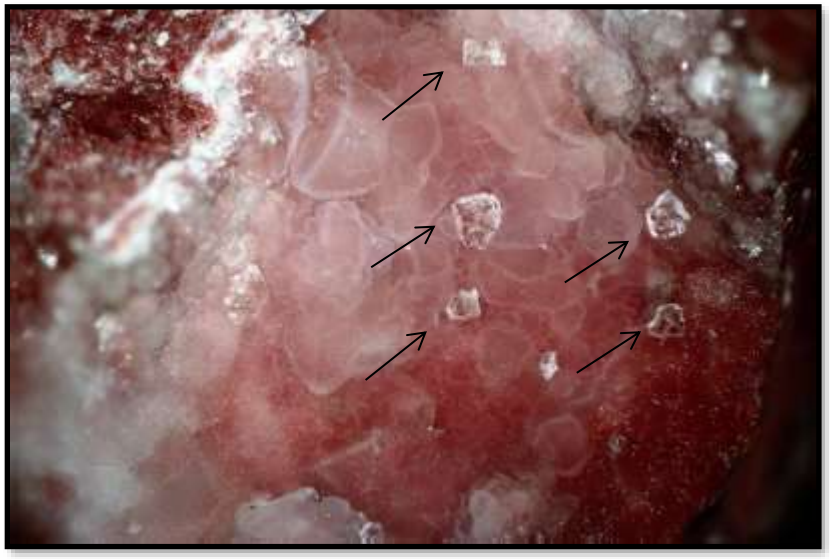

Figure 233. *Rare group of melanophlogite crystals on chalcedony. FOV = 2 mm.*

Melanterite, $FeSO_4 \cdot 7H_2O$

Greenish crusts of melanterite were noted forming by the oxidation of marcasite, as soon as mine workings are opened at the Cordero mine (Fisk 1968).

Microcline, $KAlSi_3O_8$

Potassium feldspar (microcline, variety adularia, cf. Noble et al. 1988) is almost ubiquitous in the tuffs as a diagenetic and hydrothermal alteration product of volcanic glass, particularly in the coarser-grained units and more intensely altered rocks (Glanzman and Rytuba 1979). Subhedral and euhedral crystals of microcline occur in the breccia at the McDermitt mine. The mineral has been observed as individual crystals within quartz-lined cavities. One particularity interesting sample was discovered within a breccia void containing two microcline crystals perched on their edges. Upon further examination, a "worm-shaped" mineral was noted attached to the center of each microcline crystal. It would appear that this "worm-like" mineral formed first, and then both microcline crystals nucleated on it. Following this event, the "worm-like" mineral altered to an "illite-like" mineral or possibly a smectite-like mineral could be feasible. Since only one sample of this unusual combination was found, no attempt was made for its identification.

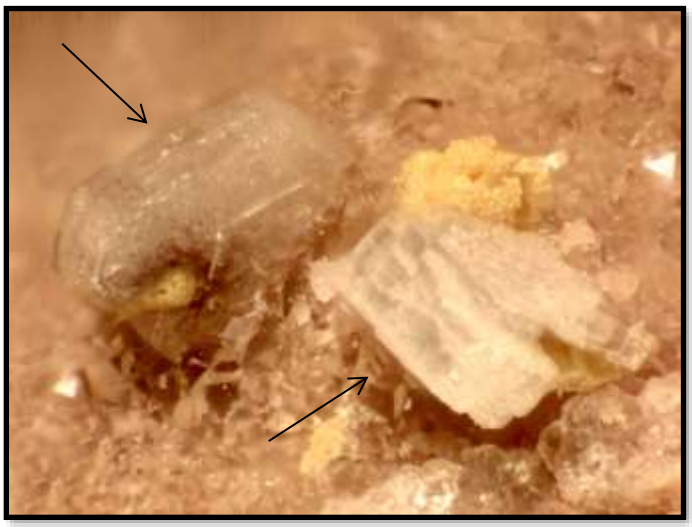

Figure 234. *Colorless to white microcline crystals on quartz. Yellow unknown at top of right crystal. FOV = 2 mm.*

Figure 235. *White microcline crystal in cavity of quartz. FOV = 3 mm.*

***Figure 236**. Unusual growth of two microcline crystals around an unknown silicate phase, possibly a smectite-like mineral, all on quartz. FOV = 2 mm.*

Montmorillonite, $(Na,Ca)_{0.3}(Al,Mg)_2Si_4O_{10}(OH)_2 \cdot nH_2O$

Montmorillonite is common in the lakebeds and breccia at the McDermitt mine (Roper 1976). It corresponds to the "low-Li dioctahedral smectite" of Glanzman and Rytuba (1979), occurring as a diagenetic and hydrothermal replacement mineral in the upper and lower "sandstone" units of the volcaniclastic sediments.

Mordenite, $(Na_2,Ca,K_2)_4(Al_8Si_{40}O_{96}) \cdot 28H_2O$

A zeolite mineral formed from volcanic glass during diagenesis and at the lowest grades of hydrothermal alteration in the upper sandstone and medial mudstone units of the volcaniclastic sediments (Glanzman and Rytuba 1979).

Opal, $SiO_2 \cdot nH_2O$

Opal fills cavities over quartz in rock samples from the McDermitt mine, and can form nodules and lenses in the medial mudstone unit of the volcaniclastic sediments (Glanzman and Rytuba 1979). It is scarce, relative to its abundance in surficial hot spring deposits (Hetherington and Cheney 1985). Spherical forms of opal occur covering pre-existing quartz in many of the rock types collected.

Pyrite, FeS_2

Pyrite is widespread with cinnabar at the Cordero mine (Bailey and Phoenix 1944). It has also been noted associated with stibnite and cinnabar from the McDermitt mine, specifically at Area 4.

Figure 237. *Vein of fine-grained pyrite with stibnite. FOV = 50 mm.*

Quartz, SiO_2

Quartz crystals are very common as vug-lining in the breccia rocks of the mines in the Opalite district (Fisk 1968). It replaces cristobalite with increasing degree of alteration of the volcaniclastic rocks (Glanzman and Rytuba 1979). Chalcedony, probably diagenetic, occurs as lenses and layers in the lacustrine sediments (Hetherington and Cheney 1985).

Figure 238. *Silica formation showing individual elongated forms. FOV = 3 mm.*

Quintinite-2H, $Mg_4Al_2(OH)_{12}CO_3{\cdot}3H_2O$

Several thin, light yellow crystals of quintinite-2H were discovered from a single rock sample recovered from the cinnabar-stibnite zone. The mineral was identified by PXRD methods. This is one of the very few minerals containing carbonate and hydroxyl.

Figure 239. *Thin, light yellow hexagonal crystals of quintinite-2H on quart associated with an iron oxide. FOV = 3 mm.*

Realgar, As_4S_4

Rare realgar has been noted with corderoite and montmorillonite at the Cordero mine (Jenkins 1981). It also has been noted in a small cut just east of the 1940 Bretz workings, where well-formed crystals of up to a centimeter are distributed along the bedding planes of carbonaceous shale (Yates 1942).

Senarmontite, Sb_2O_3

A few minute octahedrons of senarmontite occur in the oxidation zone of stibnite masses.

Stibioromeite (Stibiconite), $SbSb_2O_6(OH)$

Stibioromeite has been noted as pseudomorphic replacements of stibnite crystals in dark gray rock associated with cinnabar and sulfur.

Figure 240. *Sprays of stibiconite after stibnite surrounded by a rim of cinnabar. FOV = 30 mm.*

Figure 241. *Spray of stibiconite after stibnite with red cinnabar. FOV = 3 mm.*

Figure 242. *A group of stibiconite pseudomorphs after stibnite with cinnabar FOV = 5 mm.*

Figure 243. *Cavity of stibiconite pseudomorphs after stibnite. FOV = 15 mm.*

Figure 244. *An example of the replacement of stibnite by stibiconite. FOV = 5 mm.*

Figure 245. *An example of the replacement of stibnite by stibiconite. FOV = 5 mm.*

Stibnite, Sb_2S_3

Rare stibnite, often in delicate acicular crystals, occurs with cinnabar in rhyolite at the Cordero mine. It also occurs as divergent groups of crystals within cavities in a silica-rich rock with cinnabar, eglestonite and calomel.

Figure 246. *Cavity in silica rock containing thin stibnite crystals. FOV = 60 mm.*

Figure 247. *Stibnite vein with orbicular formation. Cinnabar to the left. FOV = 40 mm.*

Figure 248. *Orbicular stibnite surrounded by cinnabar. FOV = 50 mm.*

Figure 249. *Cavity containing delicate stibnite crystals. FOV = 35 mm.*

Figure 250. *Quartz cavity hosting delicate stibnite crystals. FOV = 6 mm.*

Sulphur, S

Both massive and crystals of sulphur have been noted associated with stibnite and stibioromeite at the McDermitt mine.

Figure 251. *Mass of sulfur on matrix. FOV = 2 mm.*

Tridymite, SiO_2

Tridymite has been reported on opalite breccia and chalcedony layers at the McDermitt mine associated with kleinite (Roper 1976).

Figure 252. *Scattering of pseudohexagonal tridymite crystals on quartz with yellow kleinite to the left. FOV = 3 mm.*

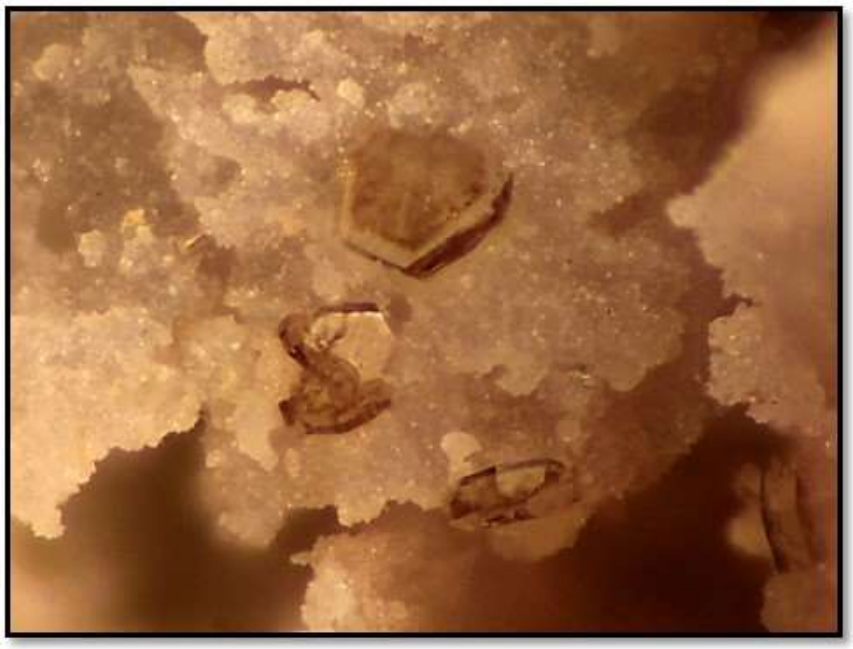

Figure 253. *View of four tridymite pseudohexagonal crystals on quartz. FOV = 1 mm.*

Tripuhyite, $Fe^{3+}Sb^{5+}O_4$

Tripuhyite has been reported from the McDermitt mine as yellow-green crystalline masses, probably as an alteration product of stibnite and pyrite (F. Cureton, personal communication, 1999).

Figure 254. *Light green mass of tripuhyite. Photo courtesy of R. Thomssen, FOV = 2 mm.*

Valentinite, Sb_2O_3

Masses of tabular crystals of valentinite occur filling cavities in partially oxidized sections of stibnite veins. Groups of clear, highly reflective crystals are associated with stibnite, stibiconite, and small crystals of quartz, often double terminated. Photographs of the valentinite on the next two pages illustrate the variety of habits and associations.

Figure 255. *Colorless crystals of valentinite surrounded by red cinnabar. FOV = 3 mm.*

Figure 256. Group of valentinite crystals surrounded by white stibiconite. FOV = 3 mm.

Figure 256b. *Different area of sample shown in Figure 256. FOV = 3 mm.*

Figure 257. A complex coating of valentinite crystals. FOV = 2 mm.

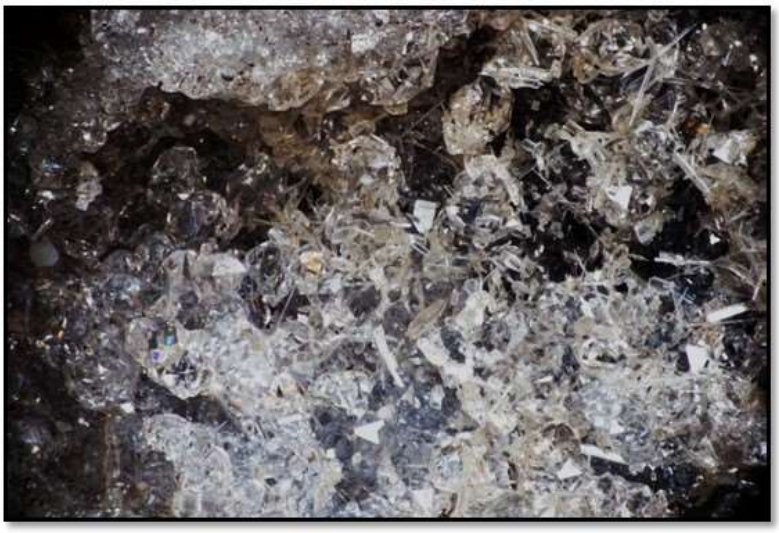

Figure 258. *Surface covering of colorless valentinite crystals. FOV = 2 mm.*

Figure 259. *Surface covering of valentinite crystals. FOV = 2 mm.*

Figure 260. *A complex crystal group of valentinite crystals in a cavity. FOV = 2 mm.*

Figure 261. *Coverage of colorless valentinite crystals. FOV = 4 mm.*

***Table 10**. Mercury-bearing minerals identified from the McDermitt Caldera Complex.*

Mineral	***Composition***	***Rarity***	***Location***
Cinnabar	HgS	Common	General Pit area
Corderoite	$Hg_3S_2Cl_2$	Common	General Pit area
Kenhsuite	$Hg_3S_2Cl_2$	Very rare	Areas #1, 4
β-$Hg_3S_2Cl_2$	$Hg_3S_2Cl_2$	Very rare	Area #1
Radtkeite	$Hg_2S_2Cl(I)$	Very rare	Area #5
Calomel	Hg_2Cl_2	Rare	Area #2
Mercury	Hg	Uncommon	Area #2, 4
Montroydite	HgO	Very rare	Area #4
Eglestonite	$Hg_6^{1+}Cl_3O(OH)$	Rare	Area #4
Schuetteite	$Hg_3(SO_4)O_2$	Uncommon	General Pit area
Shakhovite	$Hg_4SbO_3(OH)_3$	Very rare	Area #4
Terlinguaite	$[Hg_3]HgO_2Cl_2$	Rare	Area #4

Mineral	*Composition*	*Rarity*	*Location*
Terlinguacreekite	$Hg_3O_2Cl_2$*	Rare	Area #2
Kleinite	$Hg_2N(Cl,SO_4)\cdot nH_2O$	Rare	Area #2
Mosesite	$Hg_2N(Cl,Br,I,SO_4)$	Very rare	?
MCDUK-2	Hg-S-MoO_4	Very rare	Area #1
MCDUK-3	Hg-S-SO_4	Rare	Area #1
MCDUK-7	CHg_4OCl_2	Very rare	Area #3
MCDUK-16	No chem	Very rare	Area #2
MCDUK-17	Hg-S-O	Rare	Area #4
MCDUK-19	Hg-Sb-O	Very rare	Area #4
MCDUK-21	Hg-S-O	Very rare	Area #4
MCDUK-23	$Hg_3S_2Cl_2$	Rare	Area #4
MCDUK-26	HgS	Common	Area #4
MCDUK-27	Hg-O-Cl ?	Very rare	Area #4
MCDUK-28	Hg-S-O (?)	Rare	Area #4
MCDUK-29	No chem	Rare	Area #4
MCDUK-30	$Hg_3(SO)(SO_4)$	Rare	Area #4
MCDUK-31	No chem	Rare	Area #4
MCDUK-33	No chem	Rare	Area #4
MCDUK-46	No chem	Rare	Area #3

*The chemical composition of terlinguacreekite actually contains nitrogen in the structure instead of oxygen. However, a single crystal has not been found to determine the correct structure and formula.

PARAGENESIS

The mineralization of the McDermitt Caldera Complex is related to a series of vertical feeder veins that directed fluid phases into the volcanic formation. These vein systems were active over a period of about 4 Ma and produced several phases of mineralization, typical of a hot-spring environment. Local concentrations of precious metals, as well as the commonly associated indicator elements Hg, Sb, As, Se, Cu, and Mo, appear to be related to one or more hydrothermal events associated with the margins of the McDermitt Caldera Complex. These hydrothermal events were also responsible for localizing other potentially economic elements such as Li, U, Ga, Mo, Ge, Rb, Cs, and light REE's. Rytuba et al. (2003) sites examples of hydrothermal enrichment of gallium in zones of advanced argillic alteration within the Paradise Peak and McDermitt ore deposits. At McDermitt, this zone of advanced argillic alteration is similar to that associated with quartz-alunite (high sulfidation) Au-silica deposits and may have formed early in the evolution of the hydrothermal system that subsequently formed the hot-spring-type Hg deposit. Maximum Ga contents in this environment are likely to be only several hundred ppm.

Drill hole geochemistry suggest a positive correlation of anomalous precious metals mineralization with the pathfinder elements Hg, As, Sb, Se, Cu, and Mo. These pathfinder elements can be a high-level indicator of deeper low sulfidation epithermal gold-silver vein deposits. Thus, the geochemistry strongly suggests that the host rocks of the mercury mines at Cordero and McDermitt represent the preserved upper levels of a deeper, blind precious metals system. The vertical connection between near-surface Hg-silica mineralization and deeper Au-Ag veins is exposed at the contemporaneous Ivanhoe Hg-Au District (Wallace 2003), about 130 miles (210 km) SSE of McDermitt.

Hg and indicator chalcophile elements were already at unusually high levels in the rhyolites and tuffs of the McDermitt Caldera Complex, prior to leaching and concentration in the fault-controlled fluid conduits that became the ore deposits. This suggests that the sedimentary precursors that were partially melted to produce the felsic volcanics might already have been high in these metals, and may already have undergone Carlin-type enrichment in the Eocene. Marine sediments are thus the likely ultimate source of the Hg and other metals, as suggested for Mule Canyon by John et al. (2003b), albeit indirectly at McDerrmitt, through melting of sediments to produce rhyolitic magma. Marine sedimentary input into the system is also demonstrated by the presence of moderate Br

in terlinguacreekite and the iodide mineral radtkeite, since seawater provides by far the greatest concentration of these rare heavy halogen elements.

The temperature of deposition of the mercury ore bodies occurring in lake-bed sediments has been determined from fluid inclusions in quartz associated with cinnabar. Two-phase fluid inclusions are abundant in fine-grained quartz that occurs in veinlets and lining cavities within opalite. Homogenization temperatures indicate a deposition temperature of 195°C at Opalite mine, 200°C at McDermitt mine, and 205°C at Bretz mine. A minimum depth of formation of 500 feet (150 m) is necessary to prevent boiling at these temperatures, which is commensurate with the probable thickness of the lake beds within the caldera at the time of mineralization.

Fluid inclusions in quartz associated with the uranium ores are two-phase inclusions which homogenize at 340°C. A sample of unaltered rhyolite from the dome contains anomalously high uranium, 0.02%, and indicates, along with the high temperature of deposition, that the deposit is genetically related to the rhyolite intrusive (Rytuba 1976; Taylor and Powers 1955).

The following broad types of mineralization can be distinguished. Note that some of the mineral-forming processes operated over a long period of time and overlapped with each other, so they do not follow a strict temporal sequence.

Diagenetic argillic alteration

The volcanic glass in the volcaniclastic sediments was altered during diagenesis to microcline feldspar, cristobalite or quartz, smectites and zeolites. Zonation is apparent from fresh glass in the southeast of the caldera complex, through different zeolite species to zeolite-absent in the west (Glanzman and Rytuba 1979). Distinct zones of increasing alteration and temperature are indicated by (i) fresh glass and no zeolites, (ii) erionite in the sandstone units of the sediments, mordenite in the medial mudstone, (iii) clinoptilolite, (iv) analcime, (v) no glass or zeolites (Glanzman and Rytuba 1979); K-feldspar occurs in all zones except the first. Lithium was first mineralized as analcime (Rytuba and Glanzman 1979).

Hydrothermal argillic alteration

More intense hydrothermal alteration was identified at five discrete sites in the caldera complex by Glanzman and Rytuba (1979): the McDermitt mine, Bretz mine, Opalite mine, a spot 2 km south of the Bretz mine, and an area in the southwest, at the boundary of the Bull Basin and Montana Mountains. This alteration caused a rapid progression through the zeolite zones over small distances, formation of montmorillonite, “7 Å clay mineral” (probably kaolinite) and mixed-layer clay minerals, oxidation of the sediments, and graded into the two phases below.

Silicification

A distinct phase of silicic alteration started later than the argillic alteration, as evidenced by outcrop-sized relicts of relatively lightly silicified altered tuffs in more intensely silicified “opalite”. The silicification front is sharp but irregular, and cuts pre-existing stratigraphy. Silicification and associated sulfide mineralization may have used the vitric-lithic tuff as a conduit, since the most intense mineralization occurs within, just above and just below this stratigraphic layer (Hetherington and Cheney 1985).

Sulfides

Sulfide deposition appears to have started later than silicification, but overlapped strongly with it (Hetherington and Cheney 1985). McCormack (1986) states that pyrite and stibnite were deposited earlier than cinnabar. Additional sulfides include marcasite and realgar. Native gold and silver were also deposited during the early sulfide phase. The more chalcophilic elements such as Hg may have been transported as sulfide complexes (John et al. 2003b; Hampton et al. 2004). Soluble sulfide complexes are most stable in neutral or alkaline fluids, and silica most soluble under alkaline conditions, consistent with the idea that the early hydrothermal fluids were predominantly alkaline (Rytuba 1976).

Hydrothermal gangue minerals

Some non-sulfide minerals appear to have formed in ore veins about the same time as the sulfides, and often containing inclusions of sulfides. These include fluorite and baryte.

Diversification of mercury minerals

Some of the cinnabar reacted with later hydrothermal fluids to produce a diverse suite of secondary Hg minerals. Sulfohalides and nitride-halides appear to have been relatively early, followed by oxidative disproportionation of cinnabar to produce native mercury, and further reaction of mercury to produce calomel, oxyhalides and montroydite. The associated fluids are in general likely to have been more oxidized and/or acidic than the reducing, sulfide-rich, alkaline fluids of stages 3-5. These stages are delineated in detail below.

Note that under acidic or oxidizing conditions, where sulfide complexes are unstable, Hg could still be transported by complexation with chloride, which is also abundant in the system at McDermitt and can significantly mobilize Hg (Brandon et al. 2001).

1. Acid sulfate alteration

As noted above, more oxidized fluids containing sulfate rather than sulfide occurred later during the hydrothermal activity. These may have been derived from sulfidic fluids by oxidation, due to mixing with meteoric water. Note that change from the relatively weak acid hydrogen sulfide to the much stronger sulfuric acid liberates hydrogen ions, lowering the pH:

$$H_2S + 2O_2 \rightarrow SO_4^{2-} + 2H^+$$

The aggressive acidic fluid reacted not just with sulfides but also with Al-rich silicates such as glass, feldspar and kaolinite to produce alunite, and with calcite to form gypsum. An example of a possible alunite-forming reaction is:

$$^3/_2Al_2Si_2O_5(OH)_4 + 2SO_4^{2-} + 3H^+ \rightarrow KAl_3(SO_4)_2(OH)_6 + 3SiO_2 + {}^3/_2H_2O$$

kaolinite alunite

2. Solid sulfide oxidation

Exposure of pyrite and marcasite to air or aerated meteoric water formed melanterite, copiapite, fibroferrite, jarosite and ultimately goethite, hematite. The mercury sulfate schuetteite would have been formed from cinnabar at this time.

In more detail, the following paragenetic stages can be distinguished for the mercury minerals:

3. Cinnabar phase

Cinnabar was precipitated, along with other sulfides and with silicates such as microcline and quartz, from alkaline fluids. Decomposition of soluble sulfide complexes to produce solid cinnabar would have been triggered by a combination of depressurization (encouraging boiling and loss of H_2S in vapor), cooling, dilution or acidification:

$$HgS_2^{2-} + 2H^+ \rightarrow HgS + H_2S$$

4. Early mercury sulfohalide phase

A change of fluid composition towards lower pH and perhaps higher chloride activity resulted in widespread alteration of cinnabar. Experimental studies conducted by Foord et al. (1974) show that corderoite (or its high-temperature polymorph kenhsuite) is stable relative to other Hg sulfides and chlorides up to 325°C, and that corderoite forms readily by reaction of cinnabar with HCl or acidified NaCl solution at room temperature:

$$3HgS + 2Cl^- + 2H^+ \rightarrow Hg_3S_2Cl_2 + H_2S$$

The relative ease with which corderoite is formed under acid conditions, the presence of Cl^- ions as a common constituent of hot spring or ground waters, and replacement textures of cinnabar by corderoite observed in the field are all consistent with the deduction that corderoite is a low-temperature supergene mineral (Foord et al. 1974). Parks and Nordstrom (1979) give it a stability field in the Hg-S-Cl-O-H system under moderately reducing (cinnabar-mercury buffer) and strongly acidic conditions.

Replacement of cinnabar by corderoite and kenhsuite has been noted at the McDermitt mine, due to reaction with low-pH chloride-rich fluids. Kenhsuite tended to form later than corderoite, but may have been simultaneous with it, in part. Kenhsuite is the higher-temperature polymorph but can persist metastably at room temperature, so the formation of kenhsuite in preference to corderoite may imply either a rise in fluid temperature, a change in nucleation and crystallization kinetics, or stablization of the kenhsuite structure by impurities.

Coexistence of alpha, beta and gamma $Hg_3S_2Cl_2$

a. Bear in mind the Phase Rule. In general, only one of these phases has the lowest free energy at any given pressure-temperature combination. There are unique lines in P-T space where two of them coexist/can inter-transform at equilibrium, and a unique triple point where all three can do so. Then, there is also the possibility that they are unstable relative to other compounds or combinations of compounds. What we know about relative thermodynamic stability is that corderoite is the most stable of the three at low-T conditions, the beta phase is stable at higher T, and kenhsuite is never actually the most stable.

b. What occurs in nature is determined not just by thermodynamics but also by kinetics. If a crystal of an unstable phase can nucleate and grow faster than that of a stable phase, while the transformation process to the stable phase is slow, then the unstable phase will grow. There are so many physical parameters to consider, like grain size/shape/surface area as well as trace chemistry that affects kinetics, that quantitative study or predictions are a nightmare relative to their simpler thermodynamics-based equivalents!

The gray intergrowth is clearly extremely metastable. Tiny fluctuations in conditions and trace impurities/adsorbents may be favoring growth of now one phase, now another. Ultimately, it is going to want to recrystallize as corderoite.

5. Mercury nitride phase

Mercury nitrides are confined to a small area including the south end of the McDermitt open pit and the Cordero mine, consistent with the requirement for a distinctive fluid composition. High nitrogen (NH_4^+) in the ascending fluids produced kleinite, mosesite, and terlinguacreekite. The ammonium ion was likely produced when molecular N_2, originally from the atmosphere and dissolved in meteoric water, was reduced by H_2S in the hydrothermal fluids, catalyzed by iron sulfide minerals (Schoonen and Xu 2001):

$$4N_2 + 3H_2S + 12H_2O + 2H^+ \rightarrow 8NH_4^+ + 3SO_4^{2-}$$

Localization within small zones inside a very active caldera makes it unlikely that nitrogen was sourced from decaying organic material in sediments. Acidity of the hydrothermal fluid would have retained the nitrogen as ammonium, rather than allowing its loss as ammonia gas.

Kleinite is not invariably associated with cinnabar, but may have formed from dissolved Hg chloride complexes:

$$2HgCl_4^{2-} + NH_4^+ \rightarrow Hg_2NCl + 4H^+ + 7Cl^-$$

The terlinguacreekite formed sometime later than the kleinite, as some terlinguacreekite crystal groups have been observed attached to kleinite. All the Hg nitride minerals also contain Cl^-, but the terlinguacreekite also contains appreciable Br, suggesting that the Br content of the fluid may have increased through time. No contact relationships have been recorded for the mosesite.

6. Late mercury sulfohalide phase

Radtkeite is a relatively late mineral, replacing earlier corderoite or more likely kenhsuite. Radtkeite contains iodide as an essential component, which may mean that the iodide concentration in the fluid was increasing through time (cf. comment on bromide in terlinguacreekite). Radtkeite is also later than the nitride-chloride kleinite, since small masses of radtkeite have been noted attached to kleinite. Alteration of kleinite to produce radtkeite implies not only an increase in iodide activity in the fluid, but also that H_2S is still present.

$$3Hg_2NCl + 4H_2S + 4H^+ + 2I^- = 2Hg_3S_2ClI + 3NH_4^+ + Cl^-$$

The presence of sulfide, iodide and ammonium all imply that redox conditions were still reducing, overall. The presence of substantial iodide and bromide implies that marine sediments would have contributed to the hydrothermal fluids,

7. Mercury oxyhalide phase

As noted previously (Dunning et al. 2005), mercury is a highly chalcophilic element for which oxysalts are not particularly stable. Therefore, oxidation of the sulfide cinnabar produces sulfate which enters solution but is accompanied by reduction of the cation Hg^{2+} to native mercury. This is an overall reaction that can be classified as oxidative disproportionation, as shown below.

$$HgS + H_2O + {}^3/_2O_2 \rightarrow Hg + SO_4^{2-} + 2H^+$$

Subsequent oxidation of native mercury in the presence of chloride-rich fluids formed eglestonite and terlinguaite. The presence of calomel or montroydite may indicate conditions that were respectively more acidic/reducing/Cl-rich or alkaline/oxidizing/Cl-poor. Schematic reactions of native Hg to form these minerals are:

Calomel: $2Hg + 2Cl^- + 2H^+ + {}^1/_2O_2 \rightarrow Hg_2Cl_2 + H_2O$

Eglestonite: $6Hg + 3Cl^- + 3H^+ + {}^3/_2O_2 \rightarrow (Hg_2)_3Cl_3O(OH) + H_2O$

Terlinguaite: $4Hg + 2Cl^- + 2H^+ + {}^3/_2O_2 \rightarrow (Hg_3)HgO_2Cl_2 + H_2O$

Montroydite: $Hg + {}^1/_2O_2 \rightarrow HgO$

Both eglestonite and terlinguaite have not been observed in direct contact with each other. However, when they are found on the same rock sample, there is always a dividing rock phase separating them.

8. Mercury sulfate phase

At a very late stage, subaerial oxidation of cinnabar produced the Hg sulfate schuetteite as a fine-grained lite-yellow coating. Schuetteite forms under strongly acidic and oxidizing conditions (Parks and Nordstrom 1979).

$$3HgS + 2H_2O + 6O_2 \rightarrow Hg_3(SO_4)O_2 + 2SO_4^{2-} + 4H^+$$

9. Mercury carbide phase

This very rare phase is intimately associated with terlinguacreekite in a rock type that probably formed between the massive cinnabar-corderoite rock and a light gray breccia rich in kleinite and terlinguacreekite. Because of the minute size of this carbide phase, its paragenetic relationship to terlinguacreekite could not be established with any certainty. It is believed that a pre-existing aliphatic organic mineral phase was acted upon by fluids containing Hg^{2+} in an oxygen-chloride environment. It is also believed that these conditions were very similar to that which formed both kleinite and terlinguacreekite.

The unusual mercury oxy-chloride carbide is the first natural occurrence of a derivative of Hofmann's base, a compound easily made in the laboratory. In general, aromatics are difficult to break apart into single carbon atoms because of the strong bonding forces. If the iodoform-analogue hypothesis is correct, then there must have been some aliphatic 2-ol or a 2-one functional group which may have been attached to a larger aromatic molecule or not. If the molecule in question is light and highly hydroxylated, it could be dissolved in water with no other mineralogical evidence of its existence. Fragmented "humate"/fulvate" polymers from decay of former vegetation during wetter climates would suffice.

Paragenetic Flow Charts

The following two paragenetic flow charts illustrate a fair representation of the formation sequence for the McDermitt mine mercury mineralization. Flow chart Figure 262 gives the flow of the oxidation of primary cinnabar into a series of secondary minerals. This chart includes both known and unknown mercury phases and their placement is the result of observations of many samples collected from several mine locations and examined under microscopic conditions. Flow chart Figure 263 gives the flow of the oxidation of pyrite, stibnite and cinnabar from a specific mine location designated as Area 4. This locality is unique in that both primary

stibnite and pyrite are observed being surrounded by later cinnabar. The oxidation of Hg, Sb and Fe primary phases have resulted in a suite of interesting secondary phases unique to this mine.

Figure 262. *Paragenetic flow chart for minerals formed by the alteration of cinnabar from the McDermitt mine.*

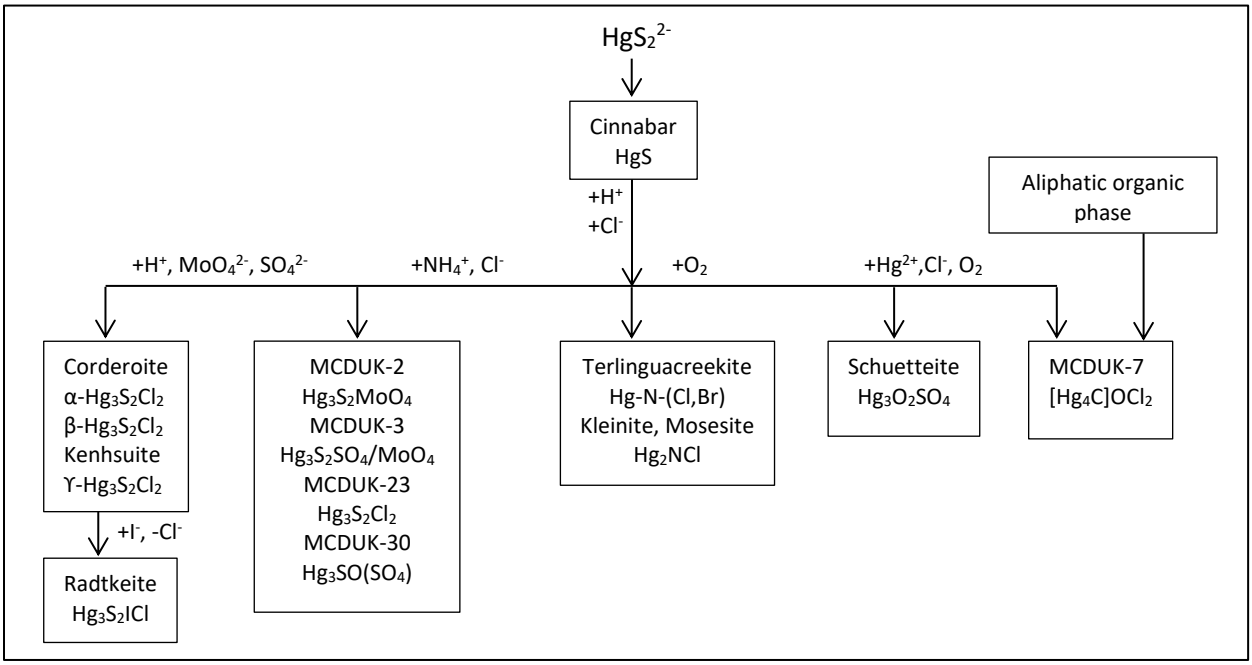

Figure 263. *Paragenetic flow chart for minerals formed by the alteration of cinnabar, stibnite, pyrite and mercury at the McDermitt mine.*

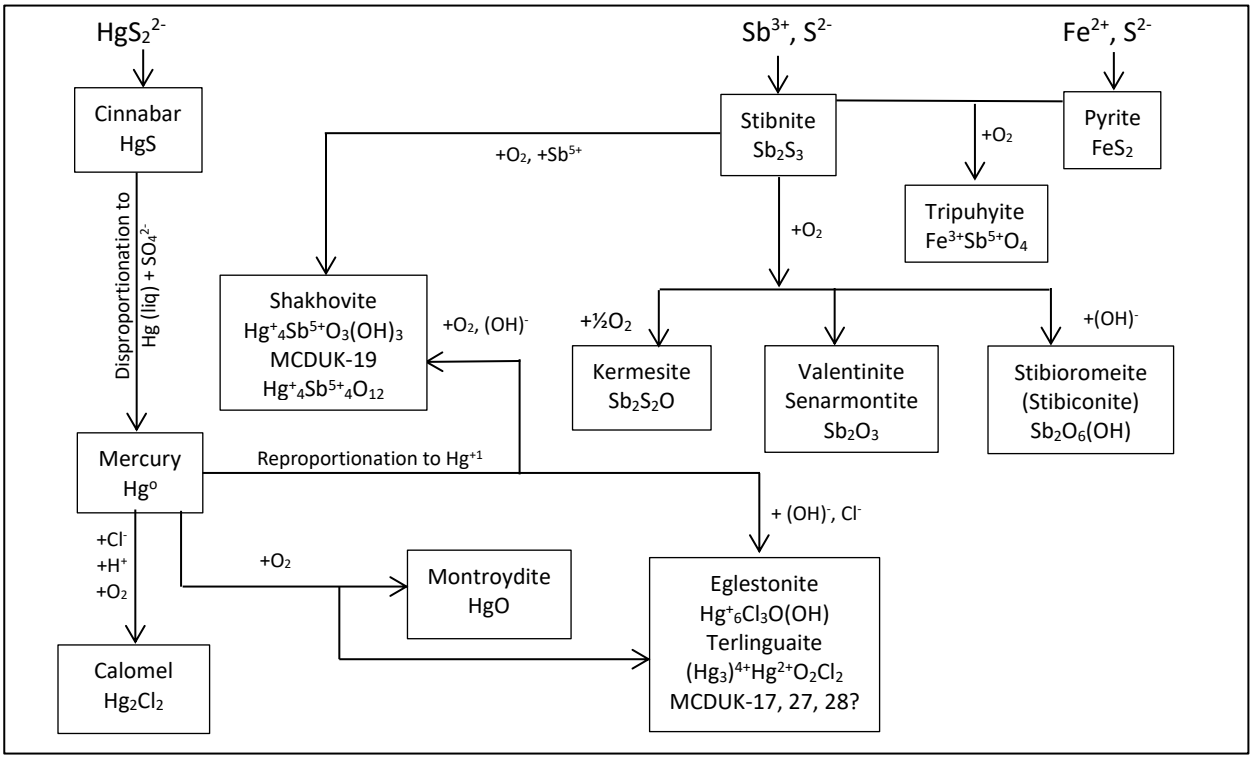

Table 11. *Paragenetic timeline for associated and mercury mineralization of the McDermitt Caldera Complex.*

Mineral	Early	Late
Quartz	———	
Fluorite	———	
Pyrite	———	
Marcasite	———	
Stibnite	———	
Cinnabar	———	
Corderoite	———	
Kenhsuite	———	
β-$Hg_3S_2Cl_2$	———	
Radtkeite	———	
Calomel	———	
Mercury	———	
Montroydite	———	
Eglestonite	———	
Schuetteite	———	
Terlinguaite	———	
Terlinguacreekite	———	
Kleinite	———	
Mosesite	———	
MCDUK-2	———	
MCDUK-3	———	
MCDUK-7	———	
MCDUK-16	———	
MCDUK-17	———?	
MCDUK-18	———?	
MCDUK-19	———?	
MCDUK-21	———?	
MCDUK-30	———?	
MCDUK-33	———?	
MCDUK-46	———?	

Table 12. *Paragenetic timeline for uranium mineralization of the McDermitt Caldera Complex.*

Mineral	Early	Late
Galena?	———	
Arsenopyrite?	———	
Chalcopyrite?	———	
Uraninite	———	
U-Rich Zircon	———	
Coffinite	———	
Meta-autunite	———?	
Metazeunerite	———?	
Metatobernite	———?	
“Gummite”	———?	

Table 13. *Paragenetic timeline for the Fe/Sb/Mn mineralization of the McDermitt Caldera Complex.*

Mineral	Early	Late
Pyrite	———	
Marcasite	———	
Stibnite	———	
Reagar	———	
Chapmanite	———	
Tripuhyite	———?	
Stibioromeite	———?	
Copiapite	———	
Fiberoferrite	———	
Geothite	———	
Hematite	———	
Melanterite	———	
Lithiophorite	———?	
Cryptomelane	———?	

Table 14. *Paragenesis sequence of minerals present at the McDermitt mine (modified after McCormack 1986).*

Mineral	Formula	Classification
Mercury Minerals		
Cinnabar	HgS	Primary Hydrothermal
Corderoite	$Hg_3S_2Cl_2$	Hydrothermal Replacement
Calomel	Hg_2Cl_2	Secondary
Eglestonite	$Hg^{+}_6Cl_3O(OH)$	Secondary
Terlinguaite	$[Hg^{+}_2Hg^{2+}]Hg^{2+}O_2Cl_2$	Secondary
Kleinite	$Hg_2N(Cl,SO_4)\cdot nH_2O$	Secondary
Terlinguacreekite	$Hg^{2+}_3O_2Cl_2$	Secondary
Schuetteite	$Hg_3(SO_4)O_2$	Secondary
Mosesite?	$Hg_2N(Cl,SO_4,MoO_4,CO_3)\cdot H_2O$	Secondary
Montroydite	HgO	Secondary
Kenhsuite	$Hg_3S_2Cl_2$	Hydrothermal Replacement
Mercury	Hg	Secondary
Radtkeite	$Hg_3S_2Cl(I)$	Secondary Hydrothermal Replacement
Shakhovite	$Hg^{+}_4Sb^{5+}O_3(OH)_3$	Secondary
Beta phase	$Hg_3S_2Cl_2$	Hydrothermal Replacement
MCDUK-2	$Hg^{2+}_3S_2(MoO_4)$	Secondary
MCDUK-3	$Hg^{2+}_3S_2(SO_4,MoO_4)$	Secondary
MCDUK-7	$C[Hg^{2+}]_4OCl_2$	Secondary
MCDUK-16	?	Secondary
MCDUK-17	Hg-S-O	Secondary
MCDUK-19	$Hg^{+}_4Sb^{5+}_4O_{12}$	Secondary
MCDUK-21	Hg-S-O	Secondary
MCDUK-23	$Hg_3S_2Cl_2$	Hydrothermal Replacement
MCDUK-27	Hg-O-Cl ?	Secondary
MCDUK-28	?	Secondary
MCDUK-30	$Hg_3SO(SO_4)$	Hydrothermal Replacement
MCDUK-31	?	Secondary ?
MCDUK-33	?	Secondary ?
MCDUK-46	?	?
Antimony Minerals		
Stibnite	Sb_2S_3	Primary Hydrothermal

Mineral	Formula	Classification
Chapmanite	$SbFe^{3+}{}_2Si_2O_8(OH)$	Primary Hydrothermal
Senarmontite	Sb_2O_3	Secondary
Stibiconite	$Sb^{3+}Sb^{5+}O^6(OH)$	Secondary
Valentinite	Sb_2O_3	Secondary
Tripuhyite	$Fe^{3+}Sb^{5+}O_4$	Secondary
Kermesite	Sb_2S_2O	Secondary
Iron/Manganese Minerals		
Pyrite	FeS_2	Primary Hydrothermal
Marcasite	FeS_2	Primary Hydrothermal
Hematite	Fe_2O_3	Secondary
Jarosite	$KFe^{3+}{}_3(SO_4)_2(OH)_6$	Secondary
Goethite	α-$Fe^{3+}O(OH)$	Secondary
Melanterite	$Fe^{2+}SO_4{\cdot}7H_2O$	Secondary
Copiapite	$Fe^{2+}Fe^{3+}{}_4(SO_4)_6(OH)_2{\cdot}20H_2O$	Secondary
Fibroferrite	$Fe^{3+}(SO_4)(OH){\cdot}H_2O$	Secondary
Cryptomelane	$K(Mn^{4+}{}_7Mn^{3+})O_{16}$	Secondary
Lithiophorite	$(Al,Li)Mn^{4+}O_2(OH)_2$	Secondary
Copper Minerals		
Conichalcite	$CaCu^{2+}(AsO_4)(OH)$	Secondary
Elements		
Gold	Au	Primary Hydrothermal
Sulfur	S	Secondary

DISCUSSION

Within the McDermitt mercury deposit, two general mineralization environments were recognized from extensive field and microscopic examinations. First, a large or mega environment was observed consisting of an initial horizontal influx of mercury-rich fluids that engulfed the area, forming massive cinnabar. This horizontal mineral zone was then acted upon by low pH chloride-rich fluids which transformed about ¼ of the cinnabar into massive corderoite.

Within and possibly along marginal edges of the cinnabar-corderoite mineralization environment a number of smaller or microenvironments formed by the action of fluids with varying pH, Eh, temperature, and ion concentrations over an unknown time period. Many of these microenvironments appear to be confined to voids in the ground rock, often quartz-lined. Within these voids, which are both uniform in size or very irregular in size, contain a variable selection of secondary mineralization resulting from the oxidation of cinnabar and/or the remobilization of previously altered phases from cinnabar.

Of particular interest is a suite of secondary minerals contained within a mass of stibnite/cinnabar containing intrusive rock. Samples of rocks from this location have resulted in a minimum of seven new mercury-bearing phases in addition to several known mercury phases. Cinnabar has been observed altering to liquid mercury and eglestonite. Rarely, the mercury has oxidized to individual clusters of montroydite. Eglestonite occurs as individual or clusters of crystals but most commonly as veins associated with liquid mercury.

Our first indication of micro void mineralogy was the discovery within a breccia containing both cinnabar and corderoite. Within these quartz-lined voids was discovered minute, colorless, prismatic crystals. These crystals were identified as kenhsuite, not previously identified in this rock type. Also within this rock type five samples were recovered that contained individual clusters of a white mineral. Upon closer examination, these clusters were composed of individual prismatic crystals attached to quartz crystals. This second phase discovered has been identified as a new mercury sulfide molybdate.

Within the same general area abundant cinnabar-corderoite bearing rock was found to contain many small irregular voids containing a dark brown cubic phase often associated with a prismatic light green to gray phase. This cubic phase was identified as corderoite, quite unlike the massive pinkish red massive corderoite derived from cinnabar. It would appear that this new habit is the result of secondary solution migration. It was also determined

that the cubic corderoite crystals formed after the light green, prismatic phase, also assumed to have formed by secondary fluids. This phase has been determined to be a mercury sulfide sulfate/molybdate.

An unusual rock type was recovered in the general area which is best described as a fine-grained silica-rich contact rock. Within this rock minute quantities of massive kleinite were identified along with crystals of terlinguacreekite. Upon further examination, individual crystals and grains of a black, prismatic mineral was identified. This phase was identified as the first mercury carbide oxychloride in Nature and a derivative of Hofmann's base. This unusual rock type appears to be a contact zone between the cinnabar-corderoite pinkish-red rock and a light gray rock rich in kleinite and terlinguacreekite.

The most prolific micro void collection of new phases has come from a mass of localized rock mass containing massive and crystallized stibnite associated with later cinnabar. Secondary fluid interaction of these primary sulfide minerals has produced a collection of unusual new mercury and antimony phases unique to this locality. So far, six new mercury and antimony phases have been identified from rock samples extracted from this locality.

We have no quantitative data for fluid compositions and other conditions at the time of growth of the various mercury minerals in the McDermitt Caldera Complex. It is also the case that there are no thermodynamic data available for most of the rarer minerals. Nevertheless, what is currently known about the stability of Hg minerals makes it clear that fluid compositions varied through time and at different locations in the caldera, as indicated in the account of paragenesis above. In particular, different minerals would have been stable under different conditions of fluid acidity (measured by pH) and redox conditions (measured by electrode potential Eh). Note that these parameters are not themselves true thermodynamic state variables like temperature, but are set locality by the concentrations of abundant species in the fluid. In particular, the ratios of Fe^{2+} to Fe^{3+} and/or sulfide species (H_2S, SH^-, S^{2-}) to SO_4^{2-} will probably have been the main determinants of redox potential, and the latter will also have been important in setting local pH, since sulfuric acid is a much stronger acid than hydrogen sulfide. Carbonate and silicate content might also have helped to determine pH.

ACKNOWLEDGMENTS

Undertaking of such a task of determining the complex mineralogy of this mine at first seemed an impossible effort. The following individuals are acknowledged and thanked for their part in the completion of this project and the knowledge that it has imparted to the science of mineralogy.

Ms. Sharon Cisneros of the Mineral Research Company provided important McDermitt mine samples for study, which were identified as terlinguacreekite. Mr. Charles Cox labored tirelessly in the field and provided nearly an endless supply of extremely hard rock and transported it back for analysis. Mr. Dan Evanich provided several photos for one of our unknowns, a rather difficult sample to photograph. Dr. Robert Housely provided SEM/EDS data for two samples. Dr. Anthony Kampf provided SEM photographs and PXRD identification of several samples which proved to be new mineral phases, including the first natural beta phase of $Hg_3S_2Cl_2$. Mr. Dick Thomssen provided important photographs and a sample for the project and obtained a tripuhyite photo from Mr. Mike Trebisky. Mr. Stephan Wolfsried provided and is thanked for several excellent photomicrographs of selected minerals for this report. Mr. Ramon Lopez furnished Cox with wonderful comparative samples of rare Hg species from Spain and Italy. Last but not least, Mark Cooper of the University of Manitoba for providing invaluable structure and identification data for a seeming endless supply of samples we submitted to him, in the hopes that at least one would be a new mercury phase not previously discovered from the McDermitt mine or elsewhere in nature. To date, thirteen potential new mercury phases have been discovered from the ore samples collected and examined.

REFERENCES

AINSWORTH, B. (2004) Geological report for Clan Resources Ltd., Vancouver, BC, Aurora Project, Malheur County, OR, SEC Exhibit 99-1, 34 pp.

ALBERS, J.P. and KLEINHAMPLE, F. (1970) Spatial relation of mineral deposits to Tertiary volcanic centers in Nevada: U.S. Geological Survey Profesional Paper 700-C, C1-C10.

ANDERSON, D. (2003) Environmental cleanup site information (ECSI) database site summary report-details for site ID: 2491, Opalite mine, ID: 2493, Bretz mine. Oregon Department of Environmental Quality, Portland, Oregon 97204. www.deq.state.or.us/.

BAILEY, E.H. and PHOENIX, D.A. (1944) Quicksilver deposits in Nevada. *University Nevada Bulletin* **38**, 206p.

BAILEY, E.H., HILDEBRAND, F.A., CHRIST, C.L. and FAHEY, J.J. (1959) Schuetteite, a new supergene mercury mineral. *American Mineralogist*, **44**, 1026-1038.

BECK, J. and HEDDERICH, S. (2000) Synthesis and crystal structure of $Hg_3E_2X_2$ family. *Journal of Solid State Chemistry*, **151**, 73-76.

BENSON, T.R., HAHOOD, G.A. and COBLE, M.A. (2013) An intense 16.5-16.0 Ma episode of rhyolitic volcanism associated with flood basalt dike emplacement at McDermitt Caldera Field and High Rock Caldera Complex, Nevada and Oregon. *American Geophysical Union Fall Meeting*, Dec., abstract V33E-2828.

BENSON, T.R., HAHOOD, G.A. and COBLE, M.A. (2014) Magmatic enrichments of energy-critical elements, Li, Ga, REE in rhyolites of McDermitt Volcanic Field, High Rock Caldera Complex, and Buff Peak intensified by *in situ* SHRIMP-RG analysis of melt inclusions in quartz. Paper 3 43-12, October. Geological Society of America Abstracts with Programs, **46**(6), 826.

BENSON, T.R., HAHOOD, G.A. and COBLE, M.A. (2015) Controls on the enrichment of energy-critical elements (Li, Ga, REE) in weakly peralkaline magmas of the Mid-Miocene McDermitt Volcanic Field, Oregon and Nevada, based on the *in situ* SHRIMP-RG analysis of quartz-hosted melt inclusions. GSA Annual Meeting, Baltimore, November.

BENSON, T.R. and HAHOOD, G.A. (2015) The oldest known caldera associated with the Yellowstone hot spot: New Geologic Mapping, Geochemistry, and 40Ar/39Ar Geochronology for the Northern McDermitt Volcanic Field, Northern Nevada and Southeastern Oregon. *American Geophysical Union Fall Meeting*, December.

BENSON, T.R., MAHOOD, G.A., COBLE, M.A. and GROVE, M.J. (2016) New geological mapping and 40Ar/39Ar geochronology demonstrate that rhyolite volcanism mirrors northwestward propagation of Mid-Miocene Columbia River Flood Basalts. *GSA Rocky Mountain Section Meeting*, Moscow, Idaho, May.

BENSEN, T.R. and MAHOOD, G.A. (2016) A tale of two swarms: mapping of calderas and 40Ar/39Ar geochronology delineate two distinct Steens Basalt fissure systems. *American Geophysical Union Fall Meeting*, December.

BENSON, T.R. (2017) Geology, 40Ar/39Ar geochronology, and lithium enrichment of the Mid-Miocene McDermitt Volcanic Field (Nevada and Oregon, United States), Ph.D. Thesis, Sanford University, 239 pp.

BENSON, T.R., MAHOOD, G.A., and GROVE, M.J. (2017) Geology and 40Ar/39Ar geochronology of the middle Miocene McDermitt volcanic field, Oregon and Nevada: Silicic volcanism associated with propagating flood basalt dikes at initiation of the Yellowstone hot spot. *Geological Society of American Bulletin* **129**(9-10), 1027-1051.

BENSON, T.R., COBLE, M.A., RYTUBA, J.J. and MAHOOD, G.A. (2017) Lithium enrichment in rhyolite magmas of intracontinental calderas leads to Li deposits in caldera basins. *Nature Communications*, **8**, article 270, 1-9.

BLUMENFELD, J. (2014) Environmental photo selection of McDermitt and Cordero mine areas. www.flickr.com/photos/epar9jeb.

BORISOV, S.V., MAGARILL, S.A., ROMANENKO, G.V. and PERBVUKHINA, N.V. (1999): Crystallochemical peculiarities of hypergene rare mercury sources in surface water – atmospheric pools. *Khimiya v interesah ustiochivogo razvitiya* **7**, 497-503.

BRANDON, N.P., FRANCIS, P.A., JEFFREY, J., KELSALL, G.H. and YIN, Q. (2001) Thermodynamics and electrochemical behaviour of Hg-S-Cl-H_2O systems. *Journal of Electroanalytical Chemistry*, **497**, 18-32.

BREITINGER, D.K., PETRIKOWSKI, G., LIEHR, G. and SENDELBECK, R. (1983) Metallomethane, VI [1] Kristallstrucktur von Tetrakis(chloroquecksilber)methan-dimethylsulfoxid $C(HgCl)_4 \cdot (CH_3)_2SO$. *Zeitschrift. Naturforsch*, **38b**, 357-364.

BRODERSEN, K., GÖBEL, G. and LIEHR, G. (1989) Terlinguaite $Hg_4O_2Cl_2$, a mineral with unusual Hg_3 units. *Zeitschrift für Anorganische und Allgemeine Chemie*, **575**, 145-153.

BROOKS, H.C. (1959) Quicksilver in Oregon. Oregon Department of Geology and Mineral Industries. Presented at the geology session of the 1959 Pacific Northwest Regional Conference, AIME.

BROOKS, H.C. (1963) Quicksilver in Oregon. *Oregon Department of Geology and Mineral Industries Bulletin* **B-055**. 223p.

CAMP, V.E., ROSS, M.E., and HANSON, W.E. (2003) Genesis of flood basalts and Basin and Range volcanic rocks from Steens Mountain to the Malheus River Gorge, Oregon, *GSA Bulletin*, Vol. **115** (1), 105-128.

CAMP, V.E., and ROSS, M.E. (2014) Radiating Volcanic Migrations: An example from the Pacific Northwest, U.S.A., downloaded from www.MantlePlumes.org, June 3, 2018, 9 pp.

CAREW, T.J. (2008) NI 43-101 Technical Report and Resource Estimation for the Cordero Gallium Project, Humboldt County, Nevada, USA, prepared for Gold Canyon Resources, Inc., 35 pp.

CARLSON, E.H. (1967) The growth of HgS and $Hg_3S_2Cl_2$ single crystals by a vapor phase method. *Journal of Crystal Growth*, **1**, 271-277.

CASTOR, S.B., HENRY, C.D. and SHEVENELL, L.A. (1996) Volcanic rock-hosted uranium deposits in northwestern Nevada and southeastern Oregon-possible sites for studies of natural analogues for the potential high-level nuclear waste repository at Yucca Mountain, Nevada. *Nevada Bureau of Mines and Geology Open File Report* **96-3**.

CASTOR, S.B. and HENRY, C.D. (2000) Geology, geochemistry, and origin of volcanic rock-hosted uranium deposits in northwestern Nevada and southeastern Oregon, US: *Ore Geology Reviews*, **16**, 1-40.

CASTOR, S.B. and FERDOCK, G.C. (2004) Minerals of Nevada. *Nevada Bureau of Mines and Geology Special Publication* **31**. University of Nevada Press, Reno and Las Vegas.

CHRISTIANSEN, R.L., FOULGER, G.R., and EVANS, J.R. (2012) Upper-mantle origin of the Yellowstone hotspot, *GSA Bulletin*, Vol. **114** (10), 1245-1256.

CHILDS, J.F. (2007) Cordero gold-silver project technical report, Cordero-43-101_09-04-07-Final.pdf, Opalite Mining District, McDermitt, Nevada. (Report prepared for Silver Predator Corporation, Reno, Nevada).

COBLE, M.A. and MAHOOD, G.A. (2008) New geologic evidence for additional 16.5-15.5 Ma silicic calderas in northwest Nevada related to initial impingement of the Yellowstone hot spot. IOP Publishing, Inc., Collapse Calderas Workshop, Conference 1 Series: Earth and Environmental Science 3, Earth and Environmental Science, 4 pp. (2008) 012002.

COBLE, M.A. and HAHOOD, G.A. (2012) Initial impingement of the Yellowstone plume located by widespread silicic volcanism contemporaneous with Columbia River flood basalts. *Geology*, **40**(7), 655-658.

COBLE, M.A. and MAHOOD, G.A. (2016) Geology of the High Rock caldera complex, northwest Nevada, and implications for intense rhyolitic volcanism associated with flood basalt magmatism and the initiation of the Snake River Plain-Yellowstone trend. *Geosphere*, **12**(1), 58-113.

CONRAD, W.K. (1984) The mineralogy and petrology of compositionally zoned ash flow tuffs, and related silicic volcanic rocks, from the McDermitt Caldera Complex, Nevada-Oregon. *Journal of Geophysical Research*, **89**, 8639-8664.

CONRAD, W.K., McKEE, E.H., RYTUBA, J.J., NASH, J.T. and UTTERBACK, W.C. (1993) Geochronology of the Sleeper Deposit, Humboldt Country, Nevada: epithermal gold-silver mineralization following emplacement of a silicic flow-dome complex. *Economic Geology*, **88**, 317-327.

COOMBS, D.S., ALBERTI, A., ARMBRUSTER, T., ARTIOLI, G., COLELLA, C., GALLI, E., GRICE, J.D., LIEBAU, F., MANDARINO, J.A., MINATO, H., NICKEL, E.H., PASSAGLIA, E., PEACOR, D.R., QUARTIERI, S., RINALDI, R., ROSS, M., SHEPPARD, R.A., TILLMANNS, E. and VEZZALINI, G. (1997) Recommended nomenclature for zeolite minerals: report

of the subcommittee on zeolites of the International Mineralogical Association, Commission on New Minerals and Mineral Names. *Canadian Mineralogist*, **35**, 1571-1606.

COOPER, M.A., ABDU, Y.A., HAWTHORNE, F.C. and KAMPF, A.R. (2013) The crystal structure of comancheite, $Hg^{2+}_{55}N^{3-}_{24}(OH,NH_2)_4(Cl,Br)_{34}$, and crystal-chemical and spectroscopic discrimination of N^{3-} and O^{2-} anions in Hg^{2+} compounds. *Mineralogical Magazine*, **77**, 3217-3237.

CURRY, D.L. (1960) The geology of the Cordero quicksilver mine area, Humboldt County, Nevada. M.S. thesis, University of Oregon, Eugene, Oregon.

DADOLY, J. (2001) Bretz mine PA report, ECSI # 2493, Oregon Department of Environmental Quality, Pendleton, Oregon.

DAYVAULT, R.D., CASTOR, S.B. and BERRY, M.R. (1985) Uranium associated with volcanic rocks of the McDermitt Caldera, Nevada and Oregon, *in* Uranium deposits in volcanic rocks: Proceedings of a technical committee meeting: Panel Proceedings Series-International Atomic Energy Agency, STI/PUB/690, 379-409.

DUNNING, G.E. and COOPER, J.F., JR. (2002) Pseudomorphic melanophlogites from California. *Mineralogical Record*, **33**, 237-242.

DUNNING, G.E., HADLEY, T. A., MAGNASCO, J., CHRISTY, A.G. and COOPER, J.F., JR. (2005) The Clear Creek mine, San Benito County, California: A unique mercury locality. *Mineralogical Record,* **36**, 337-363.

ĎUROVIČ, S. (1968) The crystal structure of γ-$Hg_3S_2Cl_2$. *Acta Crystallographica*, **B24**, 1661-1670.

ERD, R.C., ROBERTS, A.C., BONARDI, M. CRIDDLE, A.J., LEPAGE, Y., and GABE, E.J. (1993) Edoylerite, $Hg^{2+}_3S_2(Cr^{6+}O_4)$, a new mineral from the Clear Creek claim, San Benito County, California. *Mineralogical Record*, **24**, 471-475.

FISK, E.L. (1961) Cinnabar at Cordero, where they find it…how they find it. *Mining Engineering*, November, 1228-1230.

FISK, E.L. (1968) Cordero mine, Opalite mining district. In, J.D. Ridge, Ed., *Ore Deposits of the United States*, 1933-1967, vol**. 2**, 1573-1591. AIME Publ.

FOORD, E.E., BERENDSEN, P., and STOREY, L.O. (1974) Corderoite, first natural occurrence of α-$Hg_3S_2Cl_2$, from the Cordero mercury deposit, Humboldt County, Nevada. *American Mineralogist***, 59**, 652-655.

FOURIE, L. and PELDIAK, D. (2013) Independent Technical Report for the Thacker Pass Project, Humboldt County, Nevada, USA; prepared for LithiumAmericas by Advisian Burnaby, B.C., Canada, 95 pp.

FRONDEL, C. (1956) Mineral composition of gummite. *American Mineralogist*, **41,** 539-568.

FRUEH, A.J. and GRAY, N. (1968) Confirmation and refinement of the structure of $Hg_3S_2Cl_2$.. *Acta Crystallogr*aphica, **B24**, 156-157.

GARSIDE, L.J. (1973) Radioactive mineral occurrences in Nevada. *Nevada Bureau of Mines and Geology Bulletin,* **81**, 58-61.

GIESTER, G., MIKENDA, W, and PERTLIK, F. (1996) Kleinite from Terlingua, Brewster County, Texas: investigations by single-crystal X-ray diffraction and spectroscopy. *Neues Jahrbuch für Mineralogie, Monatshefte*, **1996**, 49-56.

GIRAUD, R.E. (1986) Stratigraphy of Volcanic Sediments in the McDermitt mine, Humboldt County, Nevada. M.S. thesis, University of Idaho, Moscow, Idaho.

GLANZMAN, R.K., MCCARTHY, J.H. and RYTUBA, J.J. (1978) Lithium in the McDermitt Caldera, Nevada and Oregon. *Energy*, **3**, 347-353.

GLANZMAN, R.K. and RYTUBA, J.J. (1979) Zeolite-clay mineral zonation of volcaniclastic sediments within the McDermitt caldera complex of Nevada and Oregon. *U.S. Geological Survey Open File Report*, **79-1668**.

GRDENIĆ, D., KAMENAR, B., KORPAR-ČOLIG, B., SIKIRICA, M., and JOVANOVSKI, G. (1974) Tetrakis(trifluoroacetoxymercuri)-methane and Tetrakis(acetoxymercuri)-methane as the reaction products of Hofmann's Base with the corresponding acid: X-ray crystallographic evidence. *J.C.S. Chem. Comm*. 646-647.

GRDENIĆ, D., KORPAR-ČOLIG, B. and MATKOVIĆ-ČALOGOVIĆ, D. (1996) Synthesis and crystal structures of tetrakis(nitratomercurio)methane monohydrate and bis(sulphatomercurio) bis(aquamercurio) methane. *J. Organometallic Chemistry*, **522**, 297-302.

GREENE, R.C. (1972) Preliminary geologic map of the Jordan Meadow quadrangle, Nevada-Oregon. *U.S. Geological Survey Misc. Field Studies Map* **MF-341.**

GREENE, R.C. (1976) Volcanic rocks of the McDermitt caldera, Nevada-Oregon: U.S. Geological Survey Open-File Report 76-753, 80 pp.

HAMPTON, W.A., WHITE, G.P., HOSKIN, P.W.O., BROWNE, P.R.L. and RODGERS, K.A. (2004) Cinnabar, livingstonite, stibnite and pyrite in Pliocene silica sinter from Northland, New Zealand. *Mineralogical Magazine*, **68**, 191-198.

HENRY, C.D., CASTOR, S.B., STARKEL, W.A., ELLIS, B.S., WOLFF, J.A., HEIZLER, M.T. and McINTOSH, W.C. (2012) Geologic mapping, volcanology, mineralization, and high precision 40Ar/39Ar dating of early Yellowstone hot spot magmatism: Abstract **B33B-2850** presented at 2012 Fall Meeting, AGU, San Francisco, California, 3-7 Dec.

HENRY, C.D. and JOHN, D.A. (2013) Magmatism, ash-flow tuffs, and calderas of the ignimbrite flareup in the western Nevada volcanic field, Great Basin, USA: *Geophere*, **9**, 951-1008.

HENRY, C.D., CASTOR, S.B., STARKEL, W.A., ELLIS, B.S., WOLFF, J.A., McINTOSH, W.C, and HEIZLER, M.T. (2016) Preliminary geological map of the McDermitt Caldera, Humboldt County, Nevada and Harney and Malheur Counties, Oregon. Nevada Bureau of Mines and Geology Open-File 16-1, 1-8.

HENRY, C.D., CASTOR, S.B. STARKEL, W.B., ELLIS, B.S., WOLFF, J.A., LAVARIE, J.A., MCINTOSH, W.C. and HEIZLER, M.T. (2017) Geology and evolution of the McDermitt caldera, northern Nevada and southeastern Oregon, western USA. *Geosphere*, **13** (4, July), 1066-1112.

HETHERINGTON, M.J. (1983) The Geology and Mineralization at the McDermitt Mercury Mine, Nevada. M.S. thesis, University of Washington, Seattle, Washington.

HETHERINGTON, M.J. and CHENEY, E.S. (1985) Origin of the opalite breccia at the McDermitt mercury mine, Nevada. *Economic Geology*, **80**, 1981-1987.

HOLMES, G.H., JR. (1965) Mercury in Nevada, *in*: Mercury potential of the United States, U.S. Bureau of Mines Staff, Information Circular **8252**, 215-300.

JAMBOR, J.L. and ROBERTS, A.C. (1999) New Minerals Names, Kenhsuite. *American Mineralogist*, **84**, 194.

JENKINS, R.E. (1981) Minerals of Nevada (Draft # 6). Unpublished manuscript, 280p.

JENSEN, M.C., ROTA, J.C., and FOORD, E.E. (1995) The Gold Quarry mine, Carlin-trend, Eureka County, Nevada. *Mineralogical Record*, **26**, 449-469.

JOHN, D.A., HOFSTRA, A.H., FLECK, R.J., BRUMMER, J.E. and SADERHOLM, E.C. (2003) Geologic setting and genesis of the Mule Canyon low-sulfidation epithermal gold-silver deposit, north-central Nevada. *Economic Geology*, **98**, 425-463.

KAPUSTIN, A. (2010) Mercarbide: An unusual organomercury polymer. *Coordination Chemistry Reviews,* **254**, 1290-1294.

LERCH, D.W., KLEMPERER, S.L., GLEN, J.M.G., PONCE, D.A., MILLER, E.L.S. and GOLGAN, J.P. (2007) Crustal structures of the northwestern Basin and Range Province and its transition to unextended volcanic plateaus, Geochemical, Geophysical, Geosystems*, AGU* **8**(2) 21pp.

LESZCYKOWSKI, A.M. (1987) Mineral resources of the Disaster Peak study area, Harney and Malheur Counties, Oregon and Humboldt County, Nevada. *U. S. Bureau of Mines Mineral Land Assessment*/1987 Open File Report 65-87.

LUCKETT, M., MAHOOD, G.A. and BENSON, T.R. (2013) Earliest Silicic Volcanism associated with Mid-Miocene Flood Basalts: Tuffs Interbedded with Steens Basalt, Nevada and Oregon, American Geophysical Union, Fall Meeting, Dec., Abstract V33E-2829, 1 p.

LYAKHOVITSKAYA, V.A., SOROKIN, J.I., SAFONOV, A.A. VERIN, L.A. and ANDRIANOV, V.I. (1989): Growth and structure of crystals of $Hg_3Te_2I_2$. *Kristallografiya* **34**, 836-838.

MAHOOD, G.A. and BENSON, T.R. (2016) 40Ar/39Ar ages on intercalated silicic tuffs provide precise ages for Steens Basalt lavas: implications for flood basalt effusion rates, relation to Miocene Climatic Optimum, and the age of the Steens Geomagnetic Reversal. GSA Rocky Mountain Section Meeting, Moscow, Idaho, May.

MAHOOD, G.A. and BENSON, T.R. (2017) Using 40Ar/39Ar ages of intercalated silicic tuffs to date flood basalts: precise ages for Steen Basalt Member of the Columbia River Basalt Group. *Earth and Planetary Science Letters*, **459**, 340-351.

McCORMACK, J.K. (1986) Paragenesis and origin of sediment-hosted mercury ore at the McDermitt mine, McDermitt, Nevada. M.S. thesis, University of Nevada, Reno, Nevada.

McCORMACK, J.K. (1997) Mercury sulfo-halide minerals and crystalline phases and experimental formation conditions in the system $Hg_3S_2Cl_2$-$Hg_3S_2Br_2$-$Hg_3S_2I_2$. Ph.D. thesis, University of Nevada, Reno, Nevada, 154 pp.

McCORMACK, J.K. and DICKSON, F. W. (1998) Kenhsuite, ϒ-$Hg_3S_2Cl_2$, A new mineral species from the McDermitt Mercury deposit, Humboldt County, Nevada. *Canadian Mineralogist*, **36**, 201-206.

McCORMACK, J.K., DICKSON, F.W. and LESHENDOK, M.P. (1991) Radtkeite, Hg_3S_2ClI, a new mineral from the McDermitt mercury deposit, Humboldt County, Nevada. *American Mineralogist*, **76**, 1715-1721.

McCORMACK, J.K. (2000) The darkening of cinnabar in sunlight. *Mineralium Deposita* **35**(8), 796-798.

McKEE, E.H. (1976) Origin of the McDermitt caldera in Nevada and Oregon and related mercury deposits. *Trans***. AIME 260**, 196-199.

McKEE, E H., GREENE, R.C., and FOORD, E.E. (1975). Chronology of volcanism, *Soc. America, Abs. with Programs*, **1** (5), 629-630.

MCKEE, E.H. (1976) Origin of the McDermitt caldera in Nevada and Oregon and related mercury deposits. Trans. AIME, **260,** 196-199.

MILES, M.G., PATTERSON, J H., HOBBS, C.W., HOPPER, M.J., OVEREND, J., and TOBIAS, R.S. (1968) Raman and infrared spectra of isosteric diammine and dimethyl complexes of heavy metals. *Contribution from the Department of Chemistry, University of Minnesota, Minneapolis, Minnesota 55455,* **7**, (9), 1721-1729.

MILIĆ, D., SOLDIN, Ž., GIESTER, G., POPOVIĆ, Z. and MATKOVIĆ-ČALOGOVIĆ, D. (2009) Crystal structure of the first polymeric tetramercurated methane derivative of Hofmann's Base. *Croatica Chemica Acta* **82** (2), 337-344. MINING ANNUAL REVIEW (1985). *Mining Journal*, 120.

MINOR, S.A. (1986) Stratigraphy and structure of the western Trout Creek Mountains and northern Bilk Creek Mountains, Harney County, Oregon, and Humboldt County, Nevada. M.S. thesis, University of Colorado, Boulder, 177 pp.

NAKAGAWA, T., KIHARA, K., and HARADA, K. (2001) The crystal structure of low-temperature melanophlogite. *American Mineralogist*, **86**, 1506-1512.

NASH, J.T. (2010) Volcanogenic uranium deposits: geology, geochemical processes, and criteria for resource assessment. U.S.G.S. Open File Report **2010-1001**, 17-22.

NOBLE, D.C., McCORMACK, J.K., McKEE, E.H., SILBERMAN, M.L. and WALLACE, A.B. (1988) Time of mineralization in the evolution of the McDermitt caldera complex, Nevada-Oregon, and the relation of middle Miocene mineralization in the northern Great Basin to coeval regional basaltic magmatic activity. *Economic Geology*, **83**, 859-863.

PARKS, G.A. and NORDSTROM, D.K. (1979) Estimated free energies of formation, water solubilities, and stability fields for schuetteite ($Hg_3O_2SO_4$) and corderoite ($Hg_3S_2Cl_2$) at 298 K. *In* E. Jenne, ed., *Chemical Modeling in Aqueous Systems*. ACS Symposium Series, American Chemical Society, Washington DC, 339-352.

PERVUKHINA, N.V., VASIL'EV, V.I., BORISOV, S.V., MAGARILL, S.A. and NAUMOV, D.Yu. (2003) The crystal structure of a polymorph of $Hg^{2+}{}_3S_2Br_{1.0}Cl_{0.5}I_{0.5}$. *Canadian Mineralogist*, **41**, 1445-1453.

PERVUKHINA, N.V., VASIL'EV, V.I., NAUMOV, D.Yu., BORISOV, S.V. and MAGARILL, S.A. (2004) The crystal structure of synthetic radtkeite, Hg_3S_2ClI. *Canadian Mineralogist*, **42**, 87-94.

PERVUKHINA, N.V., MAGARILL, S.A., NAUMOV, D.Yu., BORISOV, S.V., VASIL'EV, V.I. and NENASHEV, B.G. (2005) Structural chemistry of mercury chalcohalides. III. Crystal structure of $Hg_3S_2Cl_{1.5}Br_{0.5}$ polymorphs. *Journal of Structural Chemistry*, **46**, 641-646.

PIERCE, K.L. and MORGAN, L.A. (1992) The track of the Yellowstone hot spot—Volcanism, faulting, and uplift: *Geological Survey of American Memoir* **179**, p.1-53.

PLACER-AMEX STAFF (1980) The McDermitt Mine, an information brochure published by Placer Amex Inc. 8p, 16p. Nevada Bureau of Mines and Geology, Public Mining Districts website. www.data.nbmg.unr.edu/PublicMiningDistricts/3450/34500006 and34500015.

PUFF, H. and KÜSTER, J. (1962a) Die Kristallstruktur von $Hg_3S_2Cl_2$. *Naturwissenschaften*, **49**, 299-300. *Naturwissenschaften*, **53**(11), 274.

PUFF, H. and KÜSTER, J. (1962b) Die Kristallstruktur der kubischen Triquecksilber-dichalkonium-dihalogenide.

Naturwissenschaften, **49**, 464-465.

PUFF, H. and KOHLSCHMIDT, R. (1962) Quecksilberchalkogenid-halogenide. Naturwissenschaften, **49**, 299.

PUFF, H., HARPAIN, A. and HOOP, K.P. (1966) Polymorphie bie quecksilberschwefel-halogeniden. *Naturwissenschaften*, **53**(11), 274.

PUFF, H., HEINE, D. and LIECKK, G. (1968) Quicksilberschwe-felfuorid. *Naturwissenschaften*, **55**, 298.

ROBERTS, A.C., GAULT, R A., PAAR, W.H., COOPER, M.A., HAWTHORNE, F.C., BURNS, P.C., CISNEROS, S., and FOORD, E.E. (2005) Terlinguacreekite, $Hg^{2+}{}_3O_2Cl_2$, a new mineral species from the Perry pit, Mariposa mine, Terlingua mining district, Brewster County, Texas, USA. *Canadian Mineralogist,* **43**, 1055-1060.

ROPER, M.W. (1976) Hot springs mercury deposition at McDermitt mine, Humboldt County, Nevada. *Trans*. **AIME 260**, 192-195.

ROPER, M.W. and WALLACE, A.B. (1981) Geology of the Aurora uranium prospect, Malheur County, Oregon. *In* Uranium in volcanic and volcaniclastic rocks. Edited by Philip C. Goodell and Aaron C. Waters. *American Association of Petroleum Geologists*: Studies in Geology, 331 pp.

RYTUBA, J.J. (1976) Geology and ore deposits of the McDermitt caldera, Nevada-Oregon. *U. S. Geological Survey Open File Report* **76-535**.

RYTUBA, J.J. and GLANZMAN, R.K. (1978) Relation of mercury, uranium, and lithium deposits to the McDermitt caldera complex. *U.S. Geological Survey Open File Report* **78-926**, 31 p. *Nevada Bureau of Mines and Geology Report* **33**, 109-117.

RYTUBA, J.J. and GLAZMAN, R.K. (1979) Relation of mercury, uranium and lighium deposits to the McDermitt caldera complex, Nevada-Oregon. Nevada Bureau of Mines and Geology, Report **33**, 109-117.

RYTUBA, J.J. and HEROPOULOS, C. (1992) Mercury; an important byproduct in epithermal gold systems, *in* DeYoung, J. H., Jr. and Hammarstrom, J. M., eds;, Contributions to commodity geology research. *U.S. Geological Survey Bulletin* **1877,** p. D1-D8.

RYTUBA, J.J. and McKEE, E.H. (1984) Peralkaline ash flow tuffs and calderas of the McDermitt Volcanic Field, southeast Oregon and north central Nevada. *Journal of Geophysical Research*, **89**, 8616-8628.

RYTUBA, J.J., CONRAD, W.K. and GLANZMAN, R.K. (1979) Uranium, thorium, and mercury distribution through the evolution of the McDermitt caldera complex. *U. S. Geological Survey Open File Report* **79-541**.

RYTUBA and CONRAD, W.KL. (1981) Petrochemical characteristics of volcanic rocks associated with uranium deposits in the McDermitt Caldera complex, *in* GOODELL, P.C. and WATERS, A.C, eds., Uranium in volcanic and volcaniclastic rocks: American Association of Petroleum Geologists. *Studies in Geology*, **13**, 109-117.

RYTUBA, J.J., BATESON, J.T., CURTIS, D.L. and COX, G.A. (1983) Geologic map of the Little Whitehorse Creek quadrangle, Harney and Malheur Counties, Oregon. U.S. Geological Survey Miscellaneous Field Studies Map 1472, scale 1:24,000.

RYTUBA, J.J., JOHN, D.A., FOSTER, A., LUDINGTON, S.D. and KOTLYAR, B. (2003) Hydrothermal enrichment of gallium in zones of advanced argillic alteration—examples from the Paradise Peak and McDermitt ore deposits, Nevada. *In* Contributions to Industrial-Minerals Research, Chapter C, Bulletin **2209-C**, Bliss, J. D., Moyle, P. R., and Long, K. R., editors.

SCHLOTTMAN, J.D. Jr. (1987) Last Mercury Mine Closes. *California Mining Journal*, April, 17-20.

SCHOONEN, M.A.A. and XU,Y. (2001) Nitrogen reduction under hydrothermal vent conditions: implications for the prebiotic synthesis of C-H-O-N compounds. *Astrobiology*, **1**, 133-142.

SCHUETTE, C.N. (1938) Quicksilver in Oregon. *Oregon Department of geology and Mineral Industries Bulletin*, No**. 4**, 172 pp.

SHARP, B.J. (1955) Uranium occurrences at the Moonlight mine, Humboldt County, Nevada. U.S. Atomic Energy Commission Report RME-2032, pt. I, 14pp.

SHUTTY, M.C. (2015) Summary report for the 2008 Cordero, Nevada drill program. Silver Predator Corp., Hayden, Idaho.

SISSELMAN, R. (1975) New McDermitt Mine Joint Venture Emerges as Dominant Force in US Mercury Production. Engineering and Mining Journal, Dec., *in* Hollister, V.F. (1985) Discoveries of Epithermal Precious Metal Deposits, **AIME**, 120-127.

SPEER, W.E. (1977) Geology of the McDermitt mine area, Humboldt County, Nevada. M.S. thesis, University of Arizona, Tucson, Arizona.

STARKEL, W.A. (2014) Mapping, geologic evolution and petrogenesis of the McDermitt volcanic center, northern Nevada and southern Oregon, USA. Ph.D. thesis, Washington State University, School of the Environment, 407pp.

STOREY, L.O. (1985) History of the discovery of the McDermitt mine, McDermitt, Nevada. *Trans. AIME* **260**.

SWITZER, G., FOSHAG, W.F., MURATA, K.J. and FAHEY, J.J. (1953) Re-examination of mosesite. *American Mineralogist*, **38**, 1225-1234.

TAYLOR, A.O. and POWERS, J.F. (1955) Uranium occurrences at the Moonlight mine and Granite Point claims, Humboldt County, Nevada. U.S. Geological Survey, **TEM-874-A**, 16p.

TEWALT, N.A. and CARRINGTON, R.G. (2001) U. S. gallium exploration report with report on Cordero property for Gold Canyon Resources (unpublished report, 31 pp).

U.S. BUREAU OF MINES STAFF (1965) Mercury potential of the United States. USBM IC **8252**, Part 2 of 2, 224-225.

VASIL'EV, V.I., PAL'CHIK, N.A. and GRECHISHCHEV, O.K. (1984) Lavrentievite and arzakite, new natural sulfohalogenides of mercury. *Geologiya i Geofizika*, **7**, 54-63.

VASIL'EV, V.I., LAVRENT'EV, Y.G. and PAL'CHIK, N.A. (1986) The new data about arzakite and lavrentievite. *Doklady Akademii Nauk SSSR*, **290**, 948-951.

VASIL'EV, V.I., USOVA, L.V., and PAL'CHIK, N.A. (1989) Grechishchevite $Hg_3S_2(Br,Cl,I)_2$. A new supergene sulfohalogenide of mercury. *Geologiya i Geofizika*, **30**, 61-69.

VIKRE, P.G., BENSON, M.E., BLEIWAS, D.I., COLGAN, J.P., COSSETTE, P.M., DEANGELO, J., DICKEN, C.L., DRAKE, R.M. II, DU BRAY, E.A., FERNETTE, G.L., GLEN, J.M.G., HAACKE, J.E., HALL, S.M., HOFSTRA, A.H., JOHN, D.A., LUDINGTON, S., MIHALASKY, M.J., RYTUBA, J.J., SHAFFER, B.N., STILLINGS, L.L., WALLIS J.C., WILLIAMS, C.F., YAGER, D.B., and ZÜRCHER, L. (2016) Geology and Mineral Resources of the Sheldon-Hart Mountain National Wildlife Refuge Complex (Oregon and Nevada), the Southeastern Oregon and North-Central Nevada, and the Southern Idaho and Northern Nevada (and Utah) Sagebrush Focal Areas. U.S.G.S. Scientific Investigations Report **2016-5089-B**, Version 1.1, October 26, 2016, 240 pp.

VINALS, J. and CALVO, M. (2007) Corderoite, kenhsuite and perroudite, mercury sulfohalides from Chovar, Castello, Spain. *Revista de Minerales*. **3**(3): 46-49. Barcelona, Spain.

VOROSHILOV, Y.V., KHUDOLII, V.A. and PAN'KO, V.V. (1996) Phase equilibria in the HgS-HgTe-$HgCl_2$ system and the crystalline structure of beta-$Hg_3S_2Cl_2$ and Hg_3TeCl_4. *Zhurnal Neorganicheskoi Khimii*, **41**, 287-293.

WALKER, G.W. and REPENNING, C.A. (1965) Reconnaissance geologic map of the Adel quadrangle, Lake, Harney, and Malheur Counties, Oregon. U.S. Geological Survey, Miscellaneous Geologic Investigations Map I-446.

WALLACE, A.B. (2003) Geology of the Ivanhoe Hg-Au District, northern Nevada: influence of Miocene volcanism, lakes, and active faulting on epithermal mineralization. *Economic Geology*, **98**, 409-424.

WALLACE. A.B. and ROPER, M.W. (1981) Geology and uranium deposits along the Northeastern Margin, McDermitt Caldera Complex, Oregon. *In* Uranium in volcanic and volcaniclastic rocks. Edited by Philip C. Goodell and Aaron C. Waters. *American Association of Petroleum Geologis*ts: *Studies in Geology*, 331 p.

WEIL, M. (2001) $Hg_3O_2(SO_4)$, a re-investigation. *Acta Crystallographica*, **E57**, i98-i100.

WILDEN, R. (1964) Geology and mineral deposits of Humboldt County, Nevada. *Bulletin* **59**, Nevada Bureau of Mines and Geology.

WILLIAMS, G.K. (1980) Amenability studies in Kings River Summary Report. Unpublished Chevron Resources Company Report, p. 11.1-11-4.

WYLD, S.J. and WRIGHT, J.E. (2001) New evidence for Cretaceous stike-slip faulting in the U.S. Cordillera; and inplications for terrane displacement, deformation patterns and plutonism: *American Journal of Science*, V. **301**, 150-181.

YATES, R. G. (1942) Quicksilver deposits of the Opalite district, Malheur County, Oregon and Humboldt County, Nevada. *U. S. Geological Survey Bulletin* **931-N**, 319-348.

ZHUKHLISTOV, A.P. and ZVYAGIN, B.B. (1977) Determination of the crystal structures of chapmanite and bismutoferrite by high-voltage electron diffraction. *Soviet Physics and Crystallography,* **22**, 419-523.